

**Functional Analyses of ABHD17 Enzymes**

by

Melanie S. Cheung See Kit

A dissertation submitted in partial fulfillment  
of the requirements for the degree of  
Doctor of Philosophy  
(Chemistry)  
in the University of Michigan  
2019

Doctoral Committee:

Assistant Professor Brent R. Martin, Chair  
Assistant Professor Paul M. Jenkins  
Professor Anna K. Mapp  
Professor Brandon T. Ruotolo

Melanie S. Cheung See Kit

[mcheusk@umich.edu](mailto:mcheusk@umich.edu)

ORCID iD: 0000-0002-0511-1506

© Melanie S. Cheung See Kit 2019

## **Acknowledgements**

I would like to thank all the people who have made it possible for me to pursue a scientific career. I am grateful for my undergraduate mentors at St. John's University, especially Subbha Dhalladoo and Dr. Rachel Zufferey, who first introduced me to scientific research. I was lucky to have Rachel Pricer as my first mentor in graduate school. She is one of my closest friends and her support throughout graduate school has been priceless. I joined the Martin lab, where I worked with a great group of scientists. I am especially thankful to Michael Won, Sarah Haynes and Dr. Jaimeen Majmudar for their patience and help answering all the questions I had when my research projects spanned areas of science that I was not familiar with. Throughout graduate school, I was fortunate to have supportive friends, including Sarah Haynes and Sugyan Dixit.

I would like to thank my committee members (Brent, Anna, Paul and Brandon) for all their help and guidance during my time at the University of Michigan. I am grateful for all the interesting research that I worked on in the Martin lab and for the many opportunities to present my work at conferences outside of the University of Michigan. I would also like to thank our Chemistry support staff (Liz Oxford, Katie Forster, and Heather Hanosh) for all their help.

Finally, I would like to thank my family for always believing in me and encouraging me to pursue my scientific interest. I am forever grateful to my parents for giving me the chance to come to the United States nine years ago to study in college. Despite being far from home, I was lucky to have my brother in the US as well and his constant support has been invaluable.

## Table of Contents

Acknowledgements .....	ii
List of Tables .....	v
List of Figures.....	vi
Abstract.....	ix
Chapter 1 Introduction .....	1
1A. Abstract .....	1
1B. Introduction .....	2
1A. Palmitoyl protein thioesterase 1 .....	5
1B. Acyl protein thioesterases .....	6
1C. ABHD17 family thioesterases.....	12
1D. Assays for depalmitoylation.....	16
1E. Overview of thesis.....	21
Chapter 2 Biochemical Studies of ABHD17.....	24
2A. Abstract .....	24
2B. Background .....	25
2C. Results and discussion.....	28
2CI. <i>S</i> -palmitoylation across ABHD17 isoforms is regulated by a similar subset of DHHC enzymes.....	28
2CII. Protein expression and purification in different systems for use in functional activity assays.....	33
2CIII. Validation of inhibitors for full-length recombinant enzymes .....	39
2D. Conclusion .....	43
2E. Experimental.....	44

Chapter 3	Acyl-RAC Proteomics Approach to Profile Site-specific <i>S</i> -acylation .....	52
3A.	Abstract .....	52
3B.	Background .....	53
3C.	Results and discussion.....	57
3CI.	Identification of putative sites of <i>S</i> -palmitoylation in mouse embryonic fibroblasts (MEF) cells by site-specific acyl-RAC proteomics .....	57
3CII.	Profiling putative substrates of ABHD17 depalmitoylases by site-specific acyl-RAC proteomics analysis .....	61
3D.	Conclusion .....	64
3E.	Experimental.....	65
Chapter 4	Conclusion and Future Directions .....	70
4A.	Conclusion .....	70
4B.	Future directions.....	72
Appendix.....	.....	76
References	.....	89

## List of Tables

Table 2-1 Antibody information.....	46
Table 2-2 Structure of compounds used during inhibitor screening .....	50
Table 3-1 Subset of identified sites of S-palmitoylation compared to SwissPalm database.....	60
Table 3-2 Western blot antibody information .....	67

## List of Figures

Figure 1-1 Cellular pathways of protein depalmitoylation.....	4
Figure 1-2 APT inhibitor selectivity index.....	11
Figure 1-3 ABHD17 enzymes are palmitoylated and localize to the plasma membrane.....	14
Figure 1-4 Homology, depalmitoylase activity, and Palmostatin B inhibition of HDFP-sensitive serine hydrolases.....	15
Figure 2-1 Sequence alignment of the N-terminus region of ABHD17 human and mouse isoforms. ....	26
Figure 2-2 APEGS assay shows multiple S-palmitoylation sites for ABHD17 expressed in HEK-293T.....	29
Figure 2-3 ABHD17A is still S-palmitoylated after protein purification.....	29
Figure 2-4 Co-expression of ABHD17 with the full panel of 23 DHHC enzymes.....	30
Figure 2-5 Representative HA blot to verify DHHC expression.....	31
Figure 2-6 Co-expression of select DHHC and ABHD17 isoforms. ....	32
Figure 2-7 Coomassie-stained SDS-PAGE gels showing the affinity purification of ABHD17B WT fused to different N-terminal tags. ....	33
Figure 2-8 Purified ABHD17A and 17B have an active Ser labeled using FP-TAMRA. ....	34
Figure 2-9 FLAG purification of ABHD17A expressed in HEK-293T .....	35
Figure 2-10 Cobalt resin purification of ABHD17A and 17B expressed in mammalian cells. ....	35

Figure 2-11 Comparison of FP-TAMRA labeling between the unmodified and S-palmitoylated ABHD17.....	36
Figure 2-12 Purification of 6xHis-Halotag NRAS protein.....	37
Figure 2-13 In vitro experiments with NRAS expressed in HEK-293T and labeled with 17-ODYA.....	37
Figure 2-14 Alternate in vitro depalmitoylation assay strategy using a Cys alkylator conjugated to a fluorophore. ....	38
Figure 2-15 Overview of fluorogenic assay used to assess candidate inhibitors .....	39
Figure 2-16 ABHD17A and 17B are inhibited the most by oxazinone-derivative compound A. ....	40
Figure 2-17 Mechanism of inactivation by benzoxazinone derivatives.....	41
Figure 2-18 ABPP gel with ABHD17A and 17B overexpression.....	42
Figure 2-19 In vitro treatment of membrane fraction of HEK-293T lysate overexpressing ABHD17A and 17B with FLAG6xHis tag.....	42
Figure 2-20 Metabolic labeling of HAP1 cells treated with compound A or DMSO.....	43
Figure 3-1 Analysis of S-palmitoylation by acyl-RAC workflow. ....	57
Figure 3-2 S-acylated peptides in RAS mouse embryonic fibroblasts.....	59
Figure 3-3 A CRISPRi strategy was employed to target expression of ABHD17B in HAP1 cells. ....	61
Figure 3-4 Acyl-RAC gels verifying expression and S-palmitoylation of ABHD17A in THP-1 cells following CRISPRi knockdown.....	62
Figure 3-5 No significant changes in S-acylation levels observed during overexpression of ABHD17A WT and S190A (mutant) in NRAS MEF cells.....	63
Figure 3-6 NRAS palmitoylation level measured by acyl-RAC. ....	64



Figure 4-1 Quenched fluorogenic probe designed to measure depalmitoylase activity.....73

## Abstract

Post-translational modifications (PTMs) play a crucial role in trafficking proteins for many location-dependent cellular functions. Protein *S*-acylation describes the addition of long chain fatty acids (predominantly the C16:0 palmitate) to cysteines via a thioester bond. This reversible modification thus allows for controlled regulation of protein membrane tethering during various cellular processes. Indeed, *S*-palmitoylated proteins include kinases, small GTPases and transmembrane receptors, which function in response to diverse signaling events. It is important to study the enzymes that catalyze this modification since it is involved in many essential pathways. Enzymes such as APT1 and APT2 have thoroughly been studied and shown to depalmitoylate a myriad of *S*-palmitoylated substrates and the development of selective inhibitors has accelerated the discovery of new substrates. ABHD17 has more recently been shown to depalmitoylate substrates in cell-based studies. However, not much is known about its substrate recognition mechanism and cellular function and my dissertation helps to bridge this gap in knowledge. The first chapter presents a detailed introduction to protein depalmitoylases, their different cellular roles and methods that have been developed to study them. The following chapter focuses on understanding the *in vitro* activity of ABHD17 and the development of potential inhibitors to study its function. The third chapter outlines a proteomics strategy that can be used to study *S*-palmitoylation of multiple proteins at a time and was applied to understand how ABHD17 regulates *S*-palmitoylation in cells. Finally, future experiments are proposed in Chapter 4 to further improve our understanding of how ABHD17 works and what its cellular function is.

## Chapter 1 Introduction\*

### 1A. Abstract

Protein depalmitoylation describes the removal of thioester-linked long chain fatty acids from cysteine residues in proteins. For many *S*-palmitoylated proteins, this process is promoted by acyl protein thioesterase enzymes, which catalyze thioester hydrolysis to solubilize and displace substrate proteins from membranes. The closely related enzymes acyl protein thioesterase 1 (APT1; LYPLA1) and acyl protein thioesterase 2 (APT2; LYPLA2) were initially identified from biochemical assays as G protein depalmitoylases, yet later were shown to accept a number of *S*-palmitoylated protein and phospholipid substrates. Leveraging the development of isoform-selective APT inhibitors, several studies report distinct roles for APT enzymes in growth factor and hormonal signaling. In addition to APT enzymes, the ABHD17 family of hydrolases contributes to the depalmitoylation of Ras-family GTPases and synaptic proteins. Overall, enzymatic depalmitoylation ensures efficient membrane targeting by balancing the palmitoylation cycle, and may play additional roles in signaling, growth, and cell organization. This chapter provides a perspective on the biochemical and cellular analysis of protein depalmitoylases, and outline opportunities for future studies of systems-wide analysis of protein depalmitoylation.

---

\* This chapter comprises sections from a peer-reviewed review article.<sup>1</sup> My contribution to this review includes figures and assistance in writing.

## 1B. Introduction

*S*-Palmitoylation describes the addition of a long-chain fatty acid to a cysteine residue via a thioester linkage.<sup>2</sup> This hydrophobic post-translational modification promotes the membrane tethering, trafficking, and localization of a significant fraction of membrane-associated proteins. While the term “*S*-palmitoylation” implies exclusive modification by 16:0 fatty acids, the cellular profile of fatty acylated cysteine residues likely includes a variety of long chain fatty acids with differing unsaturation,<sup>3-5</sup> and is interchangeably used with the term “*S*-acylation”. Protein *S*-palmitoylation is catalyzed by a family of protein acyl transferases, termed zDHHC enzymes due to their predicted Zn<sup>2+</sup>-binding and conserved Asp-His-His-Cys motif.<sup>6-8</sup> These multi-pass transmembrane proteins catalyze acyl transfer from long chain fatty acyl-CoAs to cysteine residues in proteins. Humans express 23 zDHHC enzymes that influence many diverse cellular pathways. For example, zDHHC5 deletion blocks neuronal stem cell differentiation,<sup>9</sup> and along with its close homologue zDHHC8, localize to synapses in neurons<sup>10</sup> where they influence activity-dependent endocytic trafficking, excitability, and synaptic connectivity.<sup>11</sup> In addition, zDHHC2 palmitoylates Src-family kinases,<sup>12</sup> while inhibition of close homologue zDHHC20 prevents EGFR *S*-palmitoylation and enhances the action of EGFR inhibitors.<sup>13</sup> zDHHC9 is reported to *S*-palmitoylate Ras,<sup>14, 15</sup> and is genetically linked to X-linked mental retardation.<sup>16</sup> Across dozens of publications, zDHHC enzymes have emerged as critical regulators of protein *S*-palmitoylation and membrane targeting.<sup>2, 17</sup>

Perhaps the most intriguing aspect *S*-palmitoylation is its reversibility, since thioester hydrolysis eliminates the fatty acyl anchor to modulate membrane localization and/or function. For example, cycles of acylation and deacylation are required for the plasma membrane association of Ras-family small GTPases and G proteins,<sup>18-20</sup> establishing a distinct mode of

peripheral membrane protein directionality dependent on a continuous palmitoylation cycle.<sup>21, 22</sup> Indeed, pharmacological inhibition with promiscuous inhibitors of either zDHHC PATs or depalmitoylases block the plasma membrane targeting of Ras and G proteins.<sup>21, 23, 24</sup> Microinjection of semi-synthetic fluorescently-labeled *S*-palmitoylated Ras rapidly redistributes to the Golgi, which is established as the destination of depalmitoylated Ras.<sup>22</sup> Based on these findings, peripheral membrane protein *S*-palmitoylation requires a balanced cycle of both zDHHC enzymes and depalmitoylating enzymes for efficient transport along the flux of the secretory pathway towards the plasma membrane.<sup>21</sup> Furthermore, both Ras and G proteins are rapidly depalmitoylated in their GTP-bound state,<sup>25-27</sup> which coincides with, but is not required for agonist dependent-internalization to internal membranes.<sup>24</sup> Based on these examples, constitutive protein *S*-palmitoylation is required for proper trafficking of many peripheral membrane proteins, but may also function as a reversible signal analogous to protein phosphorylation (**Figure 1-1**). For example, serum, growth factor, or phorbol ester addition triggers deacylation of a 64 kD protein in [<sup>3</sup>H]-palmitate labeled mouse BH3C1 cells,<sup>28</sup> which in light of more recent proteomics studies,<sup>29</sup> likely corresponds to depalmitoylation of metadherin, a major driver of cancer and metastasis.<sup>30</sup> Therefore, external stimuli trigger either direct activation of depalmitoylases, or facilitate conformational changes that enhance depalmitoylase accessibility, which then tips the balance of the palmitoylation cycle to reorganize membrane distribution and signaling outputs.

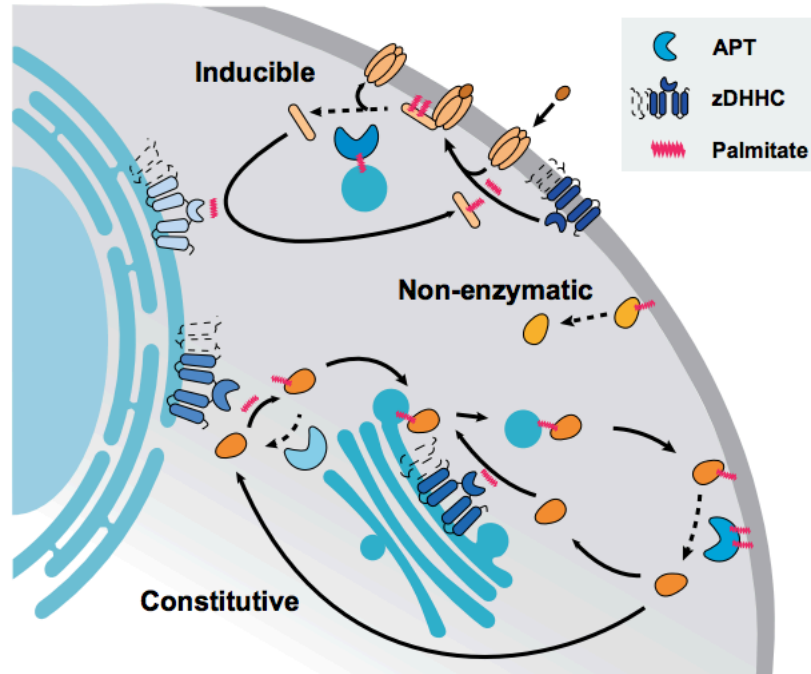


Figure 1-1 Cellular pathways of protein depalmitoylation.

Protein depalmitoylation can proceed by either non-enzymatic hydrolysis, inducible depalmitoylation, or constitutive depalmitoylation during trafficking. zDHHC enzymes are shown as transmembrane proteins.

While this model is appealing, a number of fundamental questions remain, such as 1) what enzymes catalyze depalmitoylation of different *S*-palmitoylated proteins, 2) what, if anything, triggers their activation, and 3) is there a coincident dysregulation of protein acyl transferase enzymes to block re-palmitoylation? In addition to peripheral membrane proteins, many integral membrane proteins such as channels, receptors, and adhesion proteins also require *S*-palmitoylation for proper activation, sensitization, or microdomain localization. Given the ever-expanding number of *bona fide* *S*-palmitoylated proteins,<sup>31</sup> how broad is the role for depalmitoylases in regulating *S*-palmitoylation stability? What is the scope of enzymatic depalmitoylation compared with the intrinsic hydrolysis of the high-energy thioester linkage? Through the development of new methods and model systems, these questions are central to understanding the role of dynamic *S*-palmitoylation in physiological systems.

## 1A. Palmitoyl protein thioesterase 1

Several early reports demonstrated enhanced depalmitoylation upon hormonal stimulation, suggesting activation of specific depalmitoylases might regulate intracellular signaling pathways.<sup>26, 27, 32</sup> For example, both Ras and G proteins are more rapidly depalmitoylated after activation, which was believed to contribute to more efficient internalization. Several candidate depalmitoylating enzymes were later identified by activity-guided fractionation and purification from soluble tissue homogenates.<sup>33, 34</sup> While technically feasible, this approach ignored the presence of any membrane-bound depalmitoylating enzymes. Nonetheless, the lysosomal hydrolase PPT1 was identified as the most robust H-Ras depalmitoylase *in vitro*.<sup>33</sup> PPT1 was later found to localize exclusively in lysosomes and late endosomes,<sup>35</sup> functionally separating PPT1 from depalmitoylase activity in the cytosol or on plasma membrane. PPT1 is one of 14 genes genetically linked to the family of human neuronal ceroid lipofuscinosis (NCL) lysosomal storage diseases, characterized by accumulation of lysosomal autofluorescent storage material, neurodegeneration, and childhood mortality.<sup>36</sup> Interestingly, while not localized in the lysosome, mutations in cysteine string protein alpha gene (CSP $\alpha$ ) also lead to NCL.<sup>37</sup> CSP $\alpha$  is multiply *S*-palmitoylated, and functions as a HSC70 interacting J-protein important for protein folding and synaptic vesicle function. In CSP $\alpha$  mutant cells, PPT1 is highly over-expressed.<sup>38</sup> Furthermore, PPT1 can depalmitoylate CSP $\alpha$  *in vitro*, which is reported to lead to the formation of insoluble aggregates. Acyl-RAC analysis of CSP $\alpha$  mutant cells revealed decreased *S*-palmitoylation of several synaptic proteins and neuronal signaling proteins. Overall, PPT1 is likely not contributing to plasma membrane depalmitoylation, but could play a role in vesicular depalmitoylation and lysosomal degradation of *S*-palmitoylated proteins.

## 1B. Acyl protein thioesterases

The reported lysophospholipase LYPLA1 was identified by screening soluble tissue homogenates for G protein depalmitoylase activity,<sup>34</sup> and subsequently renamed acyl protein thioesterase 1 (APT1). In addition to its depalmitoylase activity, APT1 hydrolyzes a broad profile of lysophospholipids and other long-chain mono-acyl glycerol esters, albeit at a lower catalytic efficiency than high-energy *S*-palmitoylated substrates.<sup>39, 40</sup> Since APT1 was first reported before the development of RNAi methods, much of the first decade of depalmitoylase research relied on *in vitro* biochemistry or over-expression studies. Over-expression of APT1 enhances the depalmitoylation of small GTPases,<sup>41, 42</sup> endothelial nitric oxide synthase,<sup>43</sup> and a number of other peripheral membrane proteins in transfected cells. Such over-expression could lead to a number of potential artifacts, either by disruptive fusion of epitope tags or fluorescent proteins, or through saturation of binding partners at non-physiological expression levels. If the enzyme concentration increases much beyond physiological levels, the rate of substrate hydrolysis will also increase, and potentially promote depalmitoylation of non-physiological substrates. In addition, over-expression could also impart non-physiological depalmitoylase activity to otherwise dedicated lipid modifying enzymes, particularly since thioesters are high energy bonds readily hydrolyzed by even weak nucleophiles. Over-expressing candidate *S*-palmitoylated substrates is also problematic, since high expression levels can approach the enzyme  $K_m$ , further promoting APT1-dependent depalmitoylation of non-native substrates. Even so, APT1 can depalmitoylate a number of proteins in cells. In fact, the neuronal microRNA mi138 modulates APT1 levels in synaptic spines, reportedly affecting spine volume through modulation of  $G\alpha_{13}$  *S*-palmitoylation.<sup>44</sup>



In addition to APT1, vertebrates express the highly similar depalmitoylase APT2, (68% identical, 81% similar). APT2 also hydrolyzes lysophospholipids,<sup>45</sup> but in contrast to APT1, it also hydrolyzes prostaglandin glycerol esters.<sup>46</sup> Both APT1 and APT2 act as efficient depalmitoylases *in vitro*,<sup>40</sup> and are presumed to broadly regulate *S*-palmitoylation and trafficking of peripheral membrane proteins in cells. Unfortunately, there are no quality commercial sources of APT1 and APT2 antibodies, since they are likely poorly immunogenic due to nearly exact conservation across most mammals, including mice, rabbits, and humans. Thus, most studies on APT1 and APT2 localization have used GFP or epitope fusions for subcellular analysis. The literature consensus reveals both enzymes are primarily cytoplasmic, although partially localized on internal membranes,<sup>47</sup> or in some instances on the plasma membrane.<sup>42, 48</sup> APT1 has also been found to be primarily localized and active in the mitochondria, however the mechanism by which it gets trafficked to the mitochondria is not known since it does not have a mitochondrial targeting sequence.<sup>49</sup> Both APT1 and APT2 share a cysteine at the second position immediately following the initiator methionine, and are reportedly both *S*-palmitoylated.<sup>42, 47, 50</sup> After removal of the initiator methionine, if the N-terminus is not acetylated, it may readily undergo N-acyl transfer to form a stable amide linkage. Interestingly, APT1 *S*-palmitoylation has been reported in only one proteomics experiments using hydroxylamine switch methods, but never by alkynyl fatty acid labeling.<sup>31, 50</sup> APT1 and APT2 are expressed and active across nearly all tissues,<sup>51, 52</sup> yet their absence in most large-scale profiling efforts suggests they may not be stoichiometrically *S*-palmitoylated. This low-level *S*-palmitoylation could be caused by an alternative translational start site (potentially Met- 6) or through auto-depalmitoylation. Nonetheless, knockdown of either APT1 or APT2 promotes plasma membrane association of the other APT enzyme, suggesting an interdependent *S*-palmitoylation cycle.<sup>42</sup>

Based on their predicted role in regulating peripheral membrane protein localization, peptidomimetic inhibitors of APT1 were developed that upon microinjection could mislocalize N-Ras away from the plasma membrane.<sup>53</sup> Based on these studies, derivatives of the generic natural product lipase inhibitor tetrahydrolipstatin were identified that potently inhibited both APT1 and APT2.<sup>41</sup> The  $\beta$ -lactone mechanism-based inhibitors Palmostatin B and the choline-derivative Palmostatin M<sup>40</sup> were developed as dual inhibitors of both APT enzymes. Palmostatin B treatment led to accumulation of N-Ras on internal membranes, as well as partial rescue of E-Cadherin membrane localization.<sup>41</sup> Interestingly, knockdown of APT1 was not sufficient to reproduce the pharmacological effects to statistical significance, demonstrating possible compensatory mechanisms, either by APT2 or by other unannotated depalmitoylating enzymes. Single cell studies revealed altered trafficking dynamics of over-expressed N-Ras fluorescent protein fusions and microinjection of semi-synthetic, fluorescently labeled N-Ras. Upon growth factor stimulation, Palmostatin B treated cells showed reduced Ras activation on the Golgi. Later studies demonstrated selective growth inhibition of N-Ras, but not K-Ras driven growth of myeloid progenitors.<sup>54</sup> Accordingly, Palmostatin B directly modulates N-Ras localization and activity by disrupting the Ras palmitoylation cycle.<sup>55</sup>

While Palmostatin B demonstrates high potency against both APTs ( $IC_{50} < 5$  nM),<sup>40</sup> phenotypic effects typically require  $> 20$   $\mu$ M.<sup>41, 56, 57</sup> Early studies suggested that Palmostatin derivatives are highly unstable in serum, requiring repeated cycles of inhibitor addition to maintain inactivation.<sup>44</sup> Nevertheless, this compound has been used in numerous studies to profile APT1 and APT2 function. For instance, Palmostatin B addition accelerated the incorporation of the 17-ODYA in Lck in unstimulated T-cells.<sup>58</sup> However, the compound failed to block depalmitoylation once the cells were stimulated with Fas ligand. The authors suggested

that there may be distinct pools of depalmitoylases once the receptors are activated. In addition, the neuronal RGS-binding protein R7BP accelerates the deactivation of  $G_{i/o}$  proteins. Inhibition with Palmostatin B or HDFP both redistributed R7BP from the plasma membrane to endomembranes, disrupted association with G protein-regulated inwardly rectifying potassium (GIRK) channels, and slowed GIRK channel closure.<sup>59</sup> Importantly, knockdown of both APT1 and APT2 had no effect on GIRK inactivation, suggesting the presence of additional depalmitoylated enzymes. Chronic lymphocytic leukemia (CLL) B-cells express nearly 10-fold more APT2 and 2-fold more APT1. Palmostatin B treatment or APT knockdown increased CD95-mediated apoptosis.<sup>60</sup> Activity-based protein profiling (ABPP) studies later demonstrated that Palmostatin B is not exclusive for APT1/APT2, and inactivates a number of other lipid processing serine hydrolases with somewhat weaker potency, including ABHD6, ABHD16A, ABHD17A-C, PNPLA6, and FASN.<sup>61</sup> Accordingly, Palmostatin B should be used only as a generic depalmitoylase inhibitor, with a clear understanding that multiple enzymes are blocked at concentrations required for sustainable depalmitoylase inhibition, and the biological outcomes may reflect polypharmacology summed across many enzymes.

Despite these issues, Palmostatin B remains a popular tool for blocking depalmitoylase activity, and even attenuates depalmitoylation *in vivo* after intraperitoneal injection.<sup>62</sup> The MC1R G-protein-coupled receptor triggers melanin production and enhances DNA repair after ultraviolet irradiation. Mice with red hair MC1R variants have reduced MC1R *S*-palmitoylation, weaker cAMP stimulation, and are more susceptible to developing melanoma. Remarkably, intraperitoneal injection of Palmostatin B (10 mg kg<sup>-1</sup>) prior to UV irradiation increased MC1R *S*-palmitoylation and clearance of DNA photoproducts while reducing tumor growth. While Palmostatin B is promiscuous, at this relatively low-dose, APTs are likely to be the primary

targets. APT inhibition also prevents melanoma tumor cell invasion by regulating the *S*-palmitoylation of the polarity organizing protein MCAM.<sup>32</sup> Wnt5a stimulation promotes APT1-dependent depalmitoylation of MCAM, inducing asymmetric MCAM localization to promote a more invasive state. Taken together, APT inhibitors may be valuable prophylactics in topical sunscreens to prevent melanoma. Nonetheless, the APT1 and APT2 inhibitors ML348 and ML349 had no effect on MAPK signaling or growth across several N-Ras-dependent melanoma cell lines,<sup>63</sup> demonstrating APT activity is not essential across all cancers types or stages.

A number of more selective APT inhibitors have been developed with more drug-like properties. Isoform-selective inhibitors of APT1 (ML348,  $K_i = 280$  nM) and APT2 (ML349,  $K_i = 120$  nM) were identified by high throughput screening in a competitive fluorescence polarization assay.<sup>64</sup>

<sup>66</sup> These inhibitors share a common piperazine-amide scaffold, but diverge through additional modifications to impart isoform selectivity. For example, APT1 inhibitor, ML348 has piperazine amide adjacent to a furanyl group but APT2 inhibitor, ML349 has a thiophene conjugated to thiochromane 1,1-dioxide. These isoform-selective inhibitors are active *in vivo* following intraperitoneal injection, and engage their respective targets across all major tissues.<sup>66</sup>

Furthermore, chemical proteomics analysis of biotin-conjugated ML349 confirmed largely selective inhibition across the proteome at low micromolar concentrations.<sup>67</sup> Other covalent APT1/APT2 dual inhibitors have been reported, including the commercially available triazole urea ML211<sup>68, 69</sup> and the commercially available N-hydroxyhydantoin carbamate ML378.<sup>70, 71</sup> ML211 is more potent, yet the higher reactivity reflects a smaller selectivity window limiting *in vivo* applications. ML378 also inhibits ABHD6 and FAAH in mouse brain homogenates, yet selective inhibitors to ABHD6 and FAAH can be used as anti-target controls. Based on our

studies, we highly recommend ML348 and ML349 as probes for exploring APT function in cells and model organisms (**Figure 1-2**).

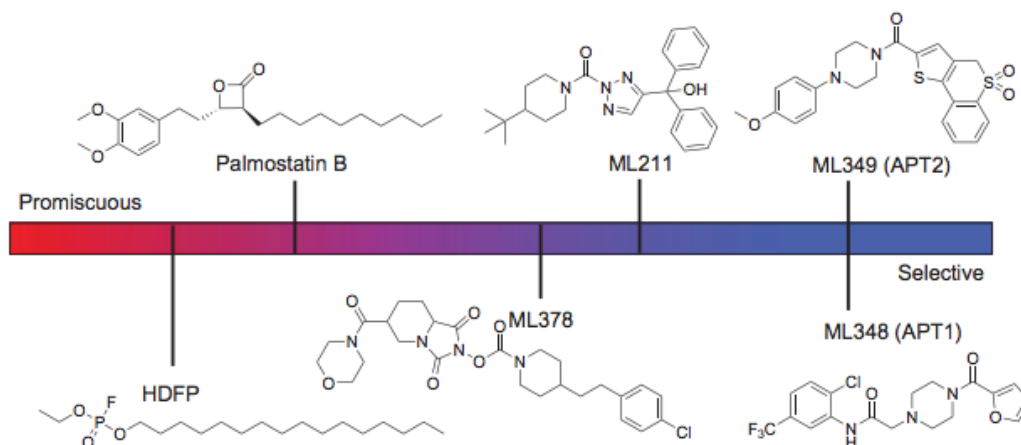


Figure 1-2 APT inhibitor selectivity index.

All listed inhibitors are commercially available, except the promiscuous lipase inhibitor HDFF. HDFF (fluorophosphonate), Palmostatin B (b-lactone), ML378 (N-hydroxyhydantoin carbamate), and ML211 (triazole urea) are covalent inhibitors, although the covalent Palmostatin B adduct is slowly reversible. ML211 inhibits ABHD11<sup>68</sup> and PPT1 (unpublished). ML378 inhibits ABHD6, FAAH, and PPT1 at higher doses.<sup>71</sup>

Beyond their role as protein depalmitoylases, APT enzymes can also hydrolyze a variety of other esters and thioester metabolites.<sup>72</sup> APT1 and APT2 were originally characterized as lysophospholipase enzymes,<sup>39, 45</sup> yet later studies demonstrated enhanced catalytic efficiency towards acyl-thioester-linked proteins.<sup>34</sup> Interestingly, APT2 was identified as the primary prostaglandin glycerol esterase, while APT1 had no significant activity.<sup>46</sup> Both APT1 and APT2 accelerate the deacylation of octanoyl-ghrelin in serum, suggesting these enzymes may also be secreted from cells.<sup>73</sup> Lipopolysaccharide treatment increased in APT1 serum levels, potentially through release from liver. Furthermore, the intracellular APT1 mRNA and protein levels were reduced after LPS stimulation, yet APT2 levels were unaffected. Overall, APTs likely hydrolyze a number of more soluble acyl-esters and thioesters, and may have broader functional roles *in vivo* beyond depalmitoylation.

To add spatial and temporal resolution to depalmitoylation enzymes, a series of mechanism-based octanoyl-thioester fluorogenic probes were developed for live cell imaging.<sup>74</sup> Approximately half of the probe fluorescence in HEK293T cells was blocked by ML348 or Palmostatin B, and APT1 siRNA knockdown reduced probe fluorescence by 25%. Interestingly, EGF stimulation reduced probe fluorescence by about 10% in live cells, suggesting some growth factor regulation of deacylase activity. While intriguing, further evidence is needed to establish if such reductions affect steady-state cellular *S*-palmitoylation levels, particularly of *S*-palmitoylated growth signaling mediators. Given the large number of candidate octanoyl-thioesterases, these probes provide a useful cell-based platform to explore deacylase activity in live cells, and measure contributions across different candidate enzymes.

### **1C. ABHD17 family thioesterases**

Until recently, APT1 was recognized as the primary depalmitoylase in cells, yet mutants in *S. cerevisiae*, *Drosophila*, and *C. elegans* have no reported phenotypes. Given that APT1 was initially described as the primary depalmitoylase regulating N-Ras activity, this was quite puzzling. Cracks in this model began to appear throughout a number of publications, most strikingly from evidence that H-Ras depalmitoylase activity was exclusively in insoluble cell fraction (P100), and not with APT1 in the soluble fraction (S100).<sup>75</sup> Later, APT1/APT2 knockdown was shown to have no effect on R7BP depalmitoylation, while treatment with Palmostatin B or HDFP both blocked activity.<sup>59</sup> This was followed by detailed activity-based profiling of Palmostatin B targets, and the realization that Palmostatin B is broadly reactive across a number of candidate depalmitoylases.<sup>61</sup> Clearly other depalmitoylase activities beyond APT1/APT2 are present in cells, and likely contribute to the depalmitoylation of plasma membrane localized targets, including Ras.

In order to identify these additional depalmitoylases, Palmostatin B-targeted hydrolases were over-expressed and *S*-palmitoylation turnover was assayed using 17-ODYA pulse-chase methods. This led to the identification of ABHD17 enzymes as candidate N-Ras depalmitoylases in COS-7 cells.<sup>61</sup> Over-expression of catalytic dead enzyme or N-terminal truncated mutants did not affect the N-Ras palmitoylation cycle, confirming ABHD17 enzymes are functional depalmitoylases in cells. ABHD17 hydrolases (ABHD17A, ABHD17B, and ABHD17C) are broadly expressed in all vertebrates, and harbor multiple conserved cysteines near their N-termini (**Figure 1-3A**). The N-terminal cysteine rich domain is essential for both *S*-palmitoylation and plasma membrane association.<sup>76</sup> Thus, ABHD17 enzymes are themselves *S*-palmitoylated, which is necessary for plasma membrane association and proximity to other *S*-palmitoylated proteins (**Figure 1-3B**). Importantly, deletion of the N-terminal cysteine rich domain has no effect on ABHD17 reactivity with fluorophosphonate activity-based probes, suggesting the palmitoylation motif is primarily responsible for directing membrane localization and does not influence enzyme activity. ABHD17A over-expression shifted N-Ras localization from the plasma membrane to internal membranes, indicative of more rapid *S*-palmitoylation turnover. Triple ABHD17 (A-C) knockdown stabilized N-Ras 17-ODYA labeling, while APT1/APT2 inhibition with ML348 and ML348 had no effect. Accordingly, ABHD17 enzymes (but not APT1/APT2) contribute to N-Ras depalmitoylation in cells.

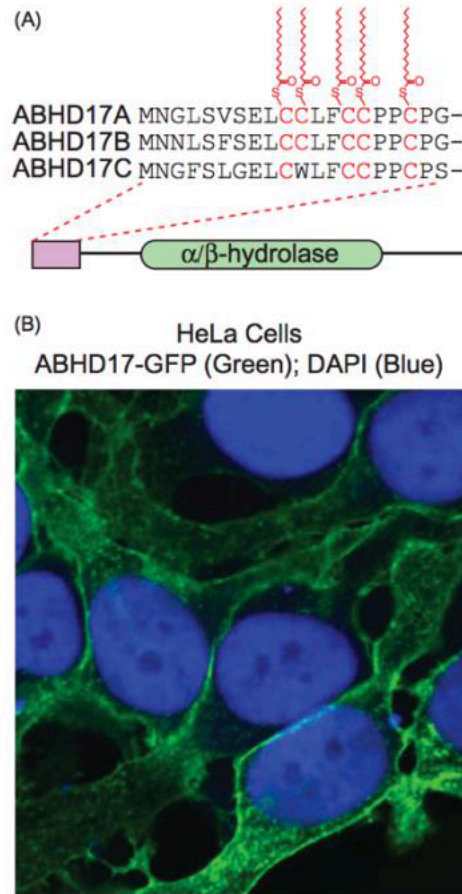


Figure 1-3 ABHD17 enzymes are palmitoylated and localize to the plasma membrane.

(A) ABHD17A-C are S-palmitoylated in a conserved N-terminal cysteine-rich motif separate from alpha-beta hydrolase domain.  
 (B) ABHD17A-GFP localization in HeLa cells demonstrates predominant plasma membrane localization.

The synaptic protein PSD-95 is rapidly de-palmitoylated after depolarization. In order to identify the PSD-95 depalmitoylase, a panel of serine hydrolases were individually co-expressed with PSD-95 in 293T and COS-7 cells.<sup>56, 77</sup> Over-expressed ABHD17 enzymes efficiently depalmitoylated PSD-95 in 293T, COS-7, and primary neuronal cultures, while other Palmostatin B targets ABHD12, ABHD13, APT1, and APT2 had only fractional reductions in PSD-95 S-palmitoylation (**Figure 1-4**). ABHD17 over-expression reduced the synaptic clusters of PSD-95 and AMPA receptors in neurons, while ABHD17A/ABHD17B/ABHD17C knockdown stabilized palmitoylated PSD-95 and prevented the decrease in synaptic PSD-95 clustering.



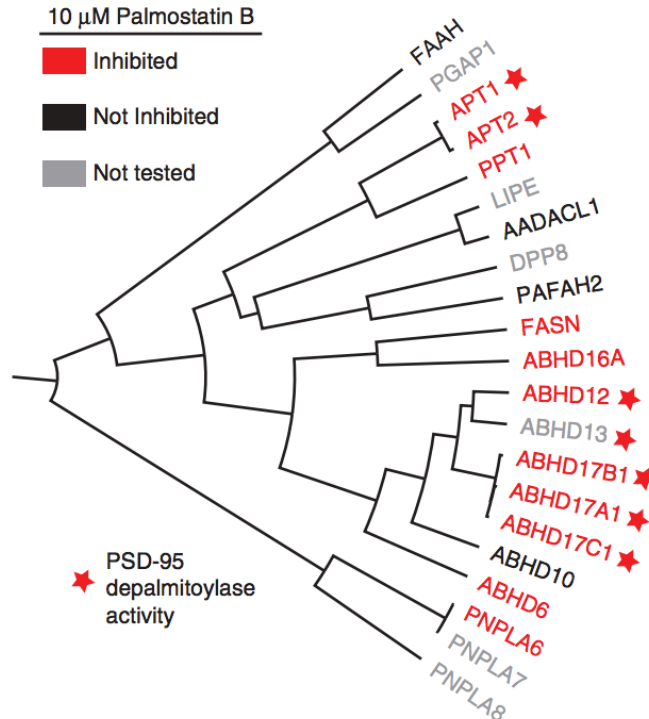


Figure 1-4 Homology, depalmitoylase activity, and Palmostatin B inhibition of HDFP-sensitive serine hydrolases.

HDFP-sensitive serine hydrolases reported from mouse B-cell hybridoma cells<sup>29</sup> are shown based on active-site anchored homology. Palmostatin B targets are highlighted in red.<sup>61, 78</sup> Enzymes that reduced PSD-95 S-palmitoylation after over-expression are labeled with a red star.<sup>56</sup>

In addition, ABHD17 overexpression in primary neurons reduces the S-palmitoylation of microtubule-associated protein 6 (MAP6), causing MAP6 retention in axons and microtubule stability.<sup>77</sup> Recently the international knockout mouse consortium identified ABHD17A as one of the top suppressors of distal cancer metastasis in mice<sup>79</sup> suggesting it may play a role in immune cell activation or surveillance. Finally, the DNA binding transcription factor TEAD is an important interactor of the co-transcriptional activator YAP, involved in the Hippo signaling pathway responsible for cell proliferation.<sup>80</sup> ABHD17A and APT2 depalmitoylate TEAD, thereby mediating its degradation by E3 ubiquitin ligase and response to cell contact during the Hippo pathway.<sup>81</sup>

Despite this growing number of cell-based ABHD17 studies, there is no biochemical evidence demonstrating *in vitro* depalmitoylation, enzyme kinetics, substrate specificity, or other

functional properties of each ABHD17 enzyme. ABHD17 enzymes may hydrolyze other lipid substrates, particularly since their plasma membrane association delivers them in proximity to a number of potential substrates. A reported biochemical high throughput screen identified moderately potent inhibitors of an N-terminal truncated ABHD17B protein, yet these inhibitors failed to inhibit full-length, mammalian cell-expressed protein (National Center for Biotechnology Information. PubChem BioAssay Database; AID=2200). Structural studies are clearly necessary to understand if the N-terminal 100 amino acids before the conserved  $\alpha/\beta$ -hydrolase domain function solely as a platform for *S*-palmitoylation and membrane tethering, or if they impart additional structural features important for substrate engagement. Future efforts are needed to explore the substrate profile, redundancy between isoforms, and physiological roles for each ABHD17 enzymes.

#### **1D. Assays for depalmitoylation**

Protein *S*-palmitoylation was first reported nearly 40 years ago,<sup>82</sup> but even the most basic experiments were hindered by the limitations of [<sup>3</sup>H]-palmitate labeling. The low radioactivity and incorporation efficiency typically required weeks to return results for a single experiment.<sup>83</sup> Furthermore, assaying [<sup>3</sup>H]-palmitate incorporation requires immunoprecipitation of a single protein, limiting the scope of the analysis to only specific hypotheses. Nonetheless, [<sup>3</sup>H]-palmitate metabolic labeling is the most accepted method for studying *S*-palmitoylation, particularly for measuring stability in pulse-chase assays. In this approach, cells are labeled with [<sup>3</sup>H]-palmitate for a fixed amount of time, followed by washes and incubation in media supplemented with excess unlabeled palmitic acid.<sup>83</sup> After immunoprecipitation and SDS-PAGE, the rate of palmitate turnover on a specific protein can be quantified by autoradiography. Through such analysis, the rate of protein *S*-palmitoylation turnover is generally faster than the rate of protein turnover, establishing that multiple

*S*-palmitoylation and depalmitoylation events occur throughout the lifetime of an *S*-palmitoylated protein.<sup>29</sup> Thus, different PATs and APT enzymes may function at different stages of protein trafficking to promote plasma membrane delivery and residency.

The recent development of non-radioactive detection methods has rejuvenated interest in *S*-palmitoylation, providing simple methods that accelerate the identification and quantitation of *S*-palmitoylated proteins.<sup>76, 84</sup> The primary method for biochemical analysis of *S*-palmitoylation uses hydroxylamine to hydrolyze all thioesters across the proteome, followed by capture of the newly liberated thiols.<sup>85-87</sup> These hydroxylamine-switch methods begin with reduction of disulfides with tris(2-carboxyethyl)phosphine (TCEP), followed by treatment with maleimide to alkylate all reduced thiols. Next, neutral hydroxylamine is added to hydrolyze thioesters, which coincidentally hydrolyzes other mechanistic protein-linked thioesters including ubiquitin ligases and lipoamide-dependent dehydrogenases. Any hydroxylamine sensitive thiols are then captured using a pyridyl-disulfide biotin conjugate for streptavidin-resin enrichment (biotin-exchange) or captured directly with pyridyl-disulfide resin (Acyl-resin assisted capture; Acyl-RAC) for further analysis.<sup>88</sup> Pyridyl-disulfide resin capture has at least three advantages. First, it limits capture to hydroxylamine-sensitive thioesters, and does not capture products from other ester or other functional groups. Second, the captured disulfide adduct is easily reversible by TCEP, allowing simple elution for gel-based or proteomic analysis of site-specific *S*-palmitoylation. Finally, since these methods avoid metabolic labeling, primary tissues can be readily analyzed to provide a snapshot of the steady state levels of *S*-palmitoylation. Most importantly, biotin-exchange and acyl-RAC have enabled mass spectrometry-based discovery and analysis across hundreds of *S*-palmitoylated proteins, allowing correlated annotation of the exact sites of *S*-palmitoylation.<sup>88</sup> Such large-scale profiling efforts provide long lists of putative *S*-palmitoylated proteins, which warrant additional biochemical validation. This is somewhat mitigated by the *S*-palmitoylation database SwissPalm,<sup>31</sup> which

provides a searchable platform to qualify candidates across published datasets and compare data from distinct experimental systems, enrichment methods, and laboratories.

The commercially available alkynyl fatty acid derivative 17-octadecynoic acid (17-ODYA) provides a second non-radioactive approach for detecting *S*-palmitoylation.<sup>76, 89, 90</sup> After addition to the cell culture media, cells process the free alkynyl fatty acid to form the coenzyme A (CoA) conjugate, which then serves as a substrate for enzymatic transfer to endogenous sites of *S*-palmitoylation. Cells collected at different time points are then lysed and conjugated by copper-catalyzed azide alkyne cycloaddition (CuAAC) to reporter-linked azides (fluorophores or biotin) for gel-based or mass spectrometry analysis. Saturated incorporation typically occurs in a few hours, although shorter time points can probe more rapid acylation events. For mass spectrometry-based analysis, lysates are conjugated to biotin-azide for streptavidin enrichment, and comparative mass spectrometry is performed using hydroxylamine-treated or palmitic acid-treated samples as controls. Additional precautions are necessary to prevent thioesterase hydrolysis during sample preparation, including addition of generic esterase inhibitors, limited total sample processing time, and careful monitoring of the pH of all reagents.<sup>91</sup> Several proteomic studies report bioorthogonal alkynyl-fatty acid labeling for profiling *S*-palmitoylation, including analyses in immune cells,<sup>9, 29, 92</sup> epithelial cells,<sup>93</sup> and protozoa.<sup>94, 95</sup> Importantly, alkynyl-fatty acid labeling provides a natural complement to hydroxylamine-switch methods, establishing two distinct enrichment methods for more confident analysis.

Alkynyl-fatty acid metabolic labeling has opened new opportunities for non-radioactive profiling of dynamic changes in *S*-palmitoylation. For example, Lck *S*-palmitoylation turnover in Jurkat T-cells was assayed using alkynyl-fatty acid pulse-chase methods and quantified by in-gel fluorescence.<sup>96</sup> Surprisingly, Lck depalmitoylation was accelerated after treatment with the phosphatase inhibitor pervanadate, yet stabilized by incubation with the non-selective hydrolase

inhibitor methyl arachidonyl fluorophosphonate (MAFP). Thus, activated T-cells increase Lck *S*-palmitoylation cycling, which is dependent on one or more MAFP-sensitive thioesterase enzymes. Using similar pulse-chase methods, proteome-wide *S*-palmitoylation dynamics were profiled by quantitative proteomics in a mouse B-cell line.<sup>29</sup> Using stable isotope labeling with amino acids in cell culture (SILAC) methods, matched “light” and “heavy” replicates were labeled with 17-ODYA over a 2 hour pulse. One of the samples was then further incubated with 10-fold excess palmitic acid in the presence of the translation inhibitor cycloheximide. After combining the two samples together, the pooled lysates were conjugated to biotin-azide for enrichment and quantitative proteomic analysis. While most *S*-palmitoylated proteins cycled palmitate at a uniform rate in the pulse-chase assay, a subset of proteins demonstrated accelerated turnover, including G proteins, Ras-family GTPases, and a number of cell polarity proteins. Furthermore, treatment with the non-selective lipase inhibitor hexadecylfluorophosphonate (HDFP) stabilized the same subset of dynamically *S*-palmitoylated proteins, confirming direct enzymatic contribution to *S*-palmitoylation dynamics on key signaling and polarity scaffolding proteins. Based on these results, the majority of *S*-palmitoylated proteins undergo basal hydrolysis, while a small subset of *S*-palmitoylated proteins are rapidly depalmitoylated by HDFP-sensitive lipases.

Alkynyl fatty acid labeling has several inherent limitations, primarily the direct incorporation of the labeled fatty acid across a variety of phospholipids. Longer incubation times lead to more extensive alkynyl-fatty acid incorporation into phospholipid pools,<sup>97</sup> reducing the effectiveness of any later chase with free palmitate. This pulse-chase suppression potentially excludes a number of proteins from dynamic analyses. Furthermore, addition of palmitate has major effects on cellular metabolism. For instance, addition of 500  $\mu$ M palmitate to human primary melanocytes expressing the variants of the melanocortin 1 receptor (MC1R) increased cAMP levels by almost 3-fold, potentially through direct enhancement of GPCR *S*-palmitoylation.<sup>62</sup> Exogenous fatty acids also

increase cellular acyl-CoA levels,<sup>5</sup> which may enhance *S*-palmitoylation levels by driving zDHHC activity or by non-enzymatic thioester exchange with accessible cysteine residues. For example, 17-ODYA in the presence of 2- bromopalmitate (a non-selective palmitoylation inhibitor) only partially reduces incorporation of the 17-ODYA.<sup>98</sup> Therefore, non-enzymatic palmitoylation levels may be enhanced by 17-ODYA incubation, elevating acyl-CoA pools to driving non-physiological thioester exchange to enhance levels of *S*-acylation.

Another major caveat is metabolic labeling can only occur at accessible, reduced cysteines. Thus, stable *S*-palmitoylated cysteines are essentially invisible, since they do not turnover to present a free thiol substrate for zDHHC PAT enzymes. Accordingly, the more stable *S*-palmitoylation site, the more challenging it is to assay by metabolic labeling. In addition, high palmitate levels can induce oxidative stress,<sup>99</sup> which may trap depalmitoylated thiols as oxidized disulfides or glutathione adducts. Different zDHHC enzymes have also been shown to prefer different fatty acyl-CoAs,<sup>5</sup> suggesting an additional level of diversity that could select against a single alkynyl fatty acid species to bias probe incorporation. Varying the acyl length of the alkynyl reporter revealed different acyl preferences, particularly since terminal azide conjugates surprisingly have little influence on zDHHC acyl specificity.<sup>5</sup> Moreover, any differential turnover rates between distinct sites in the same protein are effectively averaged in shotgun proteomics experiments, since there are no robust mass spectrometry methods to broadly profile fatty *S*-acylated peptides. [<sup>3</sup>H]-palmitate can be elongated or shortened by  $\beta$ -oxidation, further diversifying the labeled acyl species. This is particularly problematic when 17-ODYA is shortened to 15-pentadecynoic acid, which is enzymatically incorporated into N-myristoylation sites.<sup>76, 84</sup> Despite these pitfalls, metabolic labeling remains the most common approach to profile *S*-palmitoylation dynamics, on select proteins or across the proteome.

These enrichment strategies for *S*-acylated proteins can be coupled with mass spectrometry-based approaches for large scale analysis of whole proteomes. Mass spectrometry allows for the separation and detection of ions by mass to charge ( $m/z$ ) ratio, which can be used to measure the amount of a molecule of interest. This works well for samples of low complexity such as purified proteins, which can be sequenced by mass spectrometry.<sup>100, 101</sup> However, when analyzing cell extracts containing thousands of proteins, an additional separation method is necessary to prevent overlapping signals which complicate the quantification and identification of individual proteins. Thus, liquid chromatography is a compatible technique that is often added in-line prior to mass spectrometry.<sup>102</sup> ‘Bottom-up’ proteomics is commonly used to identify and measure proteins from a complex cell extract.<sup>103</sup> Proteins can be digested into smaller peptides using proteolytic enzymes such as trypsin and first separated by liquid chromatography based on their size and hydrophobicity. Then the peptides are ionized by electrospray ionization and introduced into the mass spectrometry so that their mass to charge ratios can be measured. The peptides can be further fragmented to generate ions used to map the amino acid sequence of the original peptide.<sup>104</sup> The protein sequences from specific organisms can be obtained from public databases such as Uniprot.<sup>105</sup> These sequences can be digested in silico and the resulting peptides can be fragmented to generate theoretical fragment spectra, which can be compared to the experimental spectra. Thus, the identity of the proteins can be inferred based on the list of identified peptides.<sup>106, 107</sup>

## **1E. Overview of thesis**

Cycles of *S*-palmitoylation and depalmitoylation provide a mechanism for membrane sampling and trafficking of peripheral membrane proteins to the plasma membrane.<sup>21</sup> Such directional palmitoylation cycles are demonstrated for G proteins, Ras, Scrib, and other central

regulators of cell growth and organization. G protein internalization occurs even in the presence of generic depalmitoylation inhibitors, demonstrating that while depalmitoylation may be necessary for plasma membrane trafficking, agonist-dependent internalization occurs independent of depalmitoylation.<sup>24</sup> Based on these findings, many peripheral membrane proteins require cycles of *S*-palmitoylation and depalmitoylation for plasma membrane delivery, but there are no definitive examples of post-translational regulation of depalmitoylation activity. Rather, depalmitoylation appears to depend more on sub-cellular localization and regulated expression. ABHD17 enzymes localize to the plasma membrane, where they have direct access to neuronal scaffolding proteins and growth regulators. APT enzymes are soluble, and cytoplasmic or in the mitochondria, and play active roles in maintaining the directional palmitoylation cycle important for peripheral membrane protein trafficking.

With the emergence of novel depalmitoylating enzymes, it is important to annotate the substrate profile and functional regulation by each enzyme. Chapter 2 outlines the biochemical characterization of ABHD17 in an effort to understand its function. We found that ABHD17 isoforms are palmitoylated by a similar subset of DHHC enzymes, suggesting that they do not undergo different processing pathways as they get trafficked to the plasma membrane. After comparing the rate of ABHD17 enzyme, purified from *E.coli* and HEK293T cells, we also demonstrated that *S*-palmitoylation does not impact the enzyme activity. While Palmostatin B and HDFP are useful generic inhibitors of depalmitoylases, we tested and validated a compound that inhibits the *in vitro* activity of recombinant ABHD17 enzymes. Future efforts to understand regulation of depalmitoylation will continue to leverage emerging chemical and genetic technologies. In chapter 3, we applied an acyl-RAC proteomics approach to profile sites of *S*-palmitoylation. Using our workflow, we obtained results similar to previously-published studies in addition to finding new putative palmitoylation sites on proteins. To annotate the substrates of



ABHD17A, we overexpressed the active and inactive forms of the enzyme in mouse embryonic fibroblasts that express NRAS. However, our proteomics and gel-based results showed that there were no significant changes in *S*-palmitoylation between the two treatments, hinting that ABHD17 may influence palmitate turnover through a different mechanism. Nevertheless, we have demonstrated that our method allows for the large-scale identification of sites of *S*-palmitoylation and can be a valuable tool to expedite the study of other enzymes involved in the *S*-acylation cycle, such as DHHC palmitoyltransferases.

## Chapter 2 Biochemical Studies of ABHD17<sup>#</sup>

### 2A. Abstract

*S*-palmitoylation is a dynamic post-translational modification that facilitates the trafficking and function of many membrane proteins. This process is regulated by DHHC enzymes, which usually attach a 16-carbon fatty acyl group to specific cysteines. The reverse reaction is catalyzed by depalmitoylases, including APT1, APT2 and ABHD17 enzymes. ABHD17 has three main isoforms (A, B and C) that are all *S*-palmitoylated. Cell-based studies have shown that ABHD17 depalmitoylates NRAS and PSD-95, which are involved during cancer and synaptic development, respectively. This motivated us to determine whether these enzymes are functionally redundant, characterize the *in vitro* activity, and develop inhibitors to target them. Our results show that ABHD17 isoforms are palmitoylated by a similar subset of DHHC enzymes, suggesting a uniform processing pathway for all isoforms. ABHD17 did not accept palmitoylated substrates in our *in vitro* assay, implying that its substrate preference may not be palmitate. Finally, we found some compounds that inhibited the *in vitro* activity of recombinant ABHD17A and 17B, but further probe development is needed to improve compound potency and isoform specificity. This study has contributed to the understanding of the function of ABHD17 enzymes and the identification of inhibitors that can be further developed as chemical tools.

---

<sup>#</sup> This chapter includes contribution from Timothy Precord (cloning, expression and purification of ABHD17 enzymes in *E.coli*). APT1 and APT2 proteins were purified by Sang Joon Won and Melanie S. Cheung See Kit performed the remaining experiments.

## 2B. Background

Post-translational modifications (PTMs) play a crucial role in protein trafficking for many location-dependent cellular functions.<sup>108</sup> Some PTMs are mediated via stable linkages; for example, N-palmitoylation and myristoylation,<sup>109</sup> while dynamic turnover happens to other PTMs, as is the case in *S*-palmitoylation, where a palmitate group gets attached to a cysteine via a reversible thioester linkage. *S*-acylation and *S*-palmitoylation are often used interchangeably since palmitate is the predominant long-chain fatty acid. This is regulated by two families of enzymes, namely the DHHC enzymes which acylate their substrates and the depalmitoylase enzymes which remove the acyl groups. Through PTM regulation, protein complexes can locate at the plasma membrane to regulate many cellular processes, including the control of cell polarity to establish cell-cell junctions for proper growth.<sup>110</sup>

The ABHD17 enzymes are part of a larger superfamily of serine hydrolases<sup>51</sup> and have been shown to be palmitoylated at the N-terminal region, which promotes their membrane association.<sup>76</sup> Interestingly, there are seven ABHD17 family members (A1-A3, A5, A6, B1 and C1) expressed in humans compared to three mouse orthologs (A, B, and C) and all the isoforms

share a ~ 73 % protein sequence identity and conserved cysteine-rich N terminal region (**Figure 2-1**). It is unknown whether the different isoforms have distinct functions or are redundant.

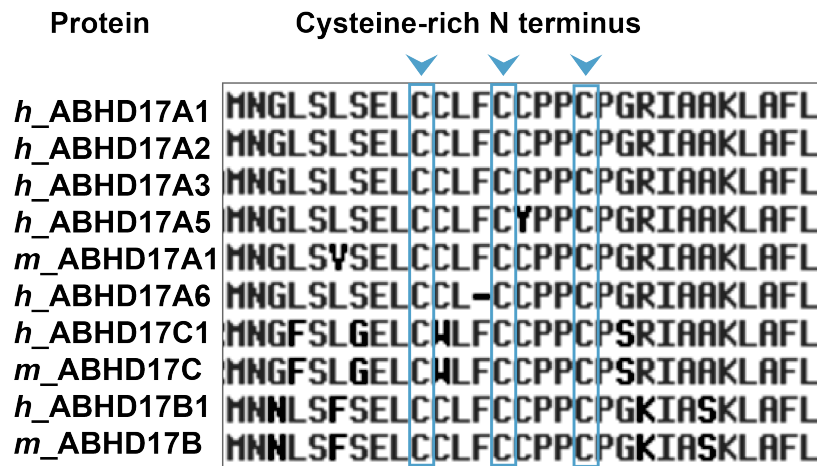


Figure 2-1 Sequence alignment of the N-terminus region of ABHD17 human and mouse isoforms.

ABHD17 exists as different human and mouse isoforms and have multiple conserved cysteines.

When overexpressed, ABHD17A is reported to depalmitoylate and mislocalize NRAS.<sup>61</sup> ABHD17 also depalmitoylates PSD-95, a scaffold protein involved in synapse development and function<sup>56</sup> as well as the microtubule-associated protein 6 (MAP6), causing MAP6 retention in axons and microtubule stability.<sup>77</sup> In addition, a recent genome-wide CRISPR screen in AML cell lines identified ABHD17B as an essential gene in NRAS dependent THP-1 cells and NRas-dependent Ba/F3 cells<sup>111</sup> and the International Mouse Phenotyping Consortium (IMPC) identified ABHD17A as one of the top suppressors of distal cancer metastasis in mice,<sup>79</sup> suggesting it may play a role in immune cell activation or surveillance. Finally, the DNA binding transcription factor TEAD is an important interactor of the co-transcriptional activator YAP, involved in the Hippo signaling pathway which is responsible for cell proliferation.<sup>80</sup> ABHD17A and APT2 depalmitoylate TEAD, thereby mediating its degradation by E3 ubiquitin ligase and response to cell contact during the Hippo pathway.<sup>81</sup> These studies all use cell-based methods to

demonstrate depalmitoylation of ABHD17 substrates; however there is no current biochemical data for their enzyme kinetics, substrate specificity, or other functional properties.

Considering that PTMs play a critical role in dictating RAS subcellular localization,<sup>112</sup> palmitoylation has been shown to mediate RAS function as an effector of growth signaling pathways,<sup>113, 114</sup> which become misregulated and trigger cancerous phenotypes.<sup>115</sup> With genetic data also suggesting a role for ABHD17 in cancer, it would be valuable to develop inhibitors for these enzymes. The non-selective lipase inhibitor hexadecylfluorophosphonate (HDFP) targets a small subset of serine hydrolases, including APTs and ABHD17s.<sup>116</sup> A high-throughput small molecule screening against ABHD17B has been carried out previously through the NIH Molecular Libraries program, resulting in the identification of putative inhibitors active against a truncated ABHD17 recombinant protein missing the first 20 amino acids<sup>117</sup> and full-length ABHD17B in a background of mouse brain membrane proteome.<sup>118</sup> This generated a promising series of oxazinones that likely inhibit through a covalent mechanism; but these compounds failed to inhibit the full-length ABHD17B protein. Since then, there has not been a drive to further validate and develop the other inhibitor chemotypes that were identified in those screens. We decided to follow up on some of the other lead scaffolds and take similar approaches, to ones previously used for APT1 and APT2, to assess the activity of the compounds. Fluorophosphonate-rhodamine (FP-TAMRA) is a fluorescent probe commonly used in activity-based protein profiling (ABPP) strategies<sup>51</sup> and can be used measure the activity of purified ABHD17s upon inhibitor treatment. We also previously used the fluorogenic substrate resorufin acetate (ResOAc) in steady-state kinetic assays to test inhibitors of APT enzymes and point mutations that would be detrimental to enzyme activity.<sup>119</sup>

Here we show that the multiple isoforms of ABHD17 are *S*-palmitoylated by a similar subset of DHHC enzymes. ABHD17 did not show depalmitoylase activity in our *in vitro* assay, implying that its substrate preference may not be palmitate. We validated some compounds that inhibited the *in vitro* activity of full length recombinant ABHD17A and 17B but further probe development is needed to improve compound potency and isoform specificity.

## 2C. Results and discussion

2CI. *S*-palmitoylation across ABHD17 isoforms is regulated by a similar subset of DHHC enzymes

Since ABHD17 is expressed as multiple mouse isoforms, we compared them (17A, B, and C) to determine how if they had different cellular roles. Steady-state *S*-palmitoylation can be assayed using different methods, including acyl-resin assisted capture (Acyl-RAC),<sup>88</sup> acyl biotin exchange (ABE)<sup>120</sup>, and acyl-PEGyl exchange gel shift (APEGs).<sup>121</sup> These rely on the biochemical exchange of the acyl groups on cysteines with different probes for enrichment strategies (Acyl-RAC and ABE) or defined mass tags (APEGs). The APEGs assay has been used to quantify the *in vitro* palmitoylation stoichiometry of PSD-95, HRAS,<sup>56</sup> and DHHC6.<sup>52</sup> Using a similar strategy, we demonstrated that ABHD17A and 17C expressed in mammalian cells have three sites of palmitoylation. ABHD17B did not display any mass shift, despite published data showing that it is also *S*-palmitoylated at the N terminus (**Figure 2-2, Figure 2-3**).<sup>76</sup>

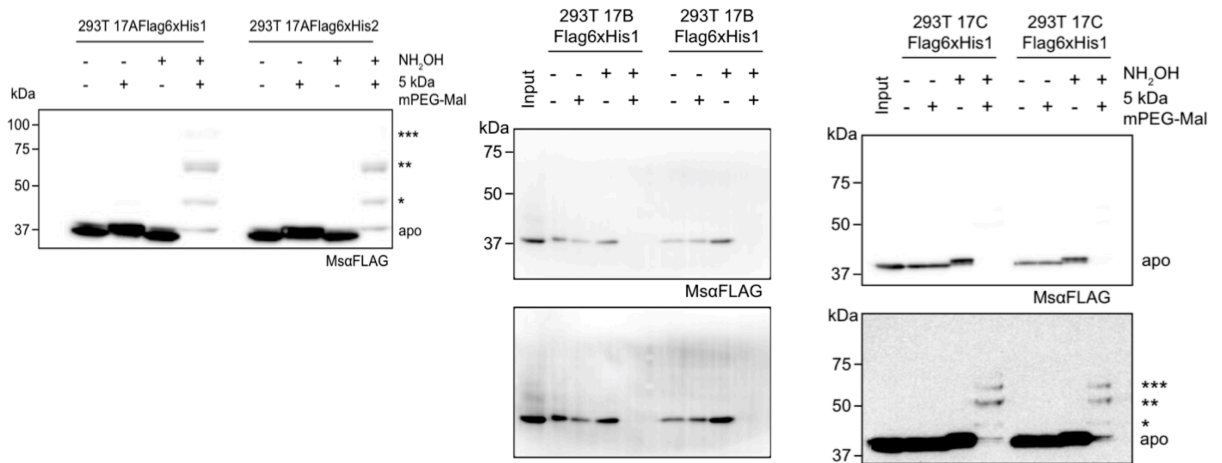


Figure 2-2 APEGS assay shows multiple *S*-palmitoylation sites for ABHD17 expressed in HEK-293T.

ABHD17A and C both have three sites of *S*-palmitoylation. There were no observed mass shift for ABHD17B despite published data showing that it is *S*-palmitoylated at its N terminus similar to 17A and 17C. Bottom row of gel images were edited at a higher contrast.

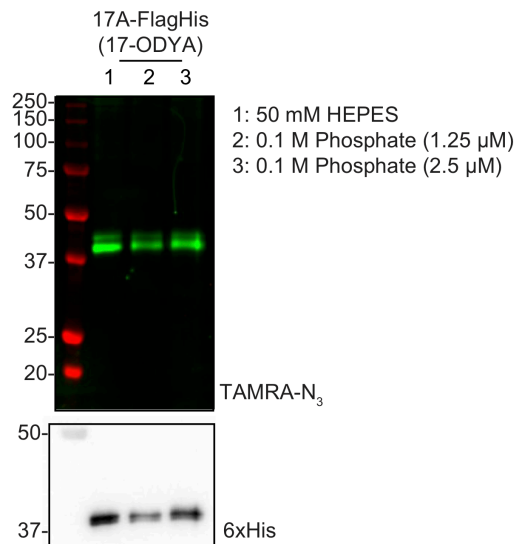


Figure 2-3 ABHD17A is still *S*-palmitoylated after protein purification.

The alkyne fatty acid is incorporated by ABHD17A and reacts to TAMRA-azide (= TAMRA-N<sub>3</sub>) after protein purification, indicating that the protein is still modified.

To identify the DHHC enzymes that modify ABHD17, we co-expressed each ABHD17 isoform with a panel of the mouse DHHCs in HEK-293T and used a metabolic labeling approach with the alkyne fatty acid mimic 17-ODYA, which gets incorporated at sites of *S*-palmitoylation.

The amount of *S*-palmitoylated protein can then be measured by in-gel fluorescence using a clickable fluorophore such as TAMRA-azide.

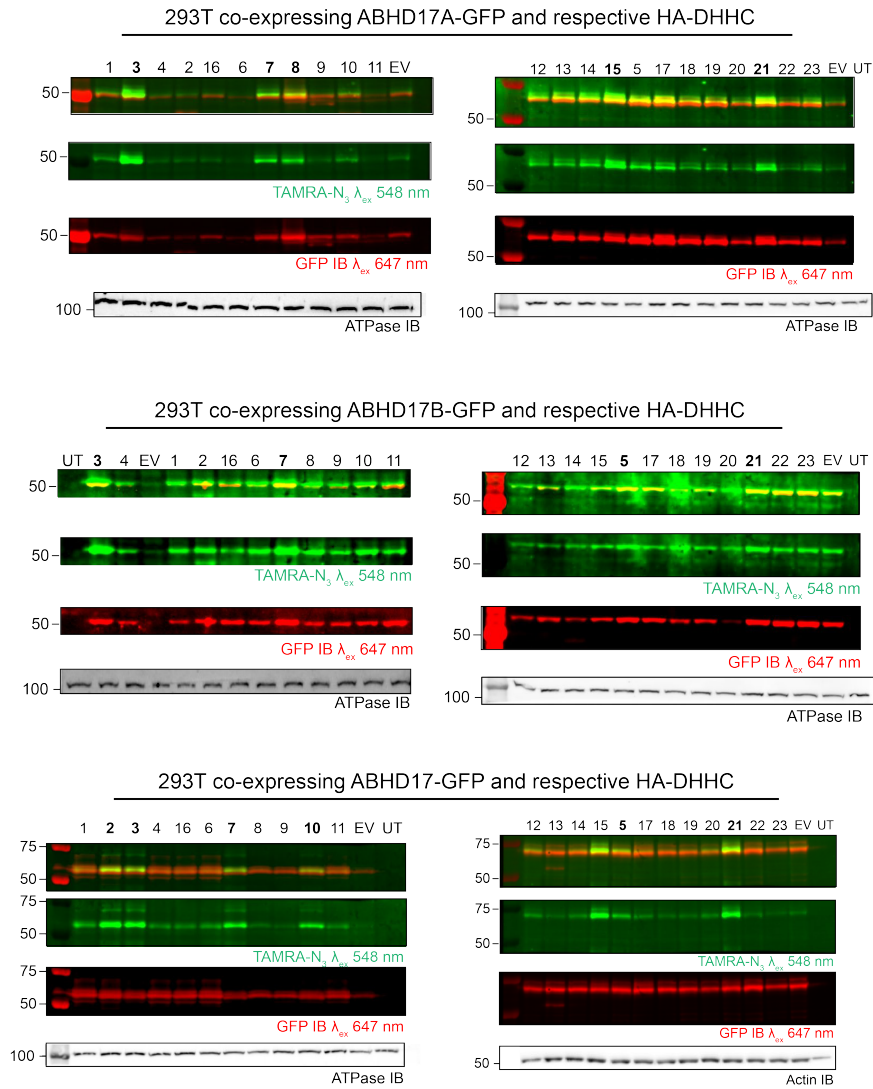


Figure 2-4 Co-expression of ABHD17 with the full panel of 23 DHHC enzymes.

ABHD17 isoforms were co-expressed with DHHC enzymes to measure *S*-palmitoylation via 17-ODYA labeling (TAMRA-N<sub>3</sub> = TAMRA-azide) and normalized to protein abundance (AF647 signal). ATPase and Actin blots are included to confirm uniform sample loading. Gel images and bar graphs to visualize palmitoylation ratio of the ABHD17 isoform with respect to distinct DHHCs. UT = untreated/ non-transfected; EV = empty vector.





confirm this for ABHD17 such as: (1) labeling ABHD17 WT and palmitoylation-deficient cysteine mutants with [<sup>35</sup>S]cysteine/methionine pulse-chase studies to monitor protein turnover or (2) inhibiting the lysosomal degradation pathway to see if that rescues expression of palmitoylation-deficient ABHD17. After confirming the multiple sites of palmitoylation for ABHD17 and finding the DHHCs that modify them, we further looked into their function by performing different *in vitro* activity assays.

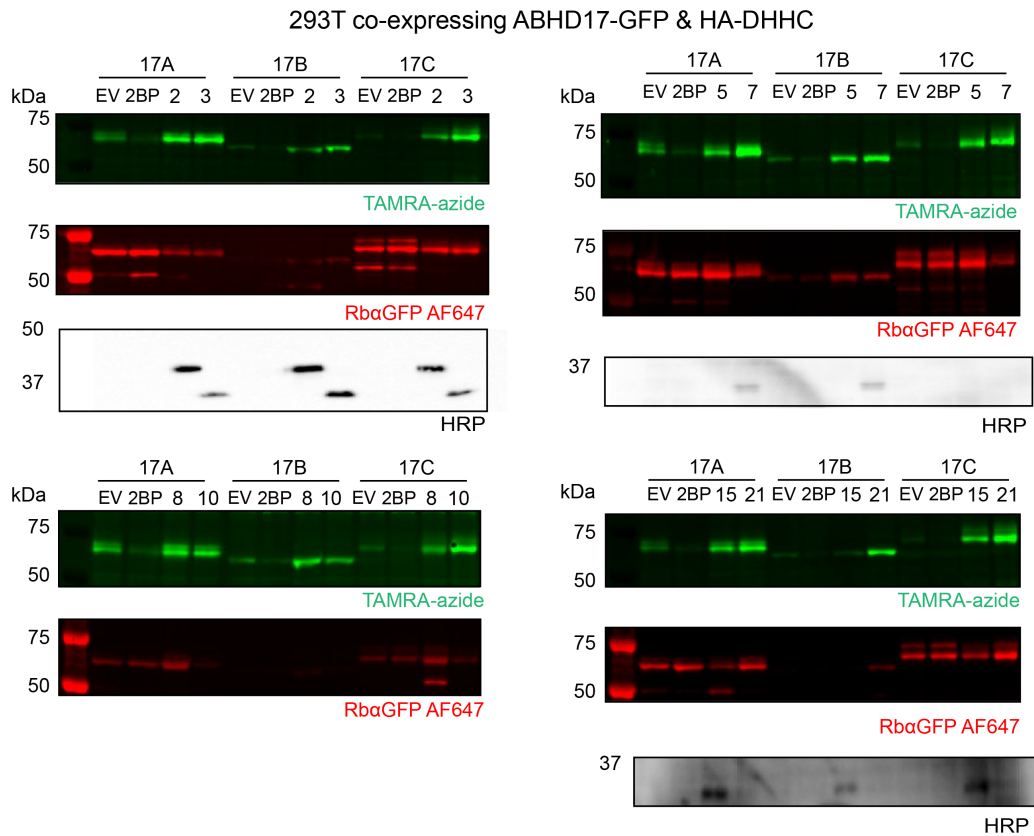


Figure 2-6 Co-expression of select DHHC and ABHD17 isoforms.

ABHD17 isoforms were co-expressed with DHHC enzymes to measure S-palmitoylation via 17-ODYA labeling (TAMRA-azide) and normalized to protein abundance (AF647 signal). HRP blots are included to confirm expression of DHHCs. Gel images to visualize palmitoylation of ABHD17 isoform with respect to overexpression of distinct DHHCs. 2BP = 2-bromopalmitate (non-specific inhibitor of DHHC); EV = empty vector; HRP = Horseradish peroxidase.

## 2CII. Protein expression and purification in different systems for use in functional activity assays

Recombinant ABHD17A and 17B (both wildtype and catalytically inactive Ser to Ala mutant) were produced from *E.coli* to test the enzymatic activity. An initial attempt to express and purify the protein with an N-terminus 6xHis tag resulted in low yield (**Figure 2-7A**). We made ABHD17 constructs with three fusion tags (MBP, GB1 and Mocr) that could help improve expression and solubility. Maltose-binding protein (MBP) has been shown to improve protein solubility and provides an additional enrichment option due to its affinity for amylose resin.<sup>125</sup> The immunoglobulin-binding domain of streptococcal protein G (GB1) has also been used as a fusion strategy owing to its small size, stability and ability for high expression in bacteria.<sup>126</sup> Finally, the bacteriophage T7 0.3 protein (named Ocr for its ability to ‘overcome classical restrictions’) can be expressed as its monomeric form, hence the name Mocr, and can be tolerated at high levels by the cell. It has been shown to improve protein solubility and yield, comparable to MBP.<sup>127</sup> MBP and GB1 both showed improved expression relative to the 6xHis tag alone (**Figure 2-7B-C**) while Mocr fusion protein did not express (not shown).

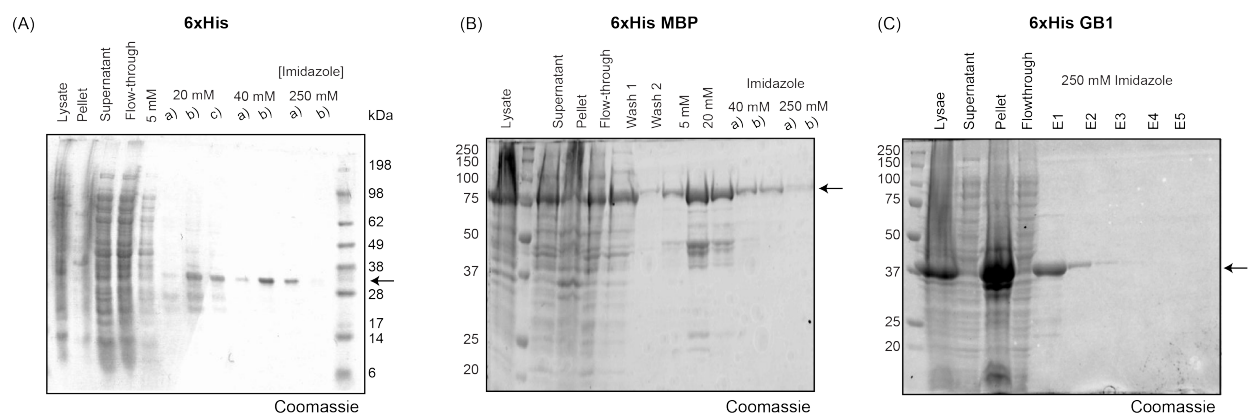


Figure 2-7 Coomassie-stained SDS-PAGE gels showing the affinity purification of ABHD17B WT fused to different N-terminal tags.

(A) With a 6xHis tag, ABHD17B WT is expressed at moderate level. (B) Adding an MBP domain (~42.5 kDa) improves the protein yield. (C) The GB1 domain (~6.2 kDa) also increases the protein expression but some remains in the insoluble fraction. E1 to E5 = Elution 1 to 5

With many non-specific contaminants eluting with the MBP fusion protein, we decided to take advantage of the MBP tag and add a second step of affinity purification, to then elute ABHD17B WT after a TEV digest. However, we were not able to fully separate the fusion protein from ABHD17B WT alone (data not shown). Since 6xHis-GB1-ABHD17B WT provided reasonable yield of protein that was active (**Figure 2-8**), it was used for our functional assays.

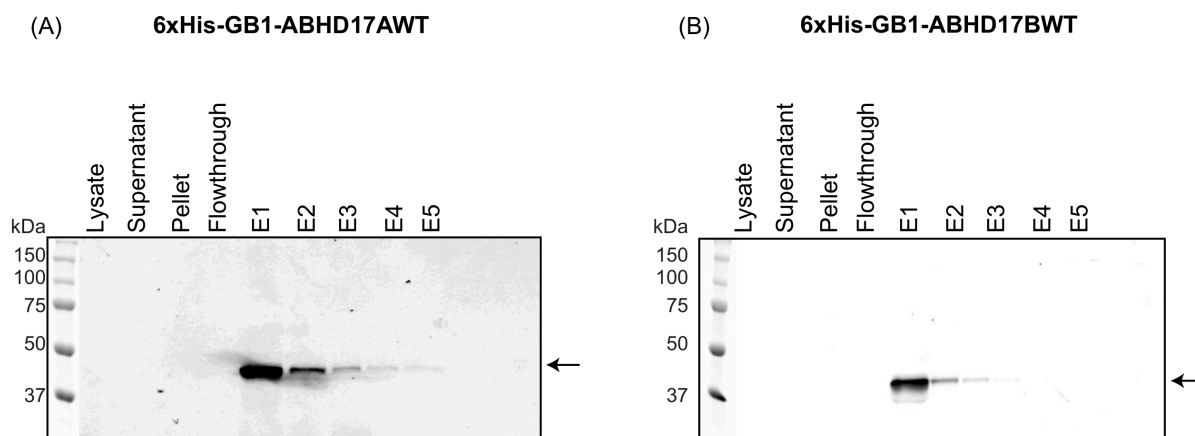


Figure 2-8 Purified ABHD17A and 17B have an active Ser labeled using FP-TAMRA.

Detection of active (A) ABHD17A WT (~ 42.8 kDa) and (B) 17B WT (~ 41.0 kDa) by FP-TAMRA in-gel fluorescence imaging at excitation wavelength = 532 nm and emission wavelength = 560 nm.

ABHD17 is *S*-palmitoylated at the N-terminus<sup>76</sup> (**Figure 2-2**, **Figure 2-3**) and we also purified recombinant enzyme from HEK-293T to determine whether the enzyme needed to be post-translationally modified in order to be recognize its substrate. In this case, we expressed an ABHD17 protein with a FLAG6xHis tag at the C-terminus. The FLAG purification (**Figure 2-9**) is cleaner compared to the 6xHis tag (Co resin) since FP-TAMRA labels only ABHD17 in eluted samples for the FLAG purification compared to the Co resin purification (**Figure 2-10**).

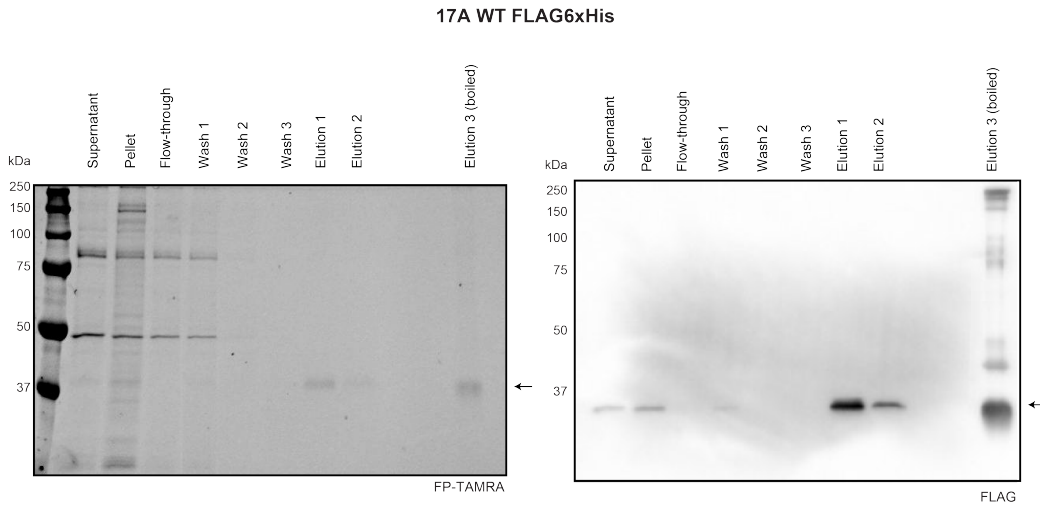


Figure 2-9 FLAG purification of ABHD17A expressed in HEK-293T

Purified ABHD17A is active and labeled by FP-TAMRA. Elution 3 shows that FLAG peptide does not elute all of the protein bound to the FLAG beads.

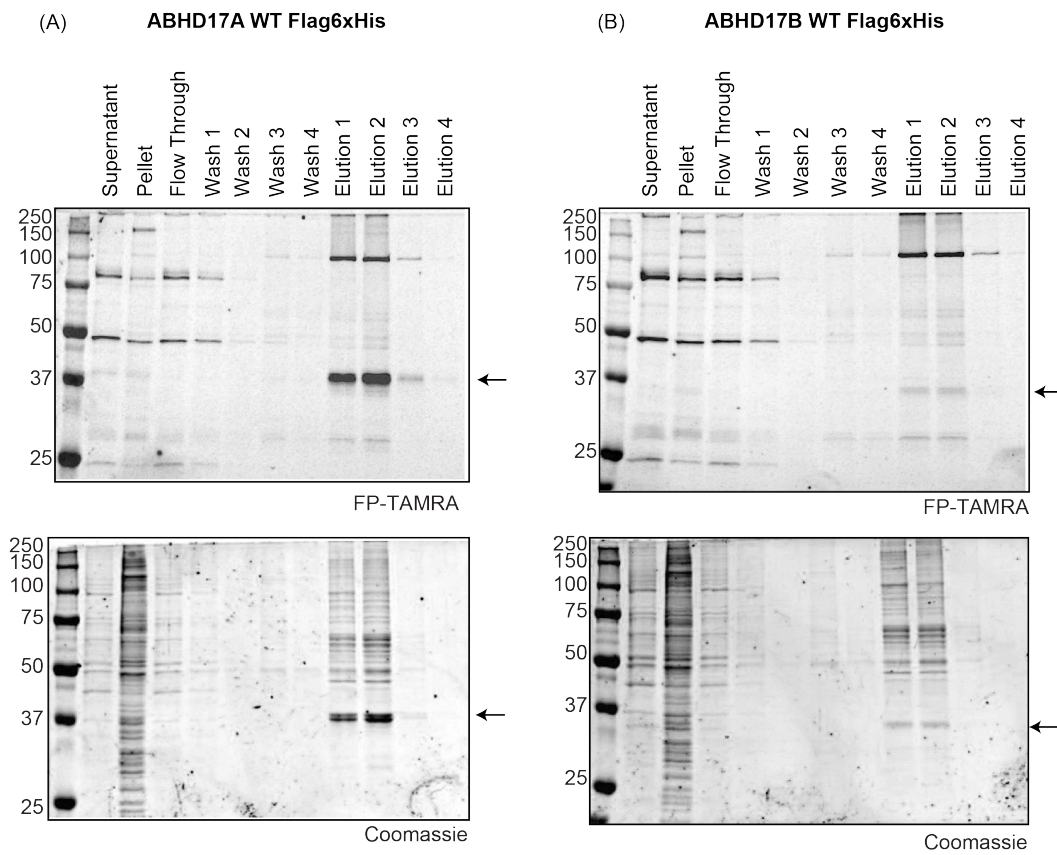


Figure 2-10 Cobalt resin purification of ABHD17A and 17B expressed in mammalian cells.

(A) Purification of ABHD17A, where top gel shows that the protein is active and is labeled with FP-TAMRA and bottom gel is the Coomassie stained gel. (B) ABHD17B is also active and is labeled by FP-TAMRA; however it expresses less than 17A.

We then compared the rate of FP-TAMRA labeling between ABHD17 purified from *E.coli* and from HEK-293T where it is *S*-palmitoylated (**Figure 2-11**). Similar rates of labeling were observed, confirming past results<sup>76</sup> where deletion of the N-terminal cysteine-rich domain has no effect on ABHD17 reactivity with fluorophosphonate activity-based probes. This suggests the palmitoylation motif is primarily responsible for trafficking to the plasma membrane and does not influence enzyme activity.

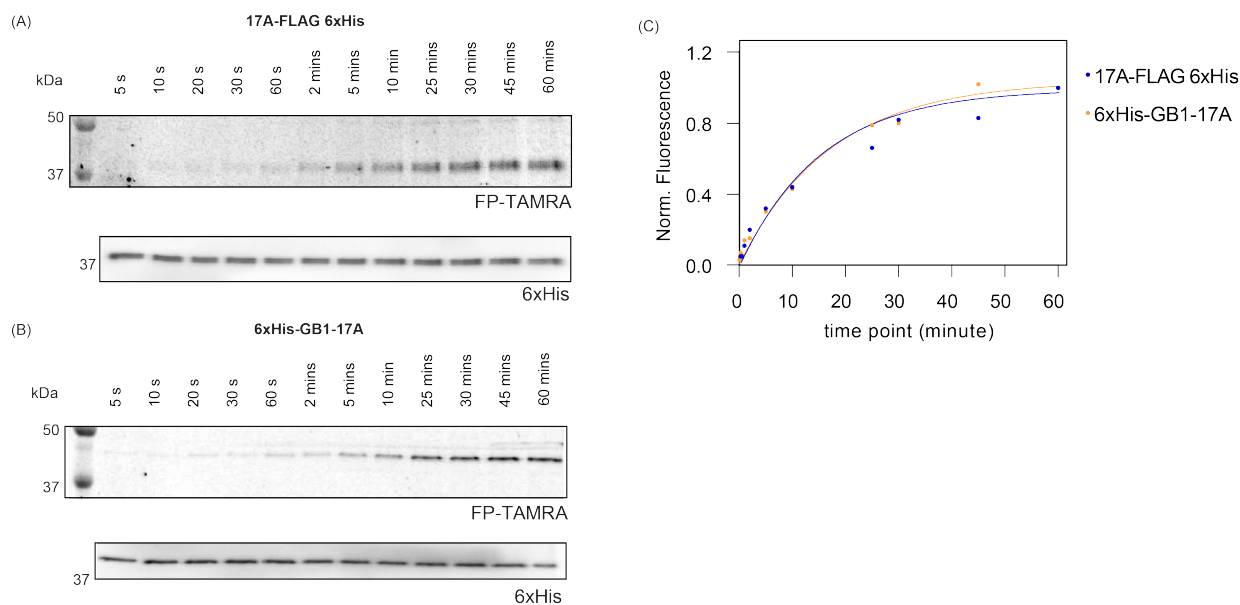


Figure 2-11 Comparison of FP-TAMRA labeling between the unmodified and *S*-palmitoylated ABHD17

FP-TAMRA labeling between the unmodified ABHD17 expressed in *E.coli* (A) and *S*-palmitoylated enzyme expressed in HEK-293T (B) show no significant differences, as displayed in this plot (C).

We also developed an *in vitro* assay to assess whether *S*-palmitoylated proteins can be depalmitoylated by ABHD17. Purifying NRAS labeled with 17-ODYA from HEK-293T (**Figure 2-12**) provided a palmitoylated substrate to test in our assay. However, our assay did not result in any reduction in 17-ODYA labeling of NRAS after incubation with depalmitoylases such as

APT1, APT2 and ABHD17A while treatment with hydroxylamine, which chemically cleaves thioester bonds, showed a decrease in signal (**Figure 2-13**).

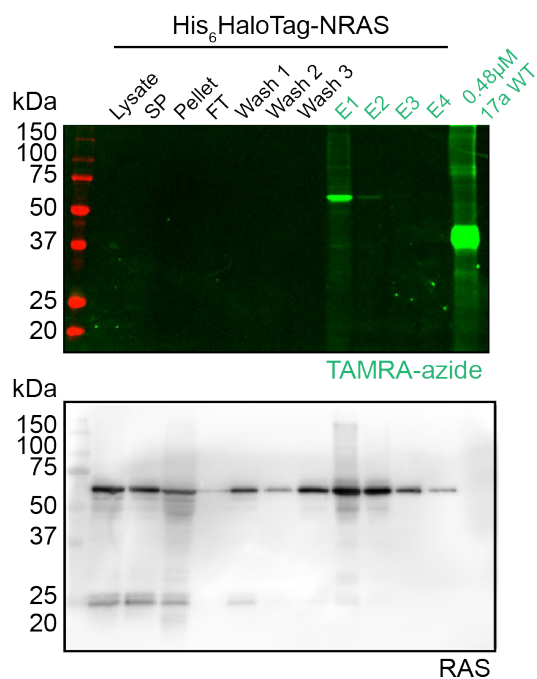


Figure 2-12 Purification of 6xHis-Halotag NRAS protein.

NRAS expressed with an N-terminus 6xHis-Halotag was purified using Halotag beads and reacted with TAMRA-azide to show that purified enzyme is still acylated (labeled with 17-ODYA).

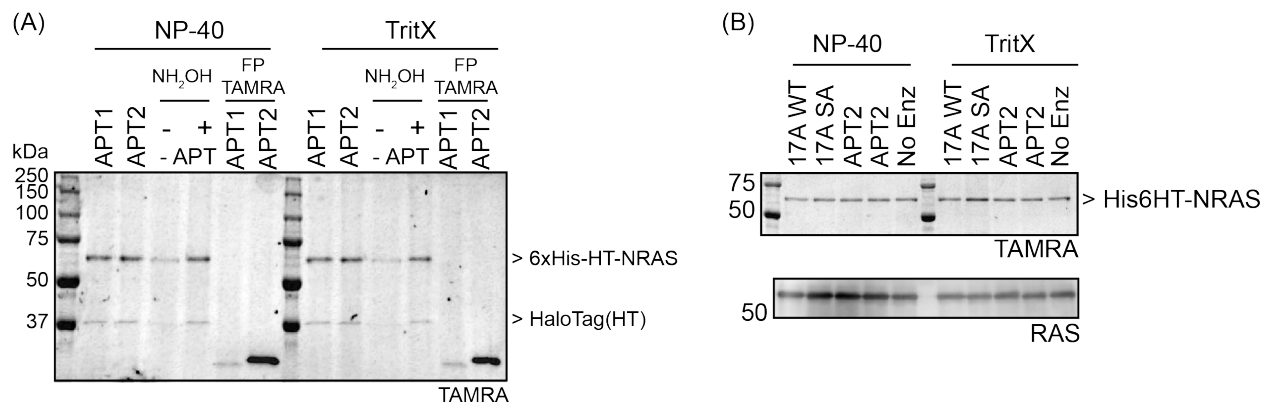


Figure 2-13 In vitro experiments with NRAS expressed in HEK-293T and labeled with 17-ODYA.

Development of in vitro assay to assess NRAS depalmitoylation by ABHD17A, APT1 and APT2, measured using signal from 17-ODYA labeled protein. Addition of hydroxylamine ( $\text{NH}_2\text{OH}$ ) causes cleavage of the thioester bond, unlike the incubation with different deacylases.

We also tried a different approach by using Acyl-RAC where the acyl group is cleaved using hydroxylamine and the newly-freed thiol is alkylated with a fluorophore. Again ABHD17 did not show any *in vitro* depalmitoylase activity (**Figure 2-14**).

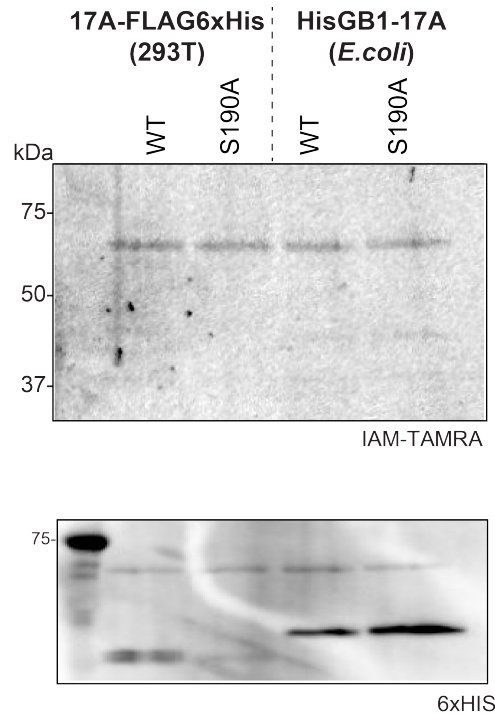


Figure 2-14 Alternate *in vitro* depalmitoylation assay strategy using a Cys alkylator conjugated to a fluorophore.

Iodoacetamide-TAMRA (IAM-TAMRA) reacts with NRAS that is palmitoylated. No change in signal is observed.

It may be that our assays are not sensitive enough to detect the changes in *S*-palmitoylation and that other methods, such as mass spectrometry, must be used to quantify the amount of protein still modified. We also did not test lipid substrates with other acyl chain lengths to demonstrate that ABHD17 have a certain lipid preference. Alternatively, it is possible that once ABHD17 is at the plasma membrane, it undergoes structural changes required for substrate recognition. Another potential explanation could be that ABHD17 regulates local availability of palmitoyl-CoA instead, which would be consistent with the cell-based results that have been published before.<sup>56, 61</sup> Therefore, further experiments are still needed to validate the substrate specificity of ABHD17 and elucidate its cellular function.



### 2CIII. Validation of inhibitors for full-length recombinant enzymes

Resorufin acetate (ResOAc) has often been used as an esterase substrate since its hydrolysis product can be measured at a different wavelength (**Figure 2-15**).<sup>128</sup> Recombinant GB1-ABHD17A and 17B enzymes were used to carry out steady-state kinetic assays with the fluorogenic ResOAc to assess the effect of different compounds selected from past screens (structures shown in **Figure 2-15**).<sup>118</sup>

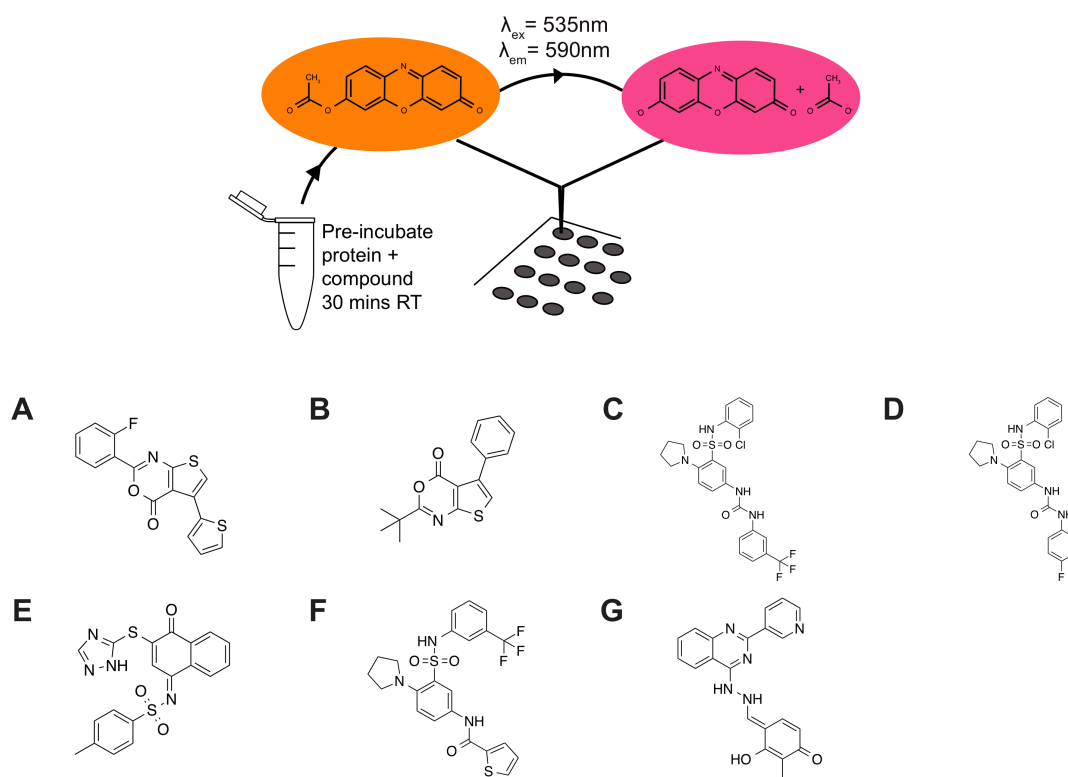


Figure 2-15 Overview of fluorogenic assay used to assess candidate inhibitors

Recombinant enzymes, either WT or catalytic dead (SA), can be pre-incubated with a compound and then reacted with ResOAc to measure hydrolysis rates in a 96-wells format. Compounds A through G were chosen for their different scaffolds.

For the steady-state kinetic assays with ResOAc, data for compound E was not included since the compound interfered with the signal generated by hydrolysis product.  $K_m$  value increases in presence of inhibitors, indicating that they are disrupting the binding affinity of the ResOAc substrate. Treatment with the benzoxazinone derivatives (compounds A and B) resulted

in a higher  $K_m$  value compared to the DMSO control and compound A showed equivalent potency towards ABHD17A and 17B isoforms (**Figure 2-16**). Substituted benzoxazin-4-ones have been previously characterized as potent irreversible inhibitors of serine proteases such as chymotrypsin.<sup>129</sup> The mechanism of inhibition involves a nucleophilic reaction between the active site serine and the carbonyl group to form a stable acyl enzyme intermediate (**Figure 2-17**).<sup>130</sup>

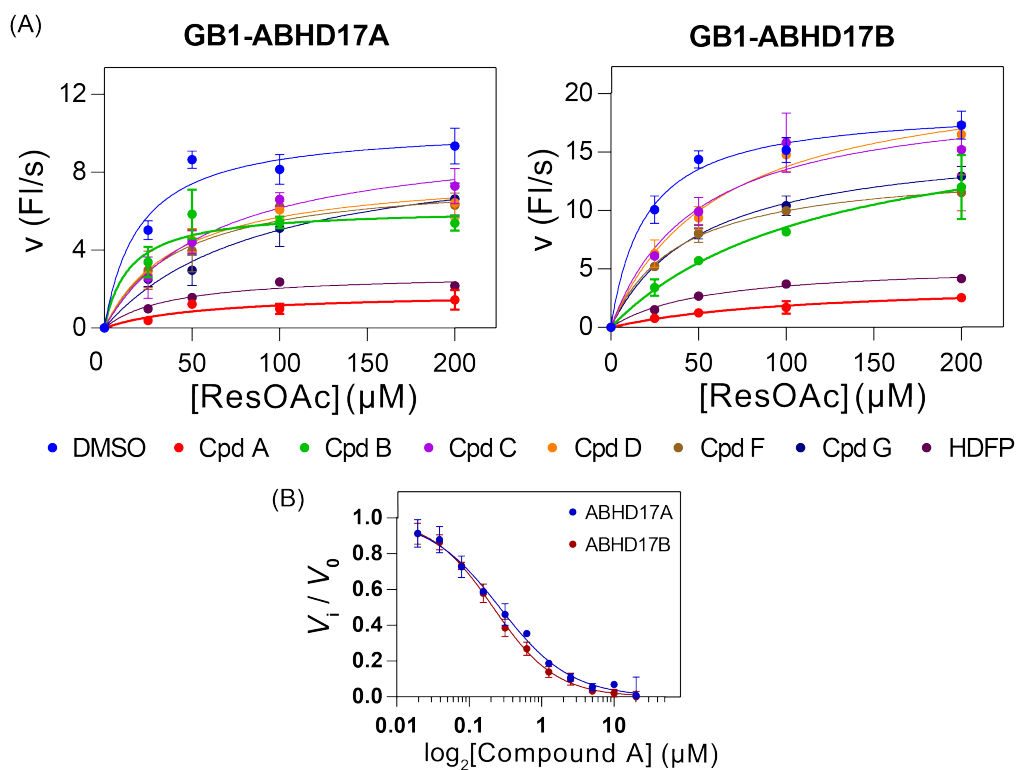


Figure 2-16 ABHD17A and 17B are inhibited the most by oxazinone-derivative compound A.

(A) Steady-state ResOAc hydrolysis rates for ABHD17A and 17B treated with different compounds. (B) Inhibition of ABHD17A and 17B by compound A.

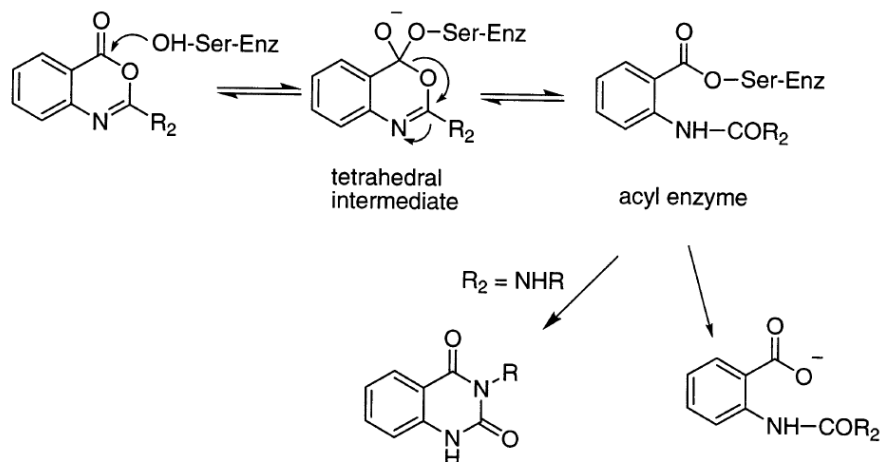


Figure 2-17 Mechanism of inactivation by benzoxazinone derivatives.

Figure was reprinted (adapted) with permission.<sup>130</sup> Copyright (2019) American Chemical Society.

In addition, we overexpressed ABHD17-GFP in HEK-293T and treated the membrane fraction with different compounds. This corroborated the results from the steady-state kinetic assays, showing that compounds A and B were effective against ABHD17A and 17B expressed in cells (**Figure 2-18**, **Figure 2-19**). Interestingly, compound E also decreased the FP-TAMRA labeling of the enzymes. As a positive control, the fractionated lysate was also treated with Palmostatin B (palmB), which is a non-specific depalmitoylase inhibitor.<sup>41</sup> The other serine hydrolases that react with FP-TAMRA do not seem to be targeted by the compounds used since the other labeled bands do not appear to decrease in intensity. Finally, we treated HAP1 cells with compound A and used 17-ODYA metabolic labeling to look at the effect on the *S*-palmitoylated proteins across the cells. However, we observed no significant changes in the palmitoylation levels with inhibitor treatment (**Figure 2-20**). Therefore, further development of the compounds is needed to improve the isoform selectivity and *in vivo* activity of the compounds.

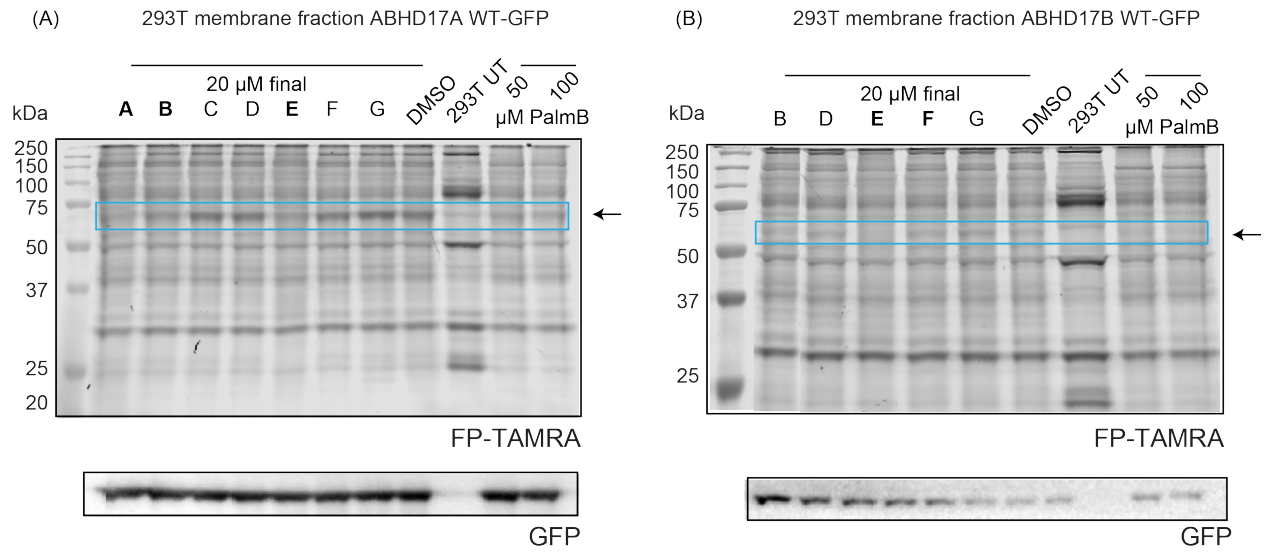


Figure 2-18 ABPP gel with ABHD17A and 17B overexpression

Treatment of Membrane fractions expressing (A) ABHD17A-GFP or (B) 17B-GFP with 20 μM compound resulted in the decrease of FP-TAMRA labeling for compounds A, B and E. PalmB is a non-specific inhibitor of depalmitoylases, which serves as a positive control.

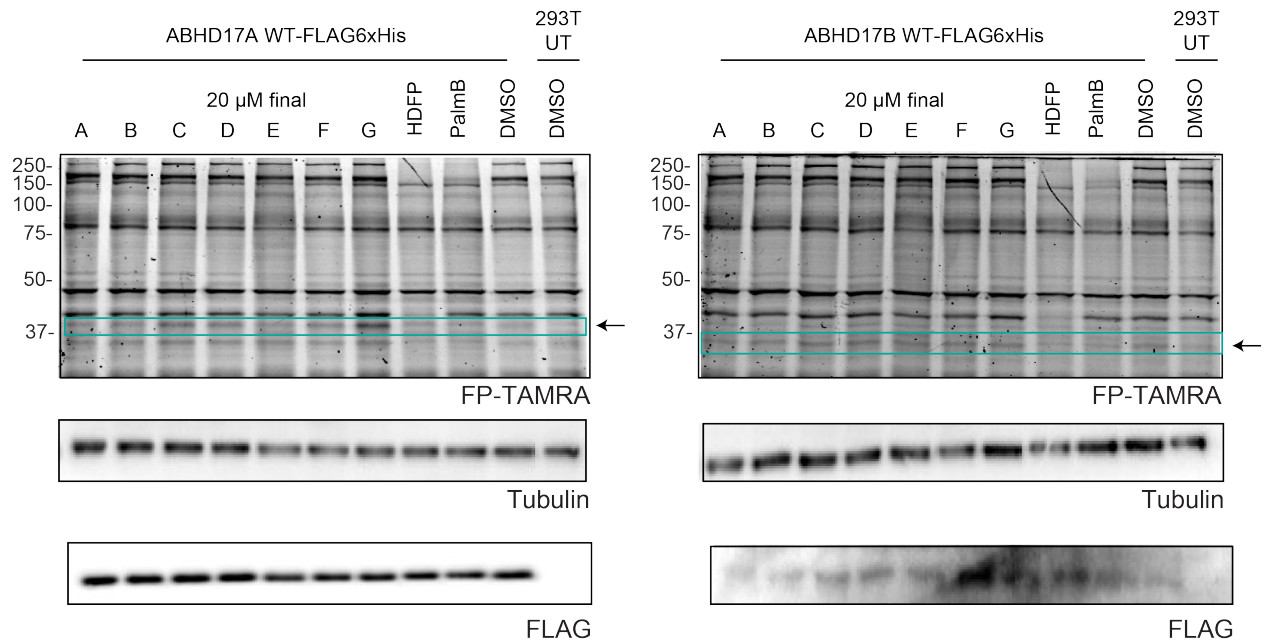


Figure 2-19 In vitro treatment of membrane fraction of HEK-293T lysate overexpressing ABHD17A and 17B with FLAG6xHis tag.

Inhibitor treatment was repeated using HEK-293T expressing a different ABHD17 fusion protein (FLAG6xHis tag) and results are similar to GFP tagged ABHD17.

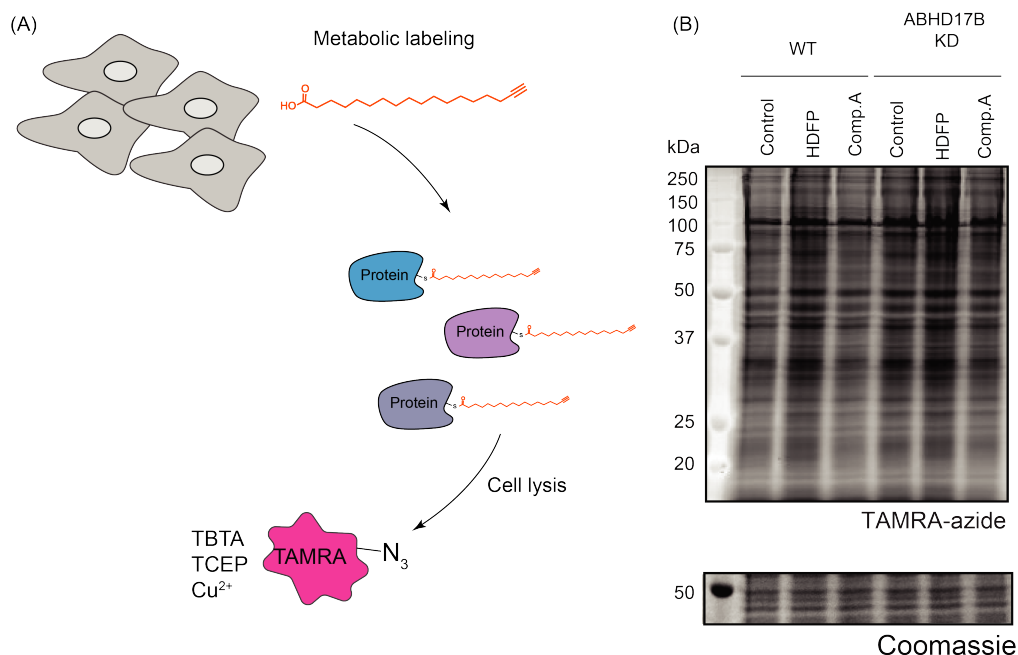


Figure 2-20 Metabolic labeling of HAP1 cells treated with compound A or DMSO.

(A) Metabolic labeling with 17-ODYA and click chemistry with a fluorophore (TAMRA-azide) to visualize *S*-palmitoylated proteins. (B) Compound A does not cause any major change in palmitoylation across HAP1 proteome, suggesting that the inhibitor does not work well *in vivo*.

## 2D. Conclusion

Our results confirmed multiple sites of *S*-fatty acylation across the ABHD17 isoforms by APEGS assay. We co-expressed DHHC enzymes and ABHD17 isoforms and analyzed the level of ABHD17 palmitoylation, by 17-ODYA labeling and conjugation to a fluorophore-azide, showing that a similar subset of DHHC enzymes acylate ABHD17. The overexpression of particular DHHCs increased the degradation of ABHD17, implying that *S*-palmitoylation may play a role in its stability. Moreover, we expressed and purified ABHD17A from *E.coli* and HEK-293T to study the *in vitro* properties of ABHD17. FP-TAMRA labeling was used to measure the activity of the enzyme and the rate of labeling between the non-modified and *S*-palmitoylated recombinant enzymes was comparable. Our assays showed that ABHD17 did not depalmitoylate recombinant NRAS protein labeled with 17-ODYA, although additional work is required to verify the lipid substrate preference of the enzymes. Finally, we tested potential

inhibitors of the recombinant enzymes *in vitro*, though further work is needed to develop the potency and isoform selectivity of the compounds.

## **2E. Experimental**

### **Cell culture and transfection**

Human HEK-293T cells were cultured in Dulbecco's Modified Eagle Media (DMEM; Invitrogen) supplemented with 1 % (v / v) 10000 Units / mL penicillin-streptomycin (Invitrogen), 4.5 g / L D-Glucose, 2 mM L-Glutamine, 110 mg / L sodium pyruvate, and 10 % (v / v) fetal bovine serum (GE Healthcare Life Sciences). Cells were transfected using Fugene HD (Promega) and Opti-MEM (reduced serum media; ThermoFisher) per the manufacturer's instructions and grown 2 additional days to reach confluency before being washed and collected for future use.

### **Acyl-PEGyl exchange gel shift (APEGS) assay**

Cells were resuspended and lysed in 50 mM HEPES pH 7.4, 100 mM NaCl, 1 mM EDTA, 2 % SDS buffer and protein concentration was quantified using DC protein assay (BioRad). 1 mg/mL protein was diluted into buffer containing 6 M urea before incubation with 10 mM tris(2-carboxyethyl)phosphine (TCEP; Sigma) for 30 minutes at room temperature (cysteine reduction step) and 50 mM iodoacetamide (IAM; Sigma) for one hour in the dark at room temperature (alkylation step). After chloroform/methanol precipitation to remove excess TCEP and IAM, protein was resuspended in 50 mM HEPES pH 7.4, 4% SDS and 5 mM EDTA buffer and mixed with a buffer containing 50 mM HEPES pH 7.4, 1%SDS, 5 mM EDTA, 1 M NH<sub>2</sub>OH, pH 7.4) for one hour at 37 °C to cleave the palmitoylation thioester bonds. As a negative control, buffer not containing hydroxylamine (NH<sub>2</sub>OH) was used. After a second chloroform-methanol precipitation step, protein was resuspended in 50 mM HEPES pH 7.4, 4% SDS buffer and

PEGylated with 20 mM 5k-mPEGs (Sigma) for 1 hr at RT to label newly exposed cysteinyl thiols. As a negative control, 20 mM NEM was used instead of mPEG (-PEG). Protein was precipitated again by chloroform-methanol and resuspended in SDS-loading buffer. Samples were heated at 95 °C for 5 minutes before being resolved by 12 % SDS-PAGE gels (180 V; 75 minutes) and analyzed by western blot as described later.

### **17-ODYA labeling across ABHD17 and DHHC co-expression panel studies**

Cells were cultured and transfected as described previously. In addition, they were treated with 20 μM 17-Octadecynoic acid (17-ODYA; Cayman Chemicals) 16 hours prior to being washed in DPBS (Dulbecco's phosphate-buffered saline; Gibco) and frozen until further use.<sup>29 131</sup> Plasmids expressing mouse DHHC genes tagged with 3xHA were a gift from Paul Jenkins lab (University of Michigan) and those expressing mouse ABHD17-GFP fusion proteins were from a previous paper.<sup>76</sup> Cells were resuspended in DPBS buffer and lysed by sonication. For in-gel analysis, 50 μg protein lysate (quantified using BioRad DC Protein Assay) was reacted with 1 mM tris(2-carboxyethyl)phosphine (TCEP; Sigma), 20 μM TAMRA azide (Click Chemistry Tools), 1 mM CuSO<sub>4</sub>, and 100 μM Tris((1-benzyl-1H-1,2,3-triazol-4-yl)methyl)amine (TBTA; Cayman) for 1 hour at room temperature and the samples were heated at 70 °C for 5 minutes before being resolved by 12 % SDS-PAGE gels (180 V; 75 minutes) and imaged using Azure c600 (Azure Biosystems). They were then analyzed by western blot.

### **Western blot analysis**

Gels were transferred to a methanol-activated Immobilon-FL membrane (Millipore) for western blot analysis. The transfer step was at 75 V for 2 hours at 4 °C in 25 mM Tris-base, 192 mM glycine, 10 % methanol buffer. Membrane was blocked in Odyssey Blocking Buffer (LI-COR) and incubated for 16 hours at 4 °C in primary antibody solutions prepared in Odyssey Blocking

Buffer supplemented with 0.2 % (v/v) Tween-20. Membrane was washed using Tris-buffered saline and 0.5 % (v/v) Tween-20 (TBS-T) before incubation with species-matched secondary antibody solutions for 1 hour at room temperature. For the DHHC and ABHD17 co-expression and metabolic labeling studies, the secondary antibody solutions contained either an anti-rabbit AlexaFluor 647 (to label GFP-tagged ABHD17) or anti-mouse horseradish peroxidase (HRP) (to label HA-tagged DHHC). HRP blots were developed using West Pico PLUS Chemiluminescent Substrate (Thermo) and the chemiluminescence signal detected by Azure c600 (Azure Biosystems) while blots treated with the AlexaFluor 647 secondary were imaged directly using the Cy5 and Cy3 channels for AlexaFluor 647 and TAMRA-azide signal. Images were processed using ImageJ software (NIH) and protein band measurements were calculated in Image Studio Lite (LI-COR). Bar graphs were plotted using RStudio.

For the remaining experiments, the secondary antibody was the species-matched HRP antibody and the blots were processed as described above.

*Table 2-1 Antibody information*

Target Protein (Dilution)	Product Information
HA (1:1000)	Roche 11583816001
6xHis (1:1000)	ThermoFisher MA121315
FLAG-M2 (1:5000)	Sigma F1804
ABHD17A (1:500)	Aviva Systems Biology ARP67573_P050
ABHD17B (1:500)	Abcam ab187665
Pan-RAS (1:1000)	Millipore 50-171-675
GFP (1:1000)	Cell Signaling Technology 2956S
Tubulin (1:2500)	Sigma T6074



Anti-rabbit AlexaFluor 647 (1:1000)	ThermoFisher A32733
Anti-mouse HRP (1:1000)	Invitrogen PI3243
Anti-rabbit HRP (1:1000)	ThermoFisher 32460

### **Cloning, expression and purification of ABHD17 fusion proteins in *E.coli* and HEK-293T**

Plasmids expressing different fusion-tagged ABHD17 were created via restriction digest and ligation into p6xHis, pMBP and pGB1 (Protein Core in the Center for Structural Biology (Life Science Institute, University of Michigan)). The mouse ABHD17 gene was amplified from plasmids previously made in the lab <sup>76</sup> and ligated using SspI and BamHI sites. BL21 (DE3) *E.coli* cultures were grown at 37 °C to OD<sub>600</sub>= 0.8 and the temperature was reduced to 18 °C for 1 hour before induction with 0.4 mM IPTG for 16 hours at 18 °C. Cell pellets were resuspended in 50 mM HEPES, 300 mM NaCl, 10% Glycerol, 2 mM 2-Mercaptoethanol and 0.005% IGEPAL buffer, lysed using a microfluidizer and centrifuged at 16000 rpm for 30 minutes. The cleared supernatant was incubated with Talon cobalt affinity beads (Clontech) for 1 hour, washed with 50 mM HEPES, 150 mM NaCl and 1 mM imidazole buffer. The protein was eluted using 50 mM HEPES, 150 mM NaCl and 150 mM imidazole buffer and dialyzed overnight to remove excess imidazole, yielding ~ 2.0 mg/mL. Sample aliquots were supplemented with 10 % glycerol and stored at -80 °C. To verify the activity of the enzymes, the purified protein samples were also incubated with 1 μM FP-TAMRA (generous gift from Gordon Amidon (University of Michigan, College of Pharmacy) for 30 minutes at room temperature prior to boiling with SDS-loading buffer (50 mM Tris-Cl, pH 6.8, 2 % (w/v) SDS (sodium dodecyl sulfate; electrophoresis grade), 0.1 % (w/v) bromophenol blue, 10 % (v/v) glycerol and 100 mM 2-mercaptoethanol).

Samples were resolved by 12 % SDS-PAGE gels (180 V; 75 minutes) and imaged using Azure c600 (Azure Biosystems).

ABHD17 protein was also expressed in HEK-293T using pcDNA3 plasmids with a FLAG-6xHis C-terminal tag.<sup>76</sup> Cells were cultured as previously described and at 90 % confluency, they were transfected using polyethylenimine (PEI; Alfa Aesar). Cells were collected the next day and washed in cold DPBS (Invitrogen) before storage at  $-80^{\circ}\text{C}$ . Cells were resuspended in 25 mM HEPES pH 7.5, 25 mM NaCl, 1 % (w/v) n-dodecyl- $\beta$ -Dmaltopyranoside (DDM, Anatrace) buffer for 1 hour at  $4^{\circ}\text{C}$ . After removal of insoluble material by ultracentrifugation ( $100,000 \times g$ , 45 minutes,  $4^{\circ}\text{C}$ ), the supernatant was incubated with Talon cobalt resin (Clontech) for 1 hour at  $4^{\circ}\text{C}$ . Resin was washed using 25 mM HEPES pH 7.5, 25 mM NaCl, 1 mM imidazole buffer and protein was eluted with 25 mM HEPES pH 7.5, 25 mM NaCl, 150 mM imidazole. Protein was buffer exchanged in 25 mM HEPES pH 7.5, 25 mM NaCl to remove excess imidazole and concentrated using Amicon Ultra centrifugal filters (Millipore). Protein aliquots were supplemented with 10 % glycerol before storage at  $-80^{\circ}\text{C}$ . Alternatively, protein was also purified using anti-FLAG M2 magnetic beads (Sigma) to reduce non-specific proteins that co-elute during Co resin affinity purification. The wash buffer contained 25 mM HEPES pH 7.5, 25 mM NaCl and the elution buffer was 25 mM HEPES pH 7.5, 25 mM NaCl and 0.1 mg/mL FLAG peptide (Sigma).

### **FP-TAMRA labeling time course to compare ABHD17A expressed from *E. Coli* and HEK-293T**

Corresponding bands from FP TAMRA and 6xHis blot were quantified using Image Lite Studio (LI-COR) so that fluorescence signal (FP-TAMRA) was normalized with respect to protein

abundance (6xHis band). Plotted values were calculated by dividing all normalized values with the maximum signal at 60 minutes. Plot was generated using Graphpad Prism 6.

### **In vitro assays to test depalmitoylase activity on lipidated NRAS (17-ODYA click chemistry and 5-TMRIA labeling assay)**

Enzyme was diluted to 200 nM using 0.1 M phosphate pH 7.4, 50 mM NaCl, 0.03 % DDM and either 0.5 % NP-40 or 0.5 % TritonX buffer. 1.25  $\mu$ M NRAS (labeled with 17-ODYA) was added to the enzyme in a total volume of 25  $\mu$ L and incubated for 45 minutes at 37 °C. Then, 25  $\mu$ L of click reaction mixture was added (1 mM TCEP, 20  $\mu$ M TAMRA azide, 1 mM CuSO<sub>4</sub>, and 100  $\mu$ M TBTA) for 45 minutes at room temperature. For the no enzyme sample, NRAS was instead mixed with 25  $\mu$ L 0.1M HA or 25  $\mu$ L buffer. Finally SDS loading buffer was added to the samples and they were heated at 75 °C for 5 minutes before being resolved by SDS-PAGE, imaged using the Azure c600 and further analyzed by western blot.

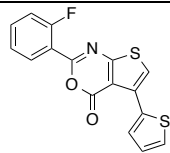
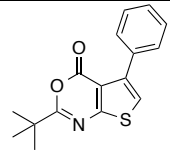
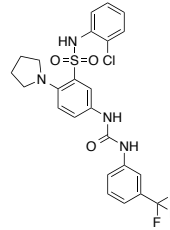
For the iodoacetamide-TAMRA experiment, a similar protocol to the one outlined in the APEGS section was used. But instead of adding 5k-mPEG probe after hydroxylamine treatment, iodoacetamide-TAMRA was added to label any new cysteines that would be depalmitoylated by ABHD17.

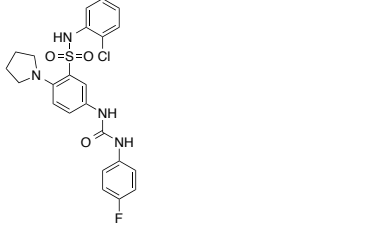
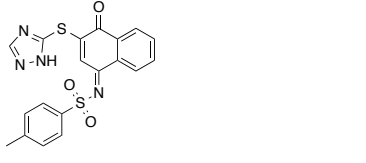
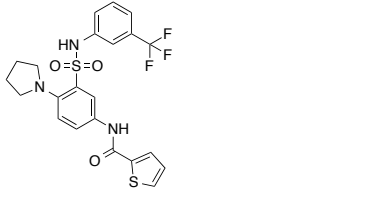
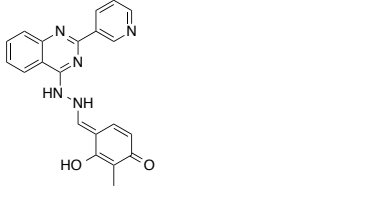
### **Resorufin acetate assay for inhibitor screening**

Steady-state kinetic assays were performed as previously described.<sup>119</sup> The rate of hydrolysis of resorufin acetate was determined for different compounds using the wild-type and the catalytic-dead enzyme (GB1-ABHD17A-S190A and GB1-ABHD17B-S170A) to subtract any spontaneous hydrolysis. Resorufin acetate (Sigma) in DMSO was titrated at various concentrations as 2  $\mu$ L aliquots in clear-bottom 96-well plates (Greiner bio-one), as well as 2  $\mu$ L aliquots of 20  $\mu$ M inhibitor in DMSO. Enzymes were diluted to 200 nM with PBS pH 6.5

supplemented with 0.1 g/L pluronic F127 (Sigma) and 96  $\mu$ L was quickly dispensed to each well and mixed by pipetting up and down multiple times, with each enzyme being tested in 2 separate runs and 4 replicates per substrate concentration. Fluorescence was measured on a Tecan F500 plate reader (525/35 nm excitation filter, 600/10 nm emission filter, and a 560 LP dichroic filter) for every 35 seconds for a total of 15 minutes. The slope of the background-subtracted (catalytic dead) fluorescence in the beginning 5 minutes was used to generate initial reaction velocities, which were then processed in Graphpad Prism 6 to derive  $K_m$  and  $V_{max}$  values.  $K_i$  values were also calculated using a similar approach, by pre-incubating 200 nM enzyme with a range of inhibitor concentrations for 30 minutes at room temperature before adding 50  $\mu$ M substrate and running the experiments in triplicates per inhibitor concentrations. Data was then processed in Graphpad Prism 6.

Table 2-2 Structure of compounds used during inhibitor screening

	Structure	CID	Vendor information
A		876987	Vita STL327592
B		786566	Vita STK869597
C		4331202	Enamine Z56262882

D		3611470	Enamine Z56262886
E		655490	Vita STK215536
F		4554648	Enamine Z26475547
G		5513860	Vita STK565259

## Chapter 3 Acyl-RAC Proteomics Approach to Profile Site-specific *S*-acylation<sup>‡</sup>

### 3A. Abstract

*S*-acylation describes a reversible post-translational modification, regulated by DHHC palmitoyltransferases which predominantly transfer a 16-carbon fatty acyl group to cysteines via a thioester link. The reverse reaction is catalyzed by depalmitoylases, including APT1, APT2 and ABHD17. This cycle facilitates the trafficking and function of proteins involved in various physiological processes, including the oncogenic RAS GTPase, where membrane tethering influences its ability to transform cells. Despite the development of chemical tools to better study *S*-palmitoylated proteins, it remains challenging to identify the sites that are modified. Here, we applied an acyl-RAC proteomics workflow to identify sites of acylation in mouse embryonic fibroblasts, which are engineered to express single RAS isoforms. Our results demonstrate that our method is comparable to other reported datasets, and we observed palmitoylated sites that were not previously annotated. Our method was also applied to identify substrates of ABHD17A; however, our results indicate that ABHD17A may not function as a depalmitoylase. The workflow described here can be further improved by additional informatics, and can be a valuable, more high-throughput strategy to identify substrates of DHHC enzymes, which are expressed as 23 distinct proteins.

---

<sup>‡</sup> This chapter includes contribution from Melanie S. Cheung See Kit, who performed all the experiments.

### 3B. Background

Protein *S*-acylation is commonly known as *S*-palmitoylation since C16:0 palmitate is the predominant fatty acid chain that gets attached to cysteines via a thioester bond. A 2011 computational survey of putative post-translational modifications (PTMs) from Swiss-Prot identified *S*-Palmitoylation as the 5<sup>th</sup> most frequent PTM.<sup>132</sup> This labile PTM is catalyzed by the DHHC family of palmitoyl transferases, which has a Cys-rich domain containing a conserved Asp-His-His-Cys (DHHC) motif. Protein depalmitoylases, including acyl-protein thioesterases 1 and 2 (APT1 and APT2) and the  $\alpha/\beta$  hydrolase domain-containing protein 17 (ABHD17), catalyze the reverse process, during which the palmitoyl group gets hydrolyzed. Protein palmitoylation has been shown to regulate the cellular trafficking of proteins across various physiological processes. For example, the oncogenic HRAS<sup>G12V</sup> mutant requires membrane tethering to cause cellular transformation and this is abrogated by a palmitoyl-deficient HRAS<sup>G12V</sup> mutant.<sup>27</sup> Postsynaptic density (PSD)-95 is a scaffolding protein involved in synaptic development and function; palmitoylation at Cys3 and Cys5 are required for its postsynaptic targeting<sup>133</sup> and it has been shown to be depalmitoylated by ABHD17.<sup>56</sup>

ABHD17 is expressed as three main isoforms (A, B, and C) and contains a cysteine-rich N-terminal domain important for *S*-palmitoylation and membrane localization.<sup>76</sup> Overexpressed ABHD17A is reported to depalmitoylate and mislocalize NRAS.<sup>61</sup> In addition, a recent genome-wide CRISPR screen in AML cell lines identified ABHD17B as an essential gene in NRAS dependent THP-1 cells and NRas-dependent Ba/F3 cells.<sup>111</sup> So far, cell-based studies have focused on specific ABHD17 substrate targets; yet no proteome-wide approach has been used to identify other substrates depalmitoylated by ABHD17.

The study of *S*-palmitoylation using bottom-up proteomics methods, has remained challenging owing to the hydrophobic and labile nature of the thioester-linked *S*-palmitoylated peptides. There has been active development of biochemical assays that either metabolically incorporate alkyne fatty acids analogs to sites of palmitoylation (which can then be captured by bioorthogonal enrichment<sup>76</sup>) or use hydroxylamine to selectively replace palmitoylation with affinity enrichment probes.<sup>120, 88</sup> The alkyne fatty acid derivative, 17-octadecynoic acid (17-ODYA), is added to cells where it can be processed to form its coenzyme (coA) conjugate, which is transferred to endogenous sites of *S*-palmitoylation by DHHC enzymes. This method is useful for dynamic studies of palmitoylation turnover since cells can be collected at different time points and the cell lysates can be tagged by copper-catalyzed azide alkyne addition (CuAAC) to azides linked to fluorophores or biotin for gel-based or mass spectrometry analyses respectively. This approach has been widely used to characterize *S*-palmitoylated proteins across multiple cell lines<sup>9, 89</sup> and organisms.<sup>95</sup> However, the alkyne fatty acid can be metabolized to other phospholipids and incorporated into other protein modifications, and high levels of palmitate can trigger oxidative stress,<sup>99</sup> causing free thiols to be trapped in disulfide bonds or glutathione adducts. Additionally, proteins with slow palmitoylation turnover may not have a free Cys available to incorporate the alkyne fatty acid analog.

An alternative approach is based on hydroxylamine-switch strategies, where hydroxylamine selectively cleaves all thioesters across the proteome to release free thiols that can then be captured. Unlike metabolic labeling, this technique can be used to profile steady-state palmitoylation levels in primary tissues. The biochemical assay starts with addition of tris(2-carboxyethyl)phosphine (TCEP) to reduce disulfides and an alkylating agent such as *N*-ethylmaleimide (NEM) or iodoacetamide (IAM) to block free thiols. Then, neutral



hydroxylamine can be added to hydrolyze thioester bonds, and the resulting thiols are captured using a pyridyl disulfide resin (acyl-resin assisted capture; acyl-RAC)<sup>88</sup> or a pyridyl disulfide biotin conjugate for subsequent streptavidin resin enrichment (acyl biotin exchange; ABE).<sup>120</sup> It is important to note that this method is not specific to *S*-palmitoylation, and other endogenous thioester-linked proteins such as ubiquitin ligases and lipoamide-dependent hydrolases are also detected. While still bound to the resin, proteins can be enzymatically digested to generate peptides for mass spectrometry (MS) analysis.

The enzymatic (usually tryptic) peptides present in the supernatant are the ones often annotated by MS to generate datasets of palmitoylated proteins.<sup>87, 116</sup> In a few cases, additional steps are performed to allow for identification of the peptides containing the *S*-palmitoylation site(s). The tryptic peptides in the supernatant are removed and the resin is washed and treated with TCEP again to release the peptides. These are either directly analyzed or blocked using a second alkylating reagent. A study of mouse forebrain tissue by site-specific acyl biotin exchange (ssABE) revealed 906 putative sites of palmitoylation mapped to 641 proteins<sup>134</sup> while acyl-RAC site analysis, comparing normal mice liver tissue and tissue deficient in DHHC13, identified 400 palmitoylation sites for 254 candidate substrates of DHHC13.<sup>135</sup> Finally, in the instance where a second alkylating reagent was used to block the free cysteine, 347 proteins were identified from naïve and LPS/IFN- $\gamma$  stimulated RAW264.7 macrophages.<sup>136</sup> These approaches provide a long list of putative sites that can be compared against the *S*-palmitoylation database SwissPalm,<sup>31</sup> thereby allowing the identification of proteins that have been previously annotated across multiple experimental methods. Additionally, sites of palmitoylation can be validated using other biochemical means, such as introducing Cys to Ala mutants of the putative site.

Here, we applied current acyl-RAC proteomics workflow (**Figure 3-1**) to identify putative sites of palmitoylation in mouse embryonic fibroblast (MEF) cell lines engineered to express individual RAS isoforms.<sup>137</sup> For our workflow, we used iodoacetamide (IAM) as the first alkylating reagent instead of methyl methanethiosulfonate (MMTS) to prevent competition with the thiopropyl beads in case of incomplete removal of excess alkylator. After eluting the tryptic peptides off the beads, we added a second alkylating reagent, MMTS to make Cys adducts that we could specifically search for during data analysis. For MEF cells expressing NRAS<sup>WT</sup> and HRAS<sup>WT</sup>, we identified 2989 sites belonging to 1533 proteins and 3695 sites mapped to 1796 proteins respectively. Further validation is required to compare our results to predicted sites of *S*-palmitoylation available from CSS-Palm,<sup>138</sup> as well as biochemically confirm the sites of palmitoylation in proteins of interest. Additionally, we applied a similar strategy in an effort to find putative substrates of ABHD17A. However, comparison of samples, overexpressing ABHD17A as the wild-type or catalytically inactive (Ser to Ala mutant; SA), did not result in any significant changes in levels of palmitoylated peptides. In agreement with our proteomics data, analysis of NRAS palmitoylation by gel-based acyl-RAC did not show any significant changes between overexpression of ABHD17A WT or ABHD17A SA. Further testing of our method, using other enzymes involved in *S*-palmitoylation such as DHHCs or APT1/2, can provide supplementary validation for its application in identifying putative *S*-palmitoylated substrates.

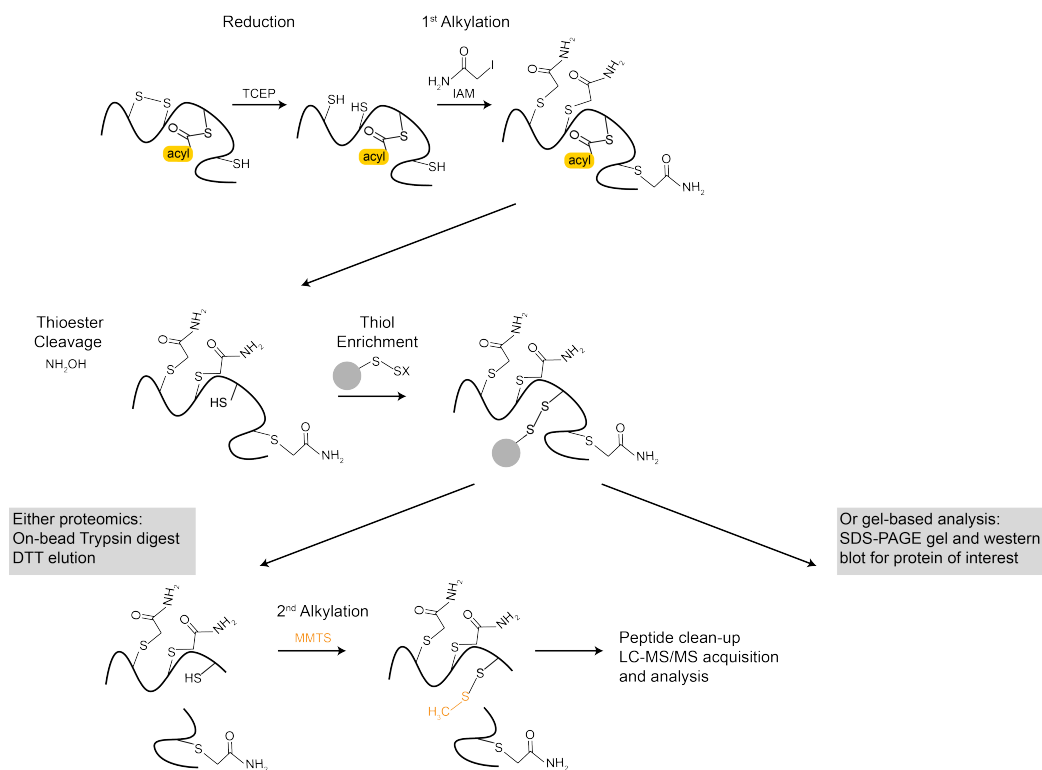


Figure 3-1 Analysis of *S*-palmitoylation by acyl-RAC workflow.

Samples can either be analyzed by proteomics to provide sites of palmitoylation across a proteome or by SDS-PAGE gel and western blot for individual proteins. TCEP = tris(2-carboxyethyl)phosphine; IAM = iodoacetamide;  $\text{NH}_2\text{OH}$  = hydroxylamine; DTT = dithiothreitol; MMTS = methyl methanethiosulfonate; LC-MS/MS = liquid chromatography-tandem mass spectrometry; SDS-PAGE = sodium dodecyl sulfate-polyacrylamide gel electrophoresis.

### 3C. Results and discussion

#### 3CI. Identification of putative sites of *S*-palmitoylation in mouse embryonic fibroblasts (MEF) cells by site-specific acyl-RAC proteomics

We decided to modify available acyl-RAC methods by using iodoacetamide (IAM) as the first alkylating reagent instead of methyl methanethiosulfonate (MMTS) and use MMTS in the later alkylating step to block thiols on peptides eluted off the thiopropyl beads. This facilitated our data analysis as we searched for Cys modified with MMTS (45.988 Da) as our sites of *S*-acylation. We used MEF cells expressing either HRAS or NRAS isoforms to test our acyl-RAC workflow (**Figure 3-1**) and identify sites of *S*-acylation from triplicate samples with or without

hydroxylamine (HA; NH<sub>2</sub>OH) treatment. Peptides were analyzed using a nanoLC-MS/MS Orbitrap, then identified and quantified using the MaxLFQ algorithm in MaxQuant,<sup>139</sup> designed for label free quantification. A statistical analysis (*t* test, permutation-based, FDR = 0.01 and *s*<sub>0</sub> = 1) was applied in order to identify peptides that were at least significantly enriched two-fold (**Figure 3-2**). For MEF cells expressing NRAS<sup>WT</sup> and HRAS<sup>WT</sup>, we identified 2989 sites belonging to 1533 proteins and 3695 sites mapped to 1796 proteins respectively. We used the SwissPalm database to compare our results to previously published datasets of *S*-palmitoylated proteins from mouse cells or tissue samples, showing that about half or more of our identified proteins have not yet been annotated as being *S*-acylated. Comparative studies between bioorthogonal metabolic labeling and hydroxylamine-switch methods<sup>116, 136</sup> have shown that they can detect distinct subsets of proteins, which could explain why some of the proteins from SwissPalm were not identified in our results.

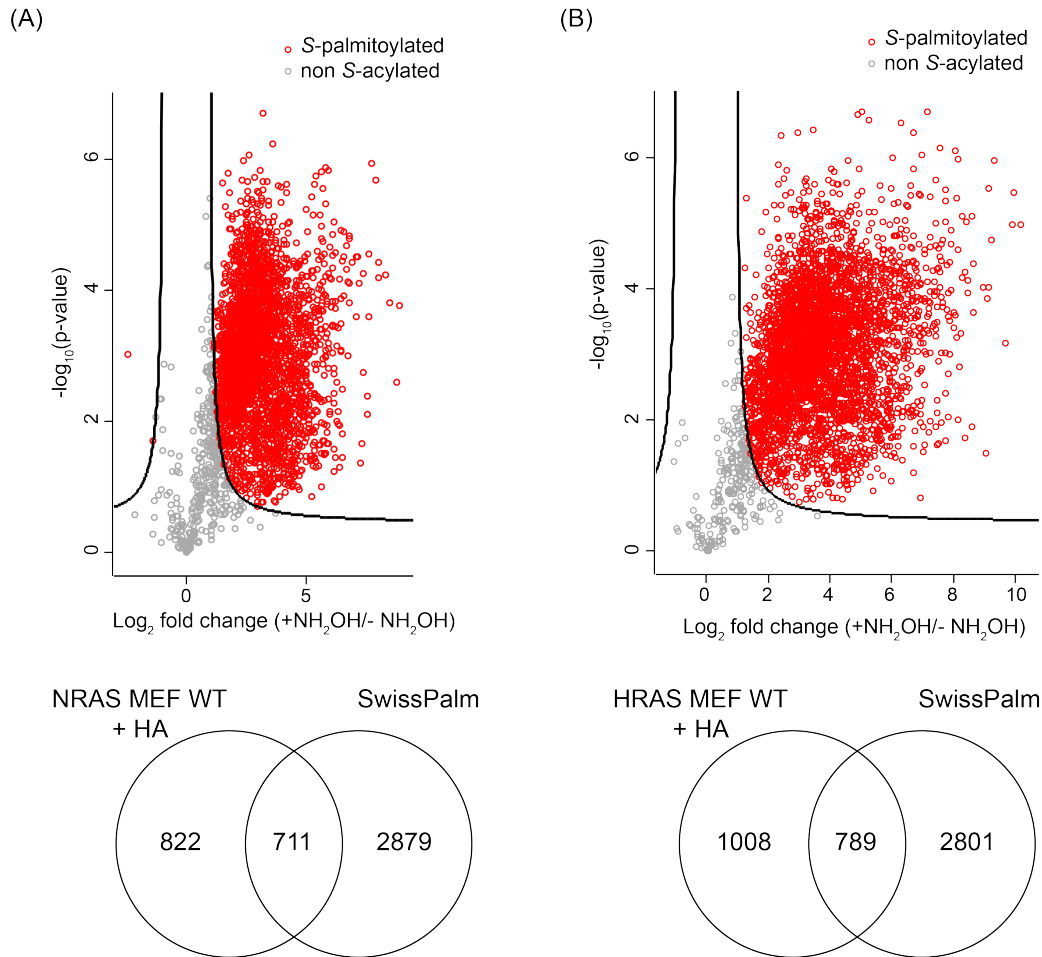


Figure 3-2 S-acylated peptides in RAS mouse embryonic fibroblasts.

Volcano plots show S-acylated peptides (labeled with MMTS) that were significantly enriched from (A) NRAS MEF and (B) HRAS MEF cells ( $p < 0.01$ ,  $\text{Log}_2(\text{Fold change}) \geq 1$ ) in a site-specific acyl-RAC proteomics experiment ( $n = 3$ , label free quantification). Venn diagrams display the overlap between the proteins identified in our experiments and the SwissPalm database containing published proteomic datasets of S-palmitoylation proteins.<sup>31</sup>

Our goal was to identify sites of S-palmitoylation and **Table 3-1** contains proteins from our dataset, that are known to be palmitoylated based on their UniProt Knowledgebase post-translational modification entry. We also compared our results to the SwissPalm database and showed similar site identifications to other published datasets which used different methods of enrichment, including acyl-RAC,<sup>135</sup> acyl biotin exchange,<sup>134</sup> and phenyl mercury enrichment.<sup>140</sup> Additional work is still needed to conduct such an analysis on a larger scale and leverage the wealth of information presented by large proteomic datasets. Computational tools can be

developed to help determine how our experimental sites of *S*-acylation measure up to predicted sites from CSS-Palm.

Table 3-1 Subset of identified sites of *S*-palmitoylation compared to SwissPalm database.

<b>Protein</b>	<b>MS/MS count</b>	<b>Cys position</b>	<b>SwissPalm sites data</b>	<b>Site validated</b>	<b>CSS-Palm prediction</b>
Lysosome membrane protein 2 (SCRIB2)	8	274	Shen et al		HC: 4, 5
Glutamine synthetase (GLNA)	5	99	Shen et al		
	6	346	Gould et al, Shen et al		
	4	229	n/a		
Calnexin (CALX)	21	367	n/a		HC: 504; MC: 8
	8	195	Gould et al		
CD81 antigen (CD81)	30	190	n/a		HC: 6, 9, 227; MC: 156, 228
	20	156	Shen et al		
		157	Shen et al		
CD9 antigen (CD9)	20	150	Collins et al		HC: 9, 76, 77, 150, 151, 216, 217; MC: 85
		151	Collins et al		
		165	Collins et al		
Ras-related protein R-Ras2 (RRAS2)	27	183	n/a		HC: 199, 201
Alpha/beta hydrolase domain-containing protein 17B (AB17B)	11	120	Collins et al		HC: 10, 11, 14, 15, 18, 39
Palmitoyltransferase ZDHHC6 (ZDHC6)	6	328	Collins et al	Abrami et al	HC: 5, 20, 135, 136, 328; MC: 101, 329, 392, 396
		329	Collins et al	Abrami et al	

n/a = not annotated; HC = high confidence; MC = medium confidence. Shen et al<sup>135</sup>; Gould et al<sup>140</sup>; Collins et al<sup>134</sup>; Abrami et

al.<sup>52</sup>

### 3CII. Profiling putative substrates of ABHD17 depalmitoylases by site-specific acyl-RAC proteomics analysis

After showing that we could obtain *S*-palmitoylation site analysis comparable to other published datasets, we decided to use our workflow to identify substrates of ABHD17A depalmitoylase. We initially tried a CRISPR interference (CRISPRi) strategy targeting ABHD17A and 17B expression at the transcriptional level<sup>141</sup> to generate cell lines with repressed expression of the enzymes. While we could obtain ABHD17B knockdown in HAP1 cells (**Figure 3-3**), our ABHD17A knockdown in THP-1 cells was not stable, and the cells recovered protein expression after multiple cell passages despite antibiotic selection (**Figure 3-4**). In the future, an alternative method such as an inducible shRNA system can be used to address cells recovering expression of essential genes.

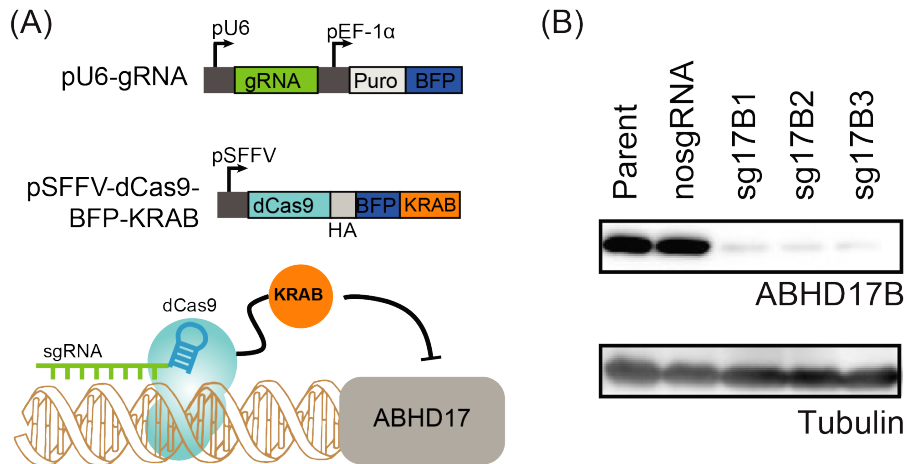


Figure 3-3 A CRISPRi strategy was employed to target expression of ABHD17B in HAP1 cells.

(A) Overview of CRISPRi technique<sup>141</sup> used to successfully knock down ABHD17B expression in HAP1 cells (B).

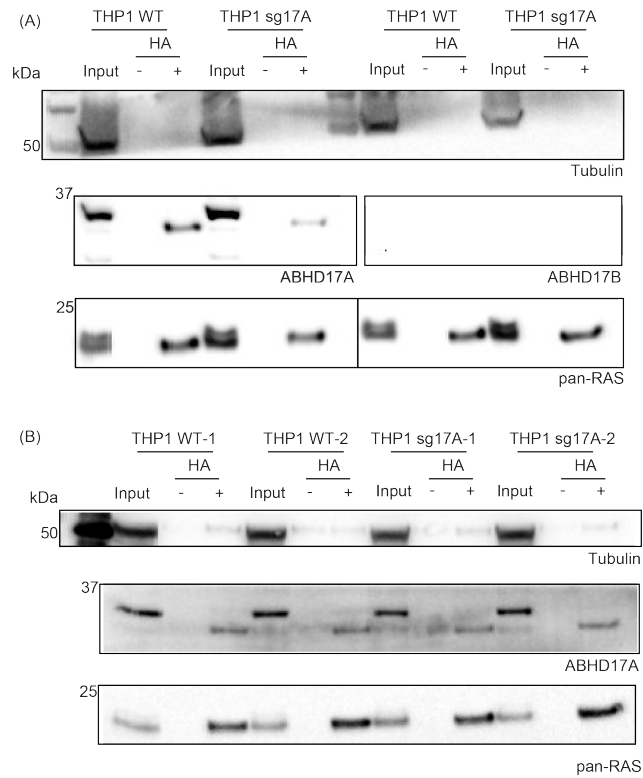


Figure 3-4 Acyl-RAC gels verifying expression and S-palmitoylation of ABHD17A in THP-1 cells following CRISPRi knockdown. ABHD17A was initially knocked down in THP-1 cells; however after passaging the cells, ABHD17A expression was recovered.

We altered our approach and instead overexpressed ABHD17 either as the wildtype active enzyme or catalytically inactive S190A mutant. Using the same workflow described earlier, we found that there were no significant changes in palmitoylation levels when ABHD17A (WT or S190A) is overexpressed in NRAS MEF cells (**Figure 3-5**).



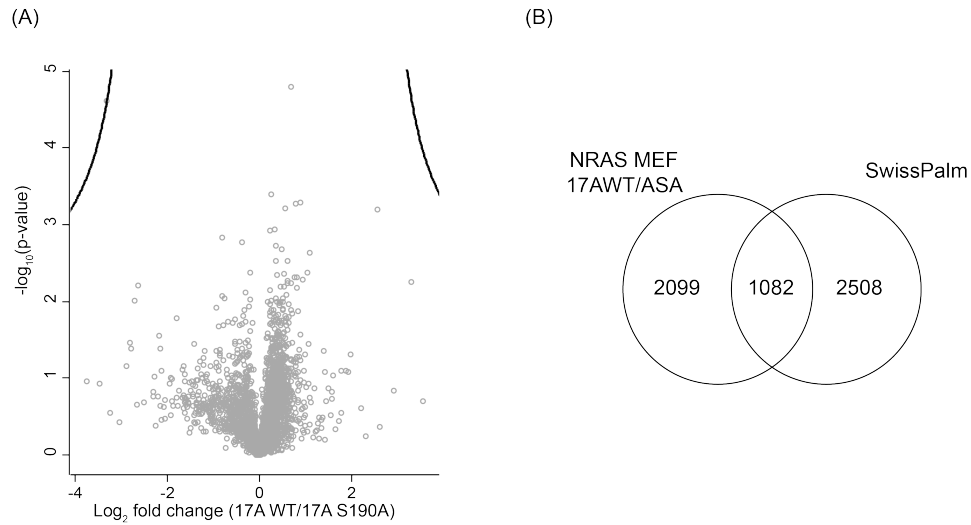


Figure 3-5 No significant changes in *S*-acylation levels observed during overexpression of *ABHD17A* WT and *S190A* (mutant) in *NRAS* MEF cells.

Volcano plot shows *S*-acylated peptides (labeled with MMTS) that were significantly enriched from *NRAS* MEF overexpressing either the active *ABHD17A* WT or catalytic inactive *S190A* mutant ( $p < 0.01$ ,  $\text{Log}_2(\text{Fold change}) \geq 1$ ) in a site-specific acyl-RAC proteomics experiment ( $n = 3$ , label free quantification). Venn diagram displays the overlap between the proteins identified in the experiments and the SwissPalm database.

To validate our proteomics result, we performed gel-based acyl-RAC and analyzed *NRAS* palmitoylation by western blot (**Figure 3-6**). Again we did not see any significant changes in endogenous *NRAS* *S*-acylation upon overexpression of *ABHD17* as the active enzyme (WT), catalytically inactive mutant (*S190A*) and the palmitoylation-deficient  $\Delta 19\text{N}$  truncation. This suggests that in our biological system, *NRAS* is not depalmitoylated by *ABHD17A*, nor does it depalmitoylate other protein substrates. As secondary validation, reciprocal strategies should be devised to either knockdown *ABHD17A* expression using a different gene editing system or develop selective and potent inhibitors of the enzyme. Moreover, there are no *in vitro* studies that demonstrate the depalmitoylase activity of *ABHD17*, leaving the possibility that it could be regulating cellular availability of palmitate through an unknown mechanism.

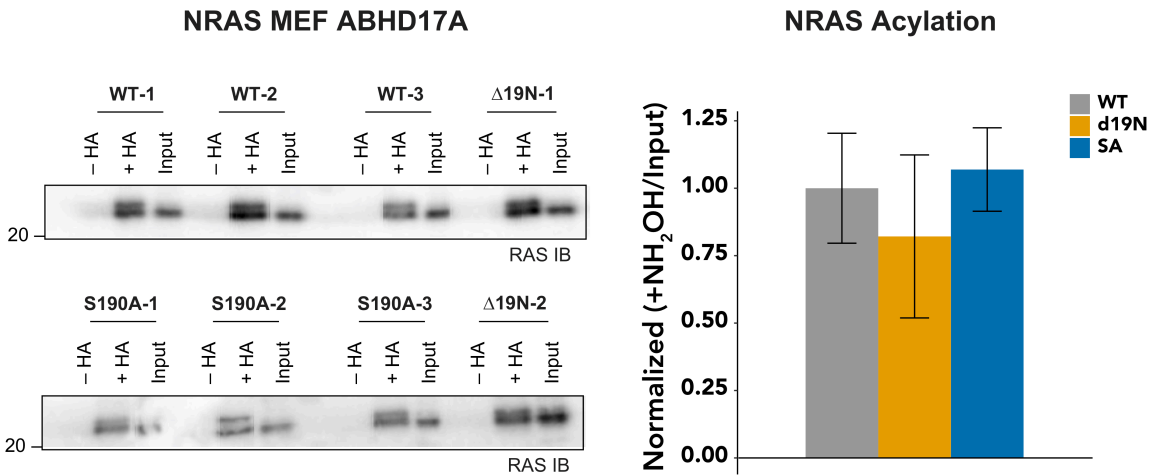


Figure 3-6 NRAS palmitoylation level measured by acyl-RAC.

ABHD17A was overexpressed as the wildtype, S190A (catalytically inactive) and Δ19N (truncation of the first 19 amino acids) in NRAS MEF cells and levels of NRAS palmitoylation measured by acyl-RAC, combined with western blot analysis.

### 3D. Conclusion

After applying our acyl-RAC proteomics methods, we identified sites of *S*-palmitoylation from MEF cells expressing either NRAS<sup>WT</sup> or HRAS<sup>WT</sup>. The proteins, along with their putative sites of palmitoylation, were compared to the SwissPalm database, which curates published proteomics datasets of *S*-palmitoylated proteins. Though our results demonstrate that a small list of putative sites are similar to ones previously identified using different methods of enrichment, we still need to improve our workflow and implement computational programming methods to analyze the whole dataset efficiently. Finally, we applied our workflow in attempt to identify putative substrates of ABHD17 enzymes. However, both our proteomics and gel-based results suggest that overexpressed ABHD17A does not cause significant changes in the palmitoylation levels in our NRAS MEF cell line, hinting that ABHD17 may influence palmitate turnover through a different mechanism. Nonetheless, this workflow could be applied for relatively high-throughput identification of putative substrates of DHHC palmitoyl transferases across various

biological systems. given that there are 23 DHHC enzymes expressed in humans. Additionally, it can be used to identify novel depalmitoylases by characterizing less studied members of the serine hydrolase superfamily.

### **3E. Experimental**

#### **Cell culture and transfection**

“RASless” mouse embryonic fibroblast (MEF) cells were obtained from the National Cancer Institute RAS Initiative. They were cultured in Dulbecco’s Modified Eagle Media (DMEM; Invitrogen) supplemented with 1 % (v / v) 10000 Units / mL penicillin-streptomycin (Invitrogen), 4.5 g / L D-Glucose, 2 mM L-Glutamine, 110 mg / L sodium pyruvate, and 10 % (v / v) fetal bovine serum (GE Healthcare Life Sciences) and at 90 % confluency, they were transfected using polyethylenimine (PEI; Alfa Aesar) and Opti-MEM (reduced serum media; ThermoFisher). Cells were collected the next day and washed in cold DPBS (Invitrogen) before storage at  $-80^{\circ}\text{C}$  for future use.

#### **Acyl-resin assisted capture (acyl-RAC)**

Cell pellets were first lysed in 50 mM HEPES pH 7.4, 100 mM NaCl, 1 mM EDTA buffer (buffer 1) by sonication and diluted using 50 mM HEPES pH 7.4, 6 M Urea, 1 mM EDTA, 1% SDS buffer (buffer 2). Proteins were then reduced using 20 mM tris(2-carboxyethyl)phosphine (TCEP; Sigma), pH 7 for 30 minutes at room temperature, followed by alkylation with 50 mM iodoacetamide (IAM; Sigma) for one hour in the dark. Proteins were then precipitated by chloroform-methanol extraction to remove excess reagents before resuspension in buffer 2, without 6 M urea (which is not compatible with protein quantification assay). Protein concentration was measured using DC protein assay (Biorad). An aliquot was saved for gel-based analysis where the sample was first incubated with 0.5 M hydroxylamine (HA, Sigma), pH

7 for 15 minutes before adding 1  $\mu$ M Tetramethylrhodamine-5-Iodoacetamide Dihydroiodide (5-TMRIA (noted IAM-TAMRA); Thermo) for 30 minutes.

The remaining sample was split equally into 2 tubes for the enrichment analysis. For plus HA treatment, 0.5 M HA, pH 7 was added to the sample in addition to  $\sim$  20 mg slurry of pre-activated thiopropyl sepharose 6B beads (Sigma). For the minus HA sample, buffer 2 was used instead to match the volume of the plus HA sample. Samples were incubated for 2 hours at room temperature. The beads were then thoroughly washed five times with buffer 2, followed by another five times using 50 mM HEPES, pH 7.4 buffer (buffer 3). For the western blot analysis, beads were resuspended in 1X loading buffer (10% glycerol, 62.5 mM tris pH 6.8, 1% 2-mercaptoethanol, 0.05% bromophenol blue, and 1% SDS) and heated for 5 minutes at 90 °C. The supernatant analyzed by SDS-PAGE. For the proteomic analysis, beads were resuspended in buffer 3 and incubated with Trypsin/ LysC mix (Promega) at 37 °C overnight. The next day, the supernatant containing the digested peptides was collected. The beads were washed five times with buffer, followed by treatment with 25 mM dithiothreitol for 45 minutes at 70 °C. Eluted peptides were transferred to a new tube and the beads were washed three times with buffer 3. After pooling the eluted peptides with the three washes, the peptides were alkylated using 60 mM methyl methanethiosulfonate (MMTS; Sigma) for 2 hours at 37 °C. Samples were then desalted with an Oasis PRIME HLB  $\mu$ Elution Plate (Waters) and dried in a Thermo Savant SpeedVac before storage at -80 °C. Peptides were resuspended in 0.1 % TFA in LC-MS grade H<sub>2</sub>O for LC-MS/MS analysis.

### **Western blot**

Gels were transferred to a methanol-activated Immobilon-FL membrane (Millipore) for western blot analysis. The transfer step was at 75 V for 2 hours at 4 °C in 25 mM Tris-base, 192 mM

glycine, 10 % methanol buffer. Membrane was blocked in Odyssey Blocking Buffer (LI-COR) and incubated for 16 hours at 4 °C in primary antibody solutions prepared in Odyssey Blocking Buffer supplemented with 0.2 % (v/v) Tween-20. Membrane was washed using Tris-buffered saline and 0.5 % (v/v) Tween-20 (TBS-T) before incubation with species-matched secondary antibody solutions for 1 hour at room temperature.

*Table 3-2 Western blot antibody information*

Target Protein (Dilution)	Product Information
6xHis (1:1000)	ThermoFisher MA121315
FLAG-M2 (1:5000)	Sigma F1804
ABHD17A (1:500)	Aviva Systems Biology ARP67573_P050
ABHD17B (1:500)	Abcam ab187665
Pan-RAS (1:1000)	Millipore 50-171-675
Anti-mouse HRP (1:1000)	Invitrogen PI3243
Anti-rabbit HRP (1:1000)	ThermoFisher 32460

### **LC-MS/MS analysis**

Label-free biological triplicates (n =3) were prepared per condition and analyzed by LC-MS/MS using an UltiMate 3000 RSLCnano liquid chromatography system (Dionex) coupled to an Orbitrap Fusion Lumos Tribrid mass spectrometer (ThermoFisher Scientific) equipped with an EasySpray source (ThermoFisher Scientific). Each sample was resolved using a nano-capillary reverse phase column (Acclaim PepMap 100 C18, 2 µm, 75 µm i.d. x 50 cm, Thermo Scientific), 300 nL / min flowrate and 120 minutes gradient (2-30 % acetonitrile/ 0.1 % formic acid). The mass spectrometer was programmed to collect one MS1 scan (Orbitrap; 60,000 resolution; AGC

target  $2 \times 10^5$ ; max IT 50 ms) followed by data-dependent, “Top Speed” (3 seconds) MS2 scans (collision induced dissociation; Orbitrap; 30,000 resolution; AGC  $1 \times 10^5$ ; max IT 22 ms).

### **MS data processing and analysis**

The data was processed using MaxQuant version 1.6.5.0 and searched against a UniProt mouse sequence database (55197 sequences; downloaded May 2019). Cysteine carbamidomethylation and cysteine modified by MMTS (Palmitoylation sites) were used as variable modifications. For the identification, the false discovery rate was set to 0.01 for proteins, peptides and sites while the minimum peptide length was set to seven amino acids. Other MaxQuant parameters were kept as the default setting. Label free quantification was performed using the “match between runs”. Dataset was further analyzed using Microsoft Office Excel 2016, BioTools.fr (for Venn diagrams) and Perseus version 1.6.5.0. Data was first filtered to remove reverse contaminants and to keep 3 valid values for plus HA samples. Replicates were grouped together and  $\log_2$  of the label free intensities was calculated. Missing (NA) values resulting from zero values for the minus HA samples were imputed with random numbers from a normal distribution (imputation criteria: width 0.3 and down shift 1.8). A two-sample test (permutation-based, 250 permutations, FDR = 0.01 and S0 value = 1) was performed to compare the plus HA sample (S-acylated proteins) with minus HA (background) and find significant peptides that were enriched with a fold change of at least 2. The Venn diagrams were

For the samples where ABHD17A WT and 17A SA were overexpressed, the data was filtered so that all 6 values for the two sets of triplicates were required and no missing value imputation was performed. A two-sample test (permutation-based, 250 permutations, FDR = 0.01 and S0 value = 1) was performed to compare the ABHD17A WT sample (plus HA) with ABHD17A SA sample

(plus HA) and find significant peptides that were enriched with a fold change of at least 2.

### **CRISPR*i* of HAP1 and THP-1 cells**

HAP1 cells were a generous gift from Gisou van der Goot (EPFL), and were cultured in Iscove's Modified Dulbecco's Medium (IMDM / Invitrogen) supplemented with 1 % (v / v) 10000 Units / mL penicillin-streptomycin, and 10 % (v / v) fetal bovine serum. THP-1 cells were cultured in Roswell Park Memorial Institute medium (RPMI 1640 / Invitrogen) supplemented with 1 % (v / v) 10000 Units / mL penicillin-streptomycin, and 10 % (v / v) fetal bovine serum. Using plasmids ordered from Addgene, optimized sgRNAs for ABHD17<sup>142</sup> (Sigma) were cloned into CRISPR*i* plasmids as previously described.<sup>143</sup> Cells were transduced with virus and allowed to grow before dilution to single cells in 96-wells plate. Cells were expanded from individual wells and screened for ABHD17 expression by western blot.

## Chapter 4 Conclusion and Future Directions

### 4A. Conclusion

*S*-palmitoylation is a dynamic post-translational modification that facilitates the trafficking and function of proteins. It is catalyzed by DHHC palmitoyltransferases, which usually attach a 16-carbon fatty acyl group to specific cysteines. Depalmitoylases can hydrolyze the thioester bond to participate in palmitate turnover and several enzymes have been reported to be depalmitoylases, including PPT1, APT1, APT2 and ABHD17 isoforms (A-C). This work focused on the biochemical characterization of the ABHD17 enzyme family in an effort to learn more about its cellular function and protein substrates.

Chapter 2 demonstrated how similar the three ABHD17 isoforms are, whereby they are presumably processed through similar processing pathways following protein production. We purified recombinant enzyme from both *E.coli* and HEK-293T cells to investigate the impact of *S*-palmitoylation on enzyme activity, and demonstrated that the rates of activity are similar based on the reaction of active site serine residue with FP-TAMRA, is comparable. Our initial development of assays, to determine whether recombinant ABHD17 can depalmitoylate a protein substrate *in vitro* were inconclusive and require additional effort to obtain a more definitive answer as to whether ABHD17 is a dedicated depalmitoylase. Given the physiological importance of the substrates ABHD17 is reported to depalmitoylate *in vivo*, it would be valuable to develop selective and potent inhibitors to further examine the cellular role of ABHD17. Similar to our lab's past efforts to develop inhibitors for APT1 and APT2 enzymes, we also



assessed compounds with different scaffolds that were initially identified in a high-throughput screen. We demonstrated that while some compounds (benzoxazinone derivatives) were effective at inhibiting recombinant full-length enzyme and HEK-293T lysate overexpressing ABHD17, the compounds did not change the overall *S*-palmitoylation levels when added directly to growing cells. Thus, future effort can be dedicated to exploring other derivatives of the benzoxazinones that are also active *in vivo*.

Chapter 3 discussed the biochemical and analytical methods available to study *S*-palmitoylation. Using our modified workflow, we obtained results similar to previously-published studies in addition to finding new putative palmitoylation sites on proteins not previously known to have them. Our method can be strengthened by developing bioinformatics tools to allow for large-scale comparisons of experimental results to the SwissPalm database, and facilitate the discovery of palmitoylation sites that can be later validated using biochemical routes. We also decided to apply our workflow to identify the putative substrates of ABHD17. In this process, we obtained unexpected results that contradicted a published report where cell-based assays were used to show that overexpressed ABHD17A depalmitoylates NRAS. Nevertheless, we have demonstrated that this method allows for the identification of sites of *S*-palmitoylation and can be a valuable tool to expedite the study of other enzymes involved in the *S*-acylation cycle, such as DHHC palmitoyltransferases.

The work presented here contributes to the understanding of ABHD17. However, numerous questions remain unanswered and would benefit from future studies. For example, the lipid substrate preference of ABHD17 remains unknown and would inform on their mechanism of action. There is still much to learn about the opposite side of *S*-palmitoylation cycle and regulation by DHHC enzymes. We hope that our modified workflow can spur more large-scale

proteomics studies to tease apart the contribution of specific DHHCs in regulating *S*-palmitoylation across various biological contexts.

#### **4B. Future directions**

Additional effort is still needed to understand the mechanism of action of ABHD17 enzymes. There has been some recent development of palmitoylated probes, which can be used to assess the depalmitoylating activity of ABHD17 isoforms. The depalmitoylation probes (DPPs) have been used to measure *in vitro* kinetics for APT1 and APT2; they were also added to cells to monitor endogenous depalmitoylase activity,<sup>74</sup> hence allowing for the detection of APT1 activity in the mitochondria.<sup>49</sup> Furthermore, this study by Amara et al,<sup>144</sup> presented quenched fluorogenic substrates, containing a palmitoylated cysteine that released the quencher molecule upon thioester hydrolysis, thus generating a fluorescence signal (**Figure 4-1**). These were used to test the activity of recombinant human APT1 and APT2, as well as PPT1 expressed from *T.gondii*. They demonstrated that the substrate was mainly processed by depalmitoylases since treatment with the non-specific inhibitor Palmostatin B blocked product formation in contrast to the common esterase substrate, 4-nitrophenyl octanoate. The authors also conjugated short peptides to their quenched fluorogenic substrates, with 2 amino acids flanking the Cys residue on each side, thereby creating a positional scanning library to map the substrate specificity of depalmitoylase enzymes. They then demonstrated that a Scribble-derived peptide sequence was preferentially hydrolyzed by APT2 and not APT1 or PPT1, corroborating a published cell-based study showing that APT2 was the enzyme depalmitoylating Scribble.<sup>57</sup> Therefore, the probes discussed above can be used to test the *in vitro* depalmitoylase activity for ABHD17 and determine how different the isoforms are.

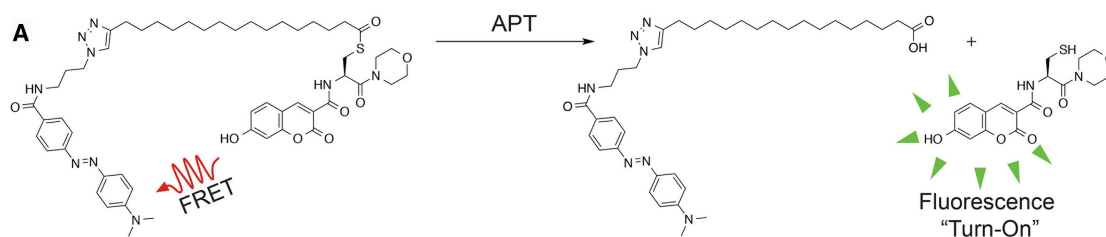


Figure 4-1 Quenched fluorogenic probe designed to measure depalmitoylase activity

The substrate contains a palmitoylated Cys that can be hydrolyzed to release the quencher molecule. License was obtained to reuse the published figure<sup>144</sup> in this document. Copyright to the licensed content publisher Elsevier.

Considering how the co-crystal structures of APT1 and APT2 with their respective isoform-selective inhibitors were instrumental in distinguishing key residues that confer inhibitor selectivity and provide structural insight into the differences between the two enzymes,<sup>119</sup> it would be valuable to pursue a similar route for ABHD17. The non-specific lipase inhibitor, HDFP has been shown to stabilize the melting temperatures of APT1 and APT2 by more than 10 °C<sup>119</sup> and could be used to mimic the long chain fatty acid of palmitate and aid in the co-crystallization of ABHD17. Having a solved structure in hand opens the possibility of taking computational approaches to (1) profile different types of lipid substrates to determine how they are accommodated in the enzyme active site to engage in the catalytic reaction and (2) simulate the docking of additional classes of compounds in an effort to find inhibitors targeting ABHD17.

Fatty acid amide hydrolase (FAAH) is involved in endocannabinoid signaling in the nervous system<sup>145</sup> and it has two important residues (Phe432 and Trp531), present at the interface between two cavities that form the enzyme active site, which are gating residues mediating active site access.<sup>146</sup> Molecular dynamics simulations, comparing the activity of wild-type and double mutant (Phe432 and Trp531) enzymes embedded in a palmitoyl-2-oleoyl-phosphatidylethanolamine (POPE) lipid bilayer, showed how the preferred fatty acid substrate, anandamide, is efficiently oriented into the active site to promote hydrolysis. Mutagenesis and kinetics experiments further confirmed the computational model.<sup>147</sup> Hence, this study could be

extended to other lipid-processing enzymes such as ABHD17 to clarify their substrate selectivity and function. Computational docking of libraries of small molecules targeting KRAS<sup>G12D</sup> mutant yielded candidate compounds that were then synthesized and shown to selectively bind to KRAS<sup>G12D</sup> and inhibit activity in primary patient samples and mouse xenograft models.<sup>148</sup> With a crystal structure of ABHD17, a similar strategy could be used to test new classes of ligands which would improve probe development to selectively target ABHD17.

In chapter 3, we used an acyl-RAC proteomics approach to identify sites of *S*-palmitoylation, where the palmitate group bound to the Cys was exchanged for an alkylating reagent following hydroxylamine treatment. However, this still remains an indirect method to measure sites of *S*-acylation. With the development of better analytical methods to address the challenge of this post-translational modification (PTM) being labile and hydrophobic, we would be able to directly assign the PTM site. Changing the column resin or adapting the mobile phase composition can extend quantitative proteomics to more hydrophobic peptides, thus allowing the direct analysis of the modified peptide and specific acyl chain. Efforts related to sample preparation methods to optimize acyl-thioester stability, separation, ionization, and fragmentation have not been explored outside of single peptide measurements. Another alternative would be to take a top-down proteomics approach, which has been used to study mutant KRAS4b purified from tumor samples proteoforms. The study identified proteoforms with specific PTMs under different cellular context, demonstrating the crosstalk between different PTMs in regulating activity of KRAS.<sup>149</sup>

Overall, the proposed experiments would contribute to a better understanding of the mechanism by which ABHD17 engages substrates and develop better chemical probes to study ABHD17 function. In addition, development of analytical strategies to directly study *S*-

palmitoylation would advance our understanding of how regulation of this PTM modulate important biological processes.

## Appendix      Enrichment of *S*-palmitoylated Proteins for Mass Spectrometry

### Analysis<sup>‡</sup>

#### Abstract

As the 10-year anniversary of their first introduction approaches, alkynyl fatty acids have revolutionized the analysis of *S*-palmitoylation dynamics, acting as functional mimics incorporated into native modification sites in cultured cells. The alkyne functional group provides a robust handle for biorthogonal Cu(I)-catalyzed azide-alkyne cycloaddition (CuAAC) to reporter-linked azides, forming a stable conjugate for enrichment for mass spectrometry analysis or in-gel fluorescence. Importantly, metabolic labeling enables time-dependent analysis of *S*-palmitoylation dynamics, which can be used to profile incorporation and turnover rates across the proteome. Here we present a protocol for cell labeling, click chemistry conjugation, enrichment, and isobaric tandem mass tag labeling for quantitative mass spectrometry analysis of protein *S*-palmitoylation.

---

<sup>‡</sup> This appendix chapter includes a book section from Protein Lipidation, Methods and Protocols (Springer 2019).<sup>131</sup> My contribution includes assistance in writing.

## Introduction

Protein *S*-palmitoylation describes the long chain fatty acylation modification of cysteine residues in proteins.<sup>2, 150</sup> zDHHC family protein acyltransferases catalyze acyl group transfer from long chain fatty acyl-CoAs to specific cysteine residues in protein substrates, which can then undergo spontaneous hydrolysis or enzyme-catalyzed depalmitoylation by protein depalmitoylases.<sup>1</sup> Hundreds of membrane-associated proteins require *S*-palmitoylation for proper localization, trafficking, and function. Despite the prevalence of *S*-palmitoylation, proteome-wide enrichment and analysis was confounded for decades by a lack of specific affinity reagents. The classic method for studying *S*-palmitoylation required metabolic addition of <sup>3</sup>[H]-labeled fatty acids analogs, immunoprecipitation of select targets, and lengthy exposure times. The introduction of hydroxylamine-switch methods (acyl-biotin exchange<sup>86</sup>, acyl-RAC<sup>88</sup>, etc.) provided the first approach to enrich and annotate *S*-acylation, demonstrating the widespread modification of hundreds of proteins in protozoa<sup>94</sup>, single cell eukaryotes<sup>120</sup>, and mammals.<sup>87, 134</sup> While this method is especially useful for analysis of primary tissues, hydroxylamine-switch methods only measure the steady-state levels of *S*-palmitoylation, and thus cannot provide any information on incorporation dynamics or turnover rates.

Alternatively, metabolic labeling with alkynyl fatty acid analogs has greatly simplified analysis of *S*-palmitoylation dynamics.<sup>151</sup> The commercially available alkynyl fatty acid analog 17-octadecynoic acid (17-ODYA) is metabolically incorporated into endogenous *S*-palmitoylation sites, enabling Cu(I)-catalyzed azide-alkyne cycloaddition (click chemistry) to fluorophore-linked azides for in-gel fluorescence or to biotin-azide for enrichment and mass spectrometry analysis.<sup>76</sup> This approach enables simple analysis of probe incorporation rates, as well as pulse-chase analysis of *S*-palmitoylation turnover dynamics.<sup>29, 96</sup> When coupled to

quantitative mass spectrometry methods, 17-ODYA labeling and enrichment has identified *S*-palmitoylated proteins with accelerated turnover kinetics, including proteins involved in cell polarity and growth.<sup>29, 57</sup> Through these methods, it is now experimentally feasible to broadly profile *S*-palmitoylation dynamics in cultured yeast<sup>152</sup>, protozoa<sup>94, 95</sup>, and mammalian cells.<sup>2, 76,</sup>  
<sup>151</sup> Here we present a workflow for multiplexed analysis of *S*-palmitoylation leveraging isobaric TMT quantitation by mass spectrometry. This protocol assumes collaboration with a mass spectrometry facility, able to perform the experiment and assist in any data analysis.

## **Materials**

Use ultrapure water (prepared by purifying deionized water, to attain a sensitivity of 18 MΩ-cm at 25 °C) and analytical grade reagents. Use phosphate buffers throughout the protocol. Do not use Tris buffers or EDTA prior to performing the click reaction, since these reagents inhibit the copper(I)-catalyzed click chemistry reaction. Discard waste materials following the appropriate waste disposal regulations.

## **Equipment and Supplies**

1. Cell culture facility including CO<sub>2</sub> incubator and biosafety cabinets cell culture hoods.
2. Branson Ultrasonics Sonifier S-450A Analog Ultrasonic Cell Disruptor/Homogenizer with double stepped tip (64 to 247 μm amplitude).
3. Beckman Optima L-70 ultracentrifuge with Sorvall F50L-24X1.5mL microrotor.
4. Absorbance spectrophotometer or plate reader to measure 700 nm absorbance measurements for protein quantitation.



5. 15 mL conical centrifuge tubes, 2 mL microcentrifuge tubes, 1.5 mL thick-walled microcentrifuge tubes (Beckman), 1.5 mL screw cap microcentrifuge tubes, mass spectrometry autosampler vials.
6. SDS-PAGE gels and electrophoresis equipment, such as BioRad Mini-PROTEAN tetra cell vertical electrophoresis system with precast 10% SDS-PAGE gels, 4X SDS loading buffer supplemented with  $\beta$ -mercaptoethanol, SDS-PAGE running buffer, and pre-stained protein molecular weight ladder.
7. Eppendorf 5810R tabletop centrifuge or equivalent with swinging bucket rotor for 15 mL tubes.
8. Promega Vac-Man Vacuum Manifold.
9. Poly-Prep chromatography column, 10 mL volume (Bio-Rad).
10. Oasis HLB  $\mu$ Elution plate (2 mg sorbent per well, 30  $\mu$ m particle size; Waters) and vacuum manifold.
11. Amersham Typhoon 5 Biomolecular Imager for in-gel fluorescence analysis.
12. Thermo Savant SPD1010 SpeedVac Concentrator System.

### **Chemicals and Reagents**

1. 20 mM 17-ODYA (1000x stock): 5.61 mg/ mL in DMSO (Cayman Chemical). Store aliquots at -80 °C.
2. ODYA labeling medium: culture medium, dialyzed serum, any required supplements, and 20  $\mu$ M 17-ODYA (1x). Sonicate the medium if necessary to dissolve 17-ODYA.
3. 20 mM palmitic acid (1000x stock): 5.13 mg / mL in DMSO. Sonicate the medium if necessary to dissolve the palmitic acid.

4. Palmitic acid labeling medium: culture medium, dialyzed serum, any required supplements, and 20  $\mu$ M palmitic acid (1x).
5. Lysis Buffer: Dulbecco's phosphate buffered saline (DPBS), 20  $\mu$ M hexadecylfluorophosphonate (HDFP) (see **note 1**).
6. DC Protein Assay Reagent (Bio-Rad).
7. TBTA solution (1x): Prepare 83 mM Tris((1-benzyl-1H-1,2,3-triazol-4-yl)methyl)amine ligand (TBTA; Click Chemistry Tools) 50x stock solution (44.25 mg / mL) in DMSO. Store at -80 °C for long-term storage. Dilute the 50x stock solution in DMSO and t-butanol following a 1:9:40 ratio respectively. Store at room temperature for extended periods.
8. TCEP solution: 50 mM stock solution (14.35 mg / mL) tris(2-carboxyethyl)phosphine (TCEP-HCl-Sigma) in DPBS and adjusted to pH 7 using concentrated base (NaOH or KOH). Prepare fresh for each use.
9. Copper sulfate solution: 50 mM stock solution (7.98 mg / mL) Copper (II) sulfate anhydrous ( $\text{CuSO}_4$ ) solution in water. Store at room temperature for extended periods.
10. Biotin-PEG3-azide solution: 10 mM stock (4.44 mg / mL) (Click Chemistry) in DMSO, and store at -80 °C.
11. TAMRA-azide solution: 1 mM stock (0.63 mg / mL) (Click Chemistry Tools) in DMSO. Store at -80 °C.
12. Resuspension buffer: 6 M Urea (360 mg / mL) and 2% w/v (20 mg / mL) sodium dodecyl sulfate (SDS), adjusting pH to 7 with HCl. Make fresh before use (see **note 2**).

13. Reducing solution: 200 mM (57.4 mg / mL) TCEP-HCl stock solution. Reconstitute with equimolar potassium hydroxide to neutralize HCl. Confirm with pH indicator strips.  
Make fresh before use.
14. Alkylating solution: 400 mM (74.0 mg / mL) Iodoacetamide (Sigma) stock solution in water. Make fresh before use. Do not store in direct light.
13. Hydroxylamine solution: 5 M (347 mg / mL) Hydroxylamine hydrochloride (Sigma), neutralized to pH 7 with concentrated NaOH or KOH. Make fresh before use.
14. Chloroform (stored in light resistant bottle)
15. Acetonitrile
16. Methanol.
17. Streptavidin-agarose beads (Pierce).
18. Wash buffer A: for streptavidin beads: DPBS with 2 M (120 mg / mL) Urea, 0.2% w / v (2 mg / mL) SDS
19. Wash buffer B: 2 M urea in DPBS, pH 7.
20. TMTsixplex Isobaric Label Reagent Set (Thermo Fisher)
21. TEAB buffer: 50 mM triethylammonium bicarbonate (TEAB, from 1 M stock solution- Thermo Fisher)
22. Mass spectrometry-grade Trypsin/Lys C (Promega). Reconstitute 20 µg in 100 µL resuspension buffer provided.
23. Acetonitrile (MS grade)
24. Equilibration solution: 0.1% Trifluoroacetic acid in Water (MS grade)
25. Elution buffer: 70% Acetonitrile in Water (MS grade)

## Methods

This procedure performs optimally when carried out in a single day, without freeze-thaw steps. In order to minimize keratin contamination, work in a clean area and frequently change gloves throughout the procedure. Be sure to prepare a sufficient number of replicates (N = 3 or more) per condition for confident analysis. Here we describe a comparison between palmitic acid and 17-ODYA treated cells.

### Metabolic cell labeling with 17-ODYA

1. Grow cells to desired density in standard culture medium. Plan for at least 3 biological replicates per condition; depending on the cell type, 15 cm dishes should provide enough protein for 1 biological replicate.
2. Wash cells gently with warm DPBS (37°C) and add ODYA Labeling Medium or Palmitic Acid Labeling Medium for the desired time. (see **note 3**).
3. Wash cells three times with cold DPBS and harvesting using a cell scraper into a 1.5 mL microcentrifuge tube.
4. Pellet cells by low speed centrifugation (500g) for 2 min at 4 °C. Aspirate DPBS and store the cell pellet at -80 °C (stable for several months).

### Preparation of cell lysates

1. Add 0.5 – 1 mL Lysis Buffer per 15 cm plate of confluent cells in the pellet. Sonicate pellet on ice for 2 x 10 s.
2. Transfer cell lysate to a thick-walled ultracentrifuge tube. Balance tube pairs and centrifuge for 45 minutes at 100,000g at 4 °C.

- Carefully remove supernatant (S100) and add 0.5 mL lysis buffer to the pellet (P100).  
Sonicate the P100 sample 1 x 10 s. The S100 fraction can be saved or discarded since it is not used in the remaining purification (see **Note 4**).
- Quantify protein concentration using the Lowry assay (DC Protein Assay) or other equivalent method. Normalize each sample to 2 mg / mL protein using Lysis Buffer.  
Aliquot 50 µg of P100 lysate to a 1.5 mL microcentrifuge tube for later in-gel fluorescence analysis.
- Add 1 - 2 mg of the P100 sample in 1 mL of Lysis Buffer and split evenly across 2 x 1.5 mL microcentrifuge tubes (0.5 mL each).
- Add 0.5 mL Methanol and 0.188 mL Chloroform and vortex. Centrifuge at max speed for 10 minutes at 4 °C. Carefully remove the aqueous and organic layers to isolate the white protein layer. Add 0.5 mL cold methanol to each tube and briefly sonicate. Recombine the samples and centrifuge at 8000g for 5 min at 4 °C. Carefully aspirate methanol and add 1 mL DPBS. Sonicate to create a disperse precipitate (see **Note 5**).

#### **Click reaction for in-gel fluorescence**

- Add 1 µL TAMRA-azide solution, 1 µL copper sulfate solution, and 3 µL TBTA solution to the 50 uL aliquot of 1 mg / mL P100 lysate in DPBS that was set aside. Vortex and let sample sit for 30 minutes at room temperature. Vortex again and wait for another 30 minutes.
- Add reducing 4X SDS sample loading buffer (supplemented with β-mercaptoethanol) to both samples. Avoid boiling to prevent thiol exchange or thioester hydrolysis. Analyze samples using standard SDS-PAGE. When the separation is complete, image the gel

using a laser scanning flatbed fluorescence imager to detect TAMRA fluorescence (with approximate excitation and emission wavelengths at 546 and 579 nm respectively).

### **Click reaction and enrichment**

1. Using 1 – 1.5 mg of P100 lysate, add 58  $\mu$ L of the Biotin-PEG3-azide solution, 23  $\mu$ L of the TCEP solution, 23  $\mu$ L of the copper sulfate solution, and 70  $\mu$ L of the TBTA solution (see **note 6**). Rotate end over end for 1 hour at room temperature.
2. Optional: For additional experimental controls for thioester-dependent labeling, to a separate series of replicates, add 1 M hydroxylamine (pH 7) and heat to 65 °C for 15 minutes.
3. Centrifuge the sample >8000g for 10 minutes at 4 °C. Decant and discard the supernatant. Add 0.5 mL cold DPBS, 0.5 mL cold methanol and sonicate a few seconds to disperse the protein pellet. Add 0.187 mL chloroform, vortex, and centrifuge >8000g for 10 minutes. Discard the aqueous and organic layers, saving the insoluble protein interface. Add 1 mL cold methanol, sonicate, and centrifuge 5 min at >8000g, and repeat. After decanting the residual methanol, add 0.5 mL Resuspension Buffer. Briefly vortex and sonicate if necessary to dissolve the protein pellet.
4. Add 25  $\mu$ L of the TCEP reducing solution (pH 7), vortex and leave at room temperature to react for 20 min. Then add 25  $\mu$ L of the iodoacetamide alkylation solution, mix and leave at room temperature for 20 min in the dark.
5. Quantify protein concentration using the Lowry assay (DC Protein Assay) or other equivalent method. Normalize each sample to a common protein concentration (see **note 7**).

6. Transfer the sample to a 15 mL capped conical vial and dilute with 5 mL DPBS. Transfer 75  $\mu$ L streptavidin-agarose bead slurry to a fresh 15 mL conical vial and wash twice with Wash Buffer A. Add to sample and rotate end over end for 90 minutes.
7. Place samples in a table top centrifuge and pellet beads at 500g for 3 minutes. Decant the supernatant. Add 10 mL of Wash Buffer A, turn vials upside down several times, and centrifuge at 500g for 3 minutes. Decant the supernatant and transfer beads in DBPS to individual Poly-prep chromatography columns.
8. Attach each chromatography column to a multi-port vacuum manifold, and add 3 x 10 mL of Wash Buffer 1, followed by 3 x 10 mL Wash Buffer B, each time allowing the buffer to nearly dry the column bed. Alternatively, the streptavidin beads can be sequentially washed with 4 cycles of centrifugation (500g x 3 min) in 10 mL Wash Buffer A and 4 cycles of centrifugation with 10 mL Wash Buffer B, carefully decanting the supernatant after each wash.

### **Digestion and desalting**

1. Transfer beads to screw cap microcentrifuge tubes in Wash Buffer B. Carefully remove any residual Wash Buffer and add 100  $\mu$ L TEAB Buffer, supplemented with 6  $\mu$ L Trypsin/LysC solution. Shake at 225 rpm at 37 °C for at least 4 hours or overnight (see **note 8**).
2. The next day, centrifuge samples at 500g for 1 minute. Transfer the supernatant to a new microcentrifuge tube. Wash the beads with an additional 50  $\mu$ L TEAB buffer and centrifuge again. Collect and combine the supernatants.

3. Resuspend each TMT label reagent (0.2 mg) in 50  $\mu\text{L}$  anhydrous acetonitrile and mix for 5 minutes. (see **note 9**). Add 45  $\mu\text{L}$  of each TMT label reagent to separate samples (*i.e.* palmitic acid control and 17-ODYA labeled;  $N = 3$ ) and leave for 1 hour to incubate at room temperature.
4. Add 1.2  $\mu\text{L}$  of 5 M Hydroxylamine (pH 7) to each sample and wait for 15 minutes to allow reaction to quench. Add 1.5  $\mu\text{L}$  of 50% Trifluoroacetic acid for a final concentration of about 0.8%. Combine labeled samples in one tube before desalting peptides.
5. Desalt using an Oasis PRIME HLB  $\mu\text{Elution}$  Plates (Waters), or equivalent solid phase extraction column. Condition resin with 200  $\mu\text{L}$  acetonitrile, followed by 200  $\mu\text{L}$  equilibration buffer. Load peptides onto the sorbent at low speed. Wash three times with 400  $\mu\text{L}$  equilibration buffer, followed by another three washes with 400  $\mu\text{L}$  water to remove salts. Elute peptides with 75  $\mu\text{L}$  of elution buffer (70% acetonitrile in water). Add an additional 75  $\mu\text{L}$  elution buffer and pool the eluents.
6. Dry the desalted elutions using a SpeedVac (Thermo) and store peptides at  $-80^{\circ}\text{C}$ .
7. Before mass spectrometry analysis, resuspend samples in MS-grade water containing 3% acetonitrile and 0.1% formic acid.
8. Contact an appropriate mass spectrometry core facility or collaborator for mass spectrometry analysis, preferably using a quadrupole Orbitrap (Q-Exactive series) or tribrid Orbitrap (Fusion series) instrument.

## Notes



1. HDFP is not commercially available, but can be substituted with other acyl fluorophosphonates, such as methyl arachidonyl fluorophosphonate. Hexadecylsulfonyl fluoride can also be used to block depalmitoylase activity.
2. It is important to measure and neutralize the pH of all buffers, since basic conditions can promote thioester hydrolysis. Be aware, 6 M Urea can shift the solution to a more basic pH, which should be equilibrated to neutral pH before use.
3. The labeling time for steady-state analysis typically requires 4 or more hours. Shorter time points can be used to measure differences in labeling rates between samples. Pulse-chase experiments require sufficient time for probe metabolic incorporation (> 90 min) prior to addition of excess palmitic acid (chase). Different cell lines have different labeling kinetics, so it is important to use in-gel fluorescence analysis to confirm labeling conditions. Also, cells labeled with palmitic acid provide a control for non-specific enrichment from streptavidin beads.
4. The S100 fraction has no detectable 17-ODYA labeling in-gel fluorescence analysis, and thus does not add any additional information to the mass spectrometry analysis. It is not essential to perform this fractionation step, but it concentrates the membrane proteome, removes soluble thioesterase enzymes, and limits nonspecific enrichment of common false positives.
5. The initial chloroform / methanol precipitation is critical to increase reproducibility by removing excess, unincorporated probe prior to click chemistry conjugation. In addition, the efficiency of the click chemistry reaction is not affected when the protein is present as an insoluble slurry.

6. Typical click chemistry reactions for proteomics analysis use 100  $\mu\text{M}$  biotin-azide. We find that increasing the biotin-azide concentration 5-fold significantly improves the reaction efficiency with alkynyl fatty acid conjugated proteins. We have not explored other commercially available copper ligands, which may further improve the reaction efficiency.
7. Following click chemistry, the chloroform / methanol precipitation and methanol washes can lead to variable levels of protein loss. It is critical to include this additional protein normalization for TMT-based mass spectrometry quantitation.
8. Agitation is used to maintain the bead slurry during digestion. The length of the digestion has not been thoroughly optimized, but longer incubations may affect thioester stability (which does not affect the analysis of tryptic peptides).
9. The TMT reagents can be diluted several-fold and used over multiple separate experiments. Experiments should be designed to match experimental groups ( $N = 3$ ) within the single multiplexed mass spectrometry experiment.

## References

1. Won, S. J.; Cheung See Kit, M.; Martin, B. R., Protein depalmitoylases. *Crit Rev Biochem Mol Biol* **2018**, *53* (1), 83-98.
2. Tom, C. T.; Martin, B. R., Fat chance! Getting a grip on a slippery modification. *ACS Chem Biol* **2013**, *8* (1), 46-57.
3. Liang, X.; Nazarian, A.; Erdjument-Bromage, H.; Bornmann, W.; Tempst, P.; Resh, M. D., Heterogeneous fatty acylation of Src family kinases with polyunsaturated fatty acids regulates raft localization and signal transduction. *J Biol Chem* **2001**, *276* (33), 30987-94.
4. Thinon, E.; Percher, A.; Hang, H. C., Bioorthogonal Chemical Reporters for Monitoring Unsaturated Fatty-Acylated Proteins. *Chembiochem* **2016**, *17* (19), 1800-1803.
5. Greaves, J.; Munro, K. R.; Davidson, S. C.; Riviere, M.; Wojno, J.; Smith, T. K.; Tomkinson, N. C.; Chamberlain, L. H., Molecular basis of fatty acid selectivity in the zDHHC family of S-acyltransferases revealed by click chemistry. *Proc Natl Acad Sci U S A* **2017**, *114* (8), E1365-E1374.
6. Lobo, S.; Greentree, W. K.; Linder, M. E.; Deschenes, R. J., Identification of a Ras palmitoyltransferase in *Saccharomyces cerevisiae*. *J Biol Chem* **2002**, *277* (43), 41268-73.
7. Fukata, M.; Fukata, Y.; Adesnik, H.; Nicoll, R. A.; Brecht, D. S., Identification of PSD-95 palmitoylating enzymes. *Neuron* **2004**, *44* (6), 987-96.
8. Gottlieb, C. D.; Zhang, S.; Linder, M. E., The Cysteine-rich Domain of the DHHC3 Palmitoyltransferase Is Palmitoylated and Contains Tightly Bound Zinc. *J Biol Chem* **2015**, *290* (49), 29259-69.
9. Li, Y.; Martin, B. R.; Cravatt, B. F.; Hofmann, S. L., DHHC5 protein palmitoylates flotillin-2 and is rapidly degraded on induction of neuronal differentiation in cultured cells. *J Biol Chem* **2012**, *287* (1), 523-30.
10. Thomas, G. M.; Hayashi, T.; Chiu, S. L.; Chen, C. M.; Haganir, R. L., Palmitoylation by DHHC5/8 targets GRIP1 to dendritic endosomes to regulate AMPA-R trafficking. *Neuron* **2012**, *73* (3), 482-96.
11. Brigidi, G. S.; Santyr, B.; Shimell, J.; Jovellar, B.; Bamji, S. X., Activity-regulated trafficking of the palmitoyl-acyl transferase DHHC5. *Nat Commun* **2015**, *6*, 8200.
12. Zeidman, R.; Buckland, G.; Cebecauer, M.; Eissmann, P.; Davis, D. M.; Magee, A. I., DHHC2 is a protein S-acyltransferase for Lck. *Mol Membr Biol* **2011**, *28* (7-8), 473-86.
13. Runkle, K. B.; Kharbanda, A.; Stypulkowski, E.; Cao, X. J.; Wang, W.; Garcia, B. A.; Witze, E. S., Inhibition of DHHC20-Mediated EGFR Palmitoylation Creates a Dependence on EGFR Signaling. *Mol Cell* **2016**, *62* (3), 385-96.
14. Swarthout, J. T.; Lobo, S.; Farh, L.; Croke, M. R.; Greentree, W. K.; Deschenes, R. J.; Linder, M. E., DHHC9 and GCP16 constitute a human protein fatty acyltransferase with specificity for H- and N-Ras. *J Biol Chem* **2005**, *280* (35), 31141-8.

15. Chai, S.; Cambronne, X. A.; Eichhorn, S. W.; Goodman, R. H., MicroRNA-134 activity in somatostatin interneurons regulates H-Ras localization by repressing the palmitoylation enzyme, DHHC9. *Proc Natl Acad Sci U S A* **2013**, *110* (44), 17898-903.
16. Raymond, F. L.; Tarpey, P. S.; Edkins, S.; Tofts, C.; O'Meara, S.; Teague, J.; Butler, A.; Stevens, C.; Barthorpe, S.; Buck, G.; Cole, J.; Dicks, E.; Gray, K.; Halliday, K.; Hills, K.; Hinton, J.; Jones, D.; Menzies, A.; Perry, J.; Raine, K.; Shepherd, R.; Small, A.; Varian, J.; Widaa, S.; Mallya, U.; Moon, J.; Luo, Y.; Shaw, M.; Boyle, J.; Kerr, B.; Turner, G.; Quarrell, O.; Cole, T.; Easton, D. F.; Wooster, R.; Bobrow, M.; Schwartz, C. E.; Gecz, J.; Stratton, M. R.; Futreal, P. A., Mutations in ZDHHC9, which encodes a palmitoyltransferase of NRAS and HRAS, cause X-linked mental retardation associated with a Marfanoid habitus. *Am J Hum Genet* **2007**, *80* (5), 982-7.
17. Lemonidis, K.; Werno, M. W.; Greaves, J.; Diez-Ardanuy, C.; Sanchez-Perez, M. C.; Salaun, C.; Thomson, D. M.; Chamberlain, L. H., The zDHHC family of S-acyltransferases. *Biochem Soc Trans* **2015**, *43* (2), 217-21.
18. Buss, J. E.; Sefton, B. M., Direct Identification of Palmitic Acid as the Lipid Attached to P21ras. *Molecular and Cellular Biology* **1986**, *6* (1), 116-122.
19. Hancock, J. F.; Magee, A. I.; Childs, J. E.; Marshall, C. J., All Ras Proteins Are Polyisoprenylated but Only Some Are Palmitoylated. *Cell* **1989**, *57* (7), 1167-1177.
20. Linder, M. E.; Middleton, P.; Hepler, J. R.; Taussig, R.; Gilman, A. G.; Mumby, S. M., Lipid modifications of G proteins: alpha subunits are palmitoylated. *Proc Natl Acad Sci U S A* **1993**, *90* (8), 3675-9.
21. Rocks, O.; Gerauer, M.; Vartak, N.; Koch, S.; Huang, Z. P.; Pechlivanis, M.; Kuhlmann, J.; Brunsveld, L.; Chandra, A.; Ellinger, B.; Waldmann, H.; Bastiaens, P. I., The palmitoylation machinery is a spatially organizing system for peripheral membrane proteins. *Cell* **2010**, *141* (3), 458-71.
22. Rocks, O.; Peyker, A.; Kahms, M.; Verveer, P. J.; Koerner, C.; Lumbierres, M.; Kuhlmann, J.; Waldmann, H.; Wittinghofer, A.; Bastiaens, P. I., An acylation cycle regulates localization and activity of palmitoylated Ras isoforms. *Science* **2005**, *307* (5716), 1746-52.
23. Webb, Y.; Hermida-Matsumoto, L.; Resh, M. D., Inhibition of protein palmitoylation, raft localization, and T cell signaling by 2-bromopalmitate and polyunsaturated fatty acids. *J Biol Chem* **2000**, *275* (1), 261-70.
24. Martin, B. R.; Lambert, N. A., Activated G Protein Gas Samples Multiple Endomembrane Compartments. *J Biol Chem* **2016**, *291* (39), 20295-20302.
25. Mumby, S. M.; Kleuss, C.; Gilman, A. G., Receptor regulation of G-protein palmitoylation. *Proc Natl Acad Sci U S A* **1994**, *91* (7), 2800-4.
26. Wedegaertner, P. B.; Bourne, H. R., Activation and depalmitoylation of Gs alpha. *Cell* **1994**, *77* (7), 1063-70.
27. Willumsen, B. M.; Cox, A. D.; Solski, P. A.; Der, C. J.; Buss, J. E., Novel determinants of H-Ras plasma membrane localization and transformation. *Oncogene* **1996**, *13* (9), 1901-9.
28. James, G.; Olson, E. N., Identification of a novel fatty acylated protein that partitions between the plasma membrane and cytosol and is deacylated in response to serum and growth factor stimulation. *J Biol Chem* **1989**, *264* (35), 20998-1006.
29. Martin, B. R.; Wang, C.; Adibekian, A.; Tully, S. E.; Cravatt, B. F., Global profiling of dynamic protein palmitoylation. *Nat Methods* **2011**, *9* (1), 84-9.
30. Wan, L.; Kang, Y., Pleiotropic roles of AEG-1/MTDH/LYRIC in breast cancer. *Adv Cancer Res* **2013**, *120*, 113-34.

31. Blanc, M.; David, F.; Abrami, L.; Migliozi, D.; Armand, F.; B,rgi, J.; van der Goot, F., *SwissPalm: Protein Palmitoylation database*. 2015; Vol. 4.
32. Wang, W.; Runkle, K. B.; Terkowski, S. M.; Ekaireb, R. I.; Witze, E. S., Protein Depalmitoylation Is Induced by Wnt5a and Promotes Polarized Cell Behavior. *J Biol Chem* **2015**, *290* (25), 15707-16.
33. Camp, L. A.; Hofmann, S. L., Purification and properties of a palmitoyl-protein thioesterase that cleaves palmitate from H-Ras. *J Biol Chem* **1993**, *268* (30), 22566-74.
34. Duncan, J. A.; Gilman, A. G., A Cytoplasmic Acyl-Protein Thioesterase That Removes Palmitate from G Protein  $\alpha$  Subunits and p21RAS. *Journal of Biological Chemistry* **1998**, *273* (25), 15830-15837.
35. Verkruyse, L. A.; Hofmann, S. L., Lysosomal targeting of palmitoyl-protein thioesterase. *J Biol Chem* **1996**, *271* (26), 15831-6.
36. Vesa, J.; Hellsten, E.; Verkruyse, L. A.; Camp, L. A.; Rapola, J.; Santavuori, P.; Hofmann, S. L.; Peltonen, L., Mutations in the palmitoyl protein thioesterase gene causing infantile neuronal ceroid lipofuscinosis. *Nature* **1995**, *376* (6541), 584-7.
37. Greaves, J.; Lemonidis, K.; Gorleku, O. A.; Cruchaga, C.; Grefen, C.; Chamberlain, L. H., Palmitoylation-induced aggregation of cysteine-string protein mutants that cause neuronal ceroid lipofuscinosis. *J Biol Chem* **2012**, *287* (44), 37330-9.
38. Henderson, M. X.; Wirak, G. S.; Zhang, Y. Q.; Dai, F.; Ginsberg, S. D.; Dolzhanskaya, N.; Staropoli, J. F.; Nijssen, P. C.; Lam, T. T.; Roth, A. F.; Davis, N. G.; Dawson, G.; Velinov, M.; Chandra, S. S., Neuronal ceroid lipofuscinosis with DNAJC5/CSPalpha mutation has PPT1 pathology and exhibit aberrant protein palmitoylation. *Acta Neuropathol* **2016**, *131* (4), 621-37.
39. Sugimoto, H.; Hayashi, H.; Yamashita, S., Purification, cDNA cloning, and regulation of lysophospholipase from rat liver. *J Biol Chem* **1996**, *271* (13), 7705-11.
40. Hedberg, C.; Dekker, F. J.; Rusch, M.; Renner, S.; Wetzel, S.; Vartak, N.; Gerding-Reimers, C.; Bon, R. S.; Bastiaens, P. I.; Waldmann, H., Development of highly potent inhibitors of the Ras-targeting human acyl protein thioesterases based on substrate similarity design. *Angew Chem Int Ed Engl* **2011**, *50* (42), 9832-7.
41. Dekker, F. J.; Rocks, O.; Vartak, N.; Menninger, S.; Hedberg, C.; Balamurugan, R.; Wetzel, S.; Renner, S.; Gerauer, M.; Scholermann, B.; Rusch, M.; Kramer, J. W.; Rauh, D.; Coates, G. W.; Brunsveld, L.; Bastiaens, P. I.; Waldmann, H., Small-molecule inhibition of APT1 affects Ras localization and signaling. *Nat Chem Biol* **2010**, *6* (6), 449-56.
42. Kong, E.; Peng, S.; Chandra, G.; Sarkar, C.; Zhang, Z.; Bagh, M. B.; Mukherjee, A. B., Dynamic palmitoylation links cytosol-membrane shuttling of acyl-protein thioesterase-1 and acyl-protein thioesterase-2 with that of proto-oncogene H-ras product and growth-associated protein-43. *J Biol Chem* **2013**, *288* (13), 9112-25.
43. Yeh, D. C.; Duncan, J. A.; Yamashita, S.; Michel, T., Depalmitoylation of endothelial nitric-oxide synthase by acyl-protein thioesterase 1 is potentiated by Ca(2+)-calmodulin. *J Biol Chem* **1999**, *274* (46), 33148-54.
44. Siegel, G.; Obernosterer, G.; Fiore, R.; Oehmen, M.; Bicker, S.; Christensen, M.; Khudayberdiev, S.; Leuschner, P. F.; Busch, C. J.; Kane, C.; Hubel, K.; Dekker, F.; Hedberg, C.; Rengarajan, B.; Drepper, C.; Waldmann, H.; Kauppinen, S.; Greenberg, M. E.; Draguhn, A.; Rehmsmeier, M.; Martinez, J.; Schratt, G. M., A functional screen implicates microRNA-138-dependent regulation of the depalmitoylation enzyme APT1 in dendritic spine morphogenesis. *Nat Cell Biol* **2009**, *11* (6), 705-16.

45. Toyoda, T.; Sugimoto, H.; Yamashita, S., Sequence, expression in Escherichia coli, and characterization of lysophospholipase II. *Biochim Biophys Acta* **1999**, *1437* (2), 182-93.
46. Manna, J. D.; Wepy, J. A.; Hsu, K. L.; Chang, J. W.; Cravatt, B. F.; Marnett, L. J., Identification of the major prostaglandin glycerol ester hydrolase in human cancer cells. *J Biol Chem* **2014**, *289* (49), 33741-53.
47. Vartak, N.; Papke, B.; Grecco, H. E.; Rossmannek, L.; Waldmann, H.; Hedberg, C.; Bastiaens, P. I., The autodepalmitoylating activity of APT maintains the spatial organization of palmitoylated membrane proteins. *Biophys J* **2014**, *106* (1), 93-105.
48. Adachi, N.; Hess, D. T.; McLaughlin, P.; Stamler, J. S., S-Palmitoylation of a Novel Site in the beta2-Adrenergic Receptor Associated with a Novel Intracellular Itinerary. *J Biol Chem* **2016**, *291* (38), 20232-46.
49. Kathayat, R. S.; Cao, Y.; Elvira, P. D.; Sandoz, P. A.; Zaballa, M. E.; Springer, M. Z.; Drake, L. E.; Macleod, K. F.; van der Goot, F. G.; Dickinson, B. C., Active and dynamic mitochondrial S-depalmitoylation revealed by targeted fluorescent probes. *Nat Commun* **2018**, *9* (1), 334.
50. Yang, W.; Di Vizio, D.; Kirchner, M.; Steen, H.; Freeman, M. R., Proteome scale characterization of human S-acylated proteins in lipid raft-enriched and non-raft membranes. *Mol Cell Proteomics* **2010**, *9* (1), 54-70.
51. Bachovchin, D. A.; Ji, T.; Li, W.; Simon, G. M.; Blankman, J. L.; Adibekian, A.; Hoover, H.; Niessen, S.; Cravatt, B. F., Superfamily-wide portrait of serine hydrolase inhibition achieved by library-versus-library screening. *Proc Natl Acad Sci U S A* **2010**, *107* (49), 20941-6.
52. Abrami, L.; Dallavilla, T.; Sandoz, P. A.; Demir, M.; Kunz, B.; Savoglidis, G.; Hatzimanikatis, V.; van der Goot, F. G., Identification and dynamics of the human ZDHHC16-ZDHHC6 palmitoylation cascade. *Elife* **2017**, *6*.
53. Deck, P.; Pendzialek, D.; Biel, M.; Wagner, M.; Popkirova, B.; Ludolph, B.; Kragol, G.; Kuhlmann, J.; Giannis, A.; Waldmann, H., Development and biological evaluation of acyl protein thioesterase 1 (APT1) inhibitors. *Angew Chem Int Ed Engl* **2005**, *44* (31), 4975-80.
54. Xu, J.; Hedberg, C.; Dekker, F. J.; Li, Q.; Haigis, K. M.; Hwang, E.; Waldmann, H.; Shannon, K., Inhibiting the palmitoylation/depalmitoylation cycle selectively reduces the growth of hematopoietic cells expressing oncogenic Nras. *Blood* **2012**, *119* (4), 1032-5.
55. Grecco, H. E.; Schmick, M.; Bastiaens, P. I., Signaling from the living plasma membrane. *Cell* **2011**, *144* (6), 897-909.
56. Yokoi, N.; Fukata, Y.; Sekiya, A.; Murakami, T.; Kobayashi, K.; Fukata, M., Identification of PSD-95 Depalmitoylating Enzymes. *J Neurosci* **2016**, *36* (24), 6431-44.
57. Hernandez, J. L.; Davda, D.; Cheung See Kit, M.; Majmudar, J. D.; Won, S. J.; Gang, M.; Pasupuleti, S. C.; Choi, A. I.; Bartkowiak, C. M.; Martin, B. R., APT2 Inhibition Restores Scribble Localization and S-Palmitoylation in Snail-Transformed Cells. *Cell Chem Biol* **2017**, *24* (1), 87-97.
58. Akimzhanov, A. M.; Boehning, D., Rapid and transient palmitoylation of the tyrosine kinase Lck mediates Fas signaling. *Proc Natl Acad Sci U S A* **2015**, *112* (38), 11876-80.
59. Jia, L.; Chisari, M.; Maktabi, M. H.; Sobieski, C.; Zhou, H.; Konopko, A. M.; Martin, B. R.; Mennerick, S. J.; Blumer, K. J., A mechanism regulating G protein-coupled receptor signaling that requires cycles of protein palmitoylation and depalmitoylation. *J Biol Chem* **2014**, *289* (9), 6249-57.
60. Berg, V.; Rusch, M.; Vartak, N.; Jüngst, C.; Schauss, A.; Waldmann, H.; Hedberg, C.; Pallasch, C. P.; Bastiaens, P. I.; Hallek, M.; Wendtner, C. M.; Frenzel, L. P., miRs-138 and

- 424 control palmitoylation-dependent CD95-mediated cell death by targeting acyl protein thioesterases 1 and 2 in CLL. *Blood* **2015**, *125* (19), 2948-57.
61. Lin, D. T.; Conibear, E., ABHD17 proteins are novel protein depalmitoylases that regulate N-Ras palmitate turnover and subcellular localization. *Elife* **2015**, *4*, e11306.
  62. Chen, S.; Zhu, B.; Yin, C.; Liu, W.; Han, C.; Chen, B.; Liu, T.; Li, X.; Chen, X.; Li, C.; Hu, L.; Zhou, J.; Xu, Z. X.; Gao, X.; Wu, X.; Goding, C. R.; Cui, R., Palmitoylation-dependent activation of MC1R prevents melanomagenesis. *Nature* **2017**, *549* (7672), 399-403.
  63. Vujic, I.; Sanlorenzo, M.; Esteve-Puig, R.; Vujic, M.; Kwong, A.; Tsumura, A.; Murphy, R.; Moy, A.; Posch, C.; Monshi, B.; Rappersberger, K.; Ortiz-Urda, S., Acyl protein thioesterase 1 and 2 (APT-1, APT-2) inhibitors palmostatin B, ML348 and ML349 have different effects on NRAS mutant melanoma cells. *Oncotarget* **2016**, *7* (6), 7297-306.
  64. Adibekian, A.; Martin, B. R.; Chang, J. W.; Hsu, K. L.; Tsuboi, K.; Bachovchin, D. A.; Speers, A. E.; Brown, S. J.; Spicer, T.; Fernandez-Vega, V.; Ferguson, J.; Cravatt, B. F.; Hodder, P.; Rosen, H., Characterization of a Selective, Reversible Inhibitor of Lysophospholipase 2 (LYPLA2). In *Probe Reports from the NIH Molecular Libraries Program*, Bethesda (MD), 2010.
  65. Adibekian, A.; Martin, B. R.; Chang, J. W.; Hsu, K. L.; Tsuboi, K.; Bachovchin, D. A.; Speers, A. E.; Brown, S. J.; Spicer, T.; Fernandez-Vega, V.; Ferguson, J.; Cravatt, B. F.; Hodder, P.; Rosen, H., Characterization of a Selective, Reversible Inhibitor of Lysophospholipase 1 (LYPLA1). In *Probe Reports from the NIH Molecular Libraries Program*, Bethesda (MD), 2010.
  66. Adibekian, A.; Martin, B. R.; Chang, J. W.; Hsu, K. L.; Tsuboi, K.; Bachovchin, D. A.; Speers, A. E.; Brown, S. J.; Spicer, T.; Fernandez-Vega, V.; Ferguson, J.; Hodder, P. S.; Rosen, H.; Cravatt, B. F., Confirming target engagement for reversible inhibitors in vivo by kinetically tuned activity-based probes. *J Am Chem Soc* **2012**, *134* (25), 10345-8.
  67. Won, S. J.; Eschweiler, J. D.; Majmudar, J. D.; Chong, F. S.; Hwang, S. Y.; Ruotolo, B. T.; Martin, B. R., Affinity-Based Selectivity Profiling of an In-Class Selective Competitive Inhibitor of Acyl Protein Thioesterase 2. *ACS Med Chem Lett* **2017**, *8* (2), 215-220.
  68. Adibekian, A.; Martin, B. R.; Speers, A. E.; Brown, S. J.; Spicer, T.; Fernandez-Vega, V.; Ferguson, J.; Cravatt, B. F.; Hodder, P.; Rosen, H., Optimization and characterization of a triazole urea dual inhibitor for lysophospholipase 1 (LYPLA1) and lysophospholipase 2 (LYPLA2). In *Probe Reports from the NIH Molecular Libraries Program*, Bethesda (MD), 2010.
  69. Adibekian, A.; Martin, B. R.; Wang, C.; Hsu, K. L.; Bachovchin, D. A.; Niessen, S.; Hoover, H.; Cravatt, B. F., Click-generated triazole ureas as ultrapotent in vivo-active serine hydrolase inhibitors. *Nat Chem Biol* **2011**, *7* (7), 469-78.
  70. Hulce, J. J.; Joslyn, C.; Speers, A. E.; Brown, S. J.; Spicer, T.; Fernandez-Vega, V.; Ferguson, J.; Cravatt, B. F.; Hodder, P.; Rosen, H., An in Vivo Active Carbamate-based Dual Inhibitor of Lysophospholipase 1 (LYPLA1) and Lysophospholipase 2 (LYPLA2). In *Probe Reports from the NIH Molecular Libraries Program*, Bethesda (MD), 2010.
  71. Cognetta, A. B., 3rd; Niphakis, M. J.; Lee, H. C.; Martini, M. L.; Hulce, J. J.; Cravatt, B. F., Selective N-Hydroxyhydantoin Carbamate Inhibitors of Mammalian Serine Hydrolases. *Chem Biol* **2015**, *22* (7), 928-37.
  72. Davda, D.; Martin, B. R., Acyl protein thioesterase inhibitors as probes of dynamic S-palmitoylation. *Medchemcomm* **2014**, *5* (3), 268-276.

73. Satou, M.; Nishi, Y.; Yoh, J.; Hattori, Y.; Sugimoto, H., Identification and characterization of acyl-protein thioesterase 1/lysophospholipase I as a ghrelin deacylation/lysophospholipid hydrolyzing enzyme in fetal bovine serum and conditioned medium. *Endocrinology* **2010**, *151* (10), 4765-75.
74. Kathayat, R. S.; Elvira, P. D.; Dickinson, B. C., A fluorescent probe for cysteine depalmitoylation reveals dynamic APT signaling. *Nat Chem Biol* **2017**, *13* (2), 150-152.
75. Ahearn, I. M.; Tsai, F. D.; Court, H.; Zhou, M.; Jennings, B. C.; Ahmed, M.; Fehrenbacher, N.; Linder, M. E.; Philips, M. R., FKBP12 binds to acylated H-ras and promotes depalmitoylation. *Mol Cell* **2011**, *41* (2), 173-85.
76. Martin, B. R.; Cravatt, B. F., Large-scale profiling of protein palmitoylation in mammalian cells. *Nat Methods* **2009**, *6* (2), 135-8.
77. Tortosa, E.; Adolfs, Y.; Fukata, M.; Pasterkamp, R. J.; Kapitein, L. C.; Hoogenraad, C. C., Dynamic Palmitoylation Targets MAP6 to the Axon to Promote Microtubule Stabilization during Neuronal Polarization. *Neuron* **2017**, *94* (4), 809-825 e7.
78. Savinainen, J. R.; Patel, J. Z.; Parkkari, T.; Navia-Paldanius, D.; Marjamaa, J. J.; Laitinen, T.; Nevalainen, T.; Laitinen, J. T., Biochemical and pharmacological characterization of the human lymphocyte antigen B-associated transcript 5 (BAT5/ABHD16A). *PLoS One* **2014**, *9* (10), e109869.
79. van der Weyden, L.; Arends, M. J.; Campbell, A. D.; Bald, T.; Wardle-Jones, H.; Griggs, N.; Velasco-Herrera, M. D.; Tuting, T.; Sansom, O. J.; Karp, N. A.; Clare, S.; Gleeson, D.; Ryder, E.; Galli, A.; Tuck, E.; Cambridge, E. L.; Voet, T.; Macaulay, I. C.; Wong, K.; Sanger Mouse Genetics, P.; Spiegel, S.; Speak, A. O.; Adams, D. J., Genome-wide in vivo screen identifies novel host regulators of metastatic colonization. *Nature* **2017**, *541* (7636), 233-236.
80. Gumbiner, B. M.; Kim, N. G., The Hippo-YAP signaling pathway and contact inhibition of growth. *J Cell Sci* **2014**, *127* (Pt 4), 709-17.
81. Kim, N. G.; Gumbiner, B. M., Cell contact and Nf2/Merlin-dependent regulation of TEAD palmitoylation and activity. *Proc Natl Acad Sci U S A* **2019**, *116* (20), 9877-9882.
82. Schlesinger, M. J.; Magee, A. I.; Schmidt, M. F., Fatty acid acylation of proteins in cultured cells. *J Biol Chem* **1980**, *255* (21), 10021-4.
83. Tsai, F. D.; Wynne, J. P.; Ahearn, I. M.; Philips, M. R., Metabolic labeling of Ras with tritiated palmitate to monitor palmitoylation and depalmitoylation. *Methods Mol Biol* **2014**, *1120*, 33-41.
84. Hang, H. C.; Geutjes, E. J.; Grotenbreg, G.; Pollington, A. M.; Bijlmakers, M. J.; Ploegh, H. L., Chemical probes for the rapid detection of Fatty-acylated proteins in Mammalian cells. *J Am Chem Soc* **2007**, *129* (10), 2744-5.
85. Drisdell, R. C.; Green, W. N., Labeling and quantifying sites of protein palmitoylation. *Biotechniques* **2004**, *36* (2), 276-85.
86. Wan, J.; Roth, A. F.; Bailey, A. O.; Davis, N. G., Palmitoylated proteins: purification and identification. *Nat Protoc* **2007**, *2* (7), 1573-84.
87. Kang, R.; Wan, J.; Arstikaitis, P.; Takahashi, H.; Huang, K.; Bailey, A. O.; Thompson, J. X.; Roth, A. F.; Drisdell, R. C.; Mastro, R.; Green, W. N.; Yates, J. R., 3rd; Davis, N. G.; El-Husseini, A., Neural palmitoyl-proteomics reveals dynamic synaptic palmitoylation. *Nature* **2008**, *456* (7224), 904-9.



88. Forrester, M. T.; Hess, D. T.; Thompson, J. W.; Hultman, R.; Moseley, M. A.; Stamler, J. S.; Casey, P. J., Site-specific analysis of protein S-acylation by resin-assisted capture. *J Lipid Res* **2011**, *52* (2), 393-8.
89. Charron, G.; Zhang, M. M.; Yount, J. S.; Wilson, J.; Raghavan, A. S.; Shamir, E.; Hang, H. C., Robust fluorescent detection of protein fatty-acylation with chemical reporters. *J Am Chem Soc* **2009**, *131* (13), 4967-75.
90. Hernandez, J. L.; Majmudar, J. D.; Martin, B. R., Profiling and inhibiting reversible palmitoylation. *Curr Opin Chem Biol* **2013**, *17* (1), 20-6.
91. Martin, B. R., Nonradioactive analysis of dynamic protein palmitoylation. *Curr Protoc Protein Sci* **2013**, *73*, Unit 14 15.
92. Yount, J. S.; Moltedo, B.; Yang, Y. Y.; Charron, G.; Moran, T. M.; Lopez, C. B.; Hang, H. C., Palmitoylome profiling reveals S-palmitoylation-dependent antiviral activity of IFITM3. *Nat Chem Biol* **2010**, *6* (8), 610-4.
93. Hernandez, J. L.; Davda, D.; Majmudar, J. D.; Won, S. J.; Prakash, A.; Choi, A. I.; Martin, B. R., Correlated S-palmitoylation profiling of Snail-induced epithelial to mesenchymal transition. *Mol Biosyst* **2016**, *12* (6), 1799-808.
94. Jones, M. L.; Collins, M. O.; Goulding, D.; Choudhary, J. S.; Rayner, J. C., Analysis of protein palmitoylation reveals a pervasive role in Plasmodium development and pathogenesis. *Cell Host Microbe* **2012**, *12* (2), 246-58.
95. Foe, I. T.; Child, M. A.; Majmudar, J. D.; Krishnamurthy, S.; van der Linden, W. A.; Ward, G. E.; Martin, B. R.; Bogyo, M., Global Analysis of Palmitoylated Proteins in *Toxoplasma gondii*. *Cell Host Microbe* **2015**, *18* (4), 501-11.
96. Zhang, M. M.; Tsou, L. K.; Charron, G.; Raghavan, A. S.; Hang, H. C., Tandem fluorescence imaging of dynamic S-acylation and protein turnover. *Proc Natl Acad Sci U S A* **2010**, *107* (19), 8627-32.
97. Thiele, C.; Papan, C.; Hoelper, D.; Kusserow, K.; Gaebler, A.; Schoene, M.; Piotrowitz, K.; Lohmann, D.; Spandl, J.; Stevanovic, A.; Shevchenko, A.; Kuerschner, L., Tracing fatty acid metabolism by click chemistry. *ACS Chem Biol* **2012**, *7* (12), 2004-11.
98. Davda, D.; El Azzouny, M. A.; Tom, C. T.; Hernandez, J. L.; Majmudar, J. D.; Kennedy, R. T.; Martin, B. R., Profiling targets of the irreversible palmitoylation inhibitor 2-bromopalmitate. *ACS Chem Biol* **2013**, *8* (9), 1912-7.
99. Xu, S.; Nam, S. M.; Kim, J. H.; Das, R.; Choi, S. K.; Nguyen, T. T.; Quan, X.; Choi, S. J.; Chung, C. H.; Lee, E. Y.; Lee, I. K.; Wiederkehr, A.; Wollheim, C. B.; Cha, S. K.; Park, K. S., Palmitate induces ER calcium depletion and apoptosis in mouse podocytes subsequent to mitochondrial oxidative stress. *Cell Death Dis* **2015**, *6*, e1976.
100. Hunt, D. F.; Yates, J. R.; Shabanowitz, J.; Winston, S.; Hauer, C. R., Protein sequencing by tandem mass spectrometry. *Proc Natl Acad Sci U S A* **1986**, *83* (17), 6233-7.
101. Biemann, K., Contributions of mass spectrometry to peptide and protein structure. *Biomed Environ Mass Spectrom* **1988**, *16* (1-12), 99-111.
102. Covey, T.; Lee, E.; Bruins, A.; Henion, J., Liquid chromatography/mass spectrometry. *Analytical Chemistry*: 1986; Vol. 58, pp 1451A-1461A

103. Zhang, Y.; Fonslow, B. R.; Shan, B.; Baek, M. C.; Yates, J. R., Protein analysis by shotgun/bottom-up proteomics. *Chem Rev* **2013**, *113* (4), 2343-94.
104. Ducret, A.; Van Oostveen, I.; Eng, J. K.; Yates, J. R.; Aebersold, R., High throughput protein characterization by automated reverse-phase chromatography/electrospray tandem mass spectrometry. *Protein Sci* **1998**, *7* (3), 706-19.
105. UniProt Consortium, T., UniProt: the universal protein knowledgebase. *Nucleic Acids Res* **2018**, *46* (5), 2699.
106. Eng, J. K.; McCormack, A. L.; Yates, J. R., An approach to correlate tandem mass spectral data of peptides with amino acid sequences in a protein database. *J Am Soc Mass Spectrom* **1994**, *5* (11), 976-89.
107. Yates, J. R.; Eng, J. K.; McCormack, A. L.; Schieltz, D., Method to correlate tandem mass spectra of modified peptides to amino acid sequences in the protein database. *Anal Chem* **1995**, *67* (8), 1426-36.
108. Deribe, Y. L.; Pawson, T.; Dikic, I., Post-translational modifications in signal integration. *Nature Structural & Molecular Biology* **2010**, *17* (6), 666-672.
109. Pepinsky, R. B.; Zeng, C. H.; Wen, D. Y.; Rayhorn, P.; Baker, D. P.; Williams, K. P.; Bixler, S. A.; Ambrose, C. M.; Garber, E. A.; Miatkowski, K.; Taylor, F. R.; Wang, E. A.; Galdes, A., Identification of a palmitic acid-modified form of human Sonic hedgehog. *Journal of Biological Chemistry* **1998**, *273* (22), 14037-14045.
110. Bilder, D., Epithelial polarity and proliferation control: links from the Drosophila neoplastic tumor suppressors. *Genes & Development* **2004**, *18* (16), 1909-1925.
111. Wang, T.; Yu, H.; Hughes, N. W.; Liu, B.; Kendirli, A.; Klein, K.; Chen, W. W.; Lander, E. S.; Sabatini, D. M., Gene Essentiality Profiling Reveals Gene Networks and Synthetic Lethal Interactions with Oncogenic Ras. *Cell* **2017**, *168* (5), 890-903.e15.
112. Laude, A. J.; Prior, I. A., Palmitoylation and localisation of RAS isoforms are modulated by the hypervariable linker domain. *Journal of Cell Science* **2008**, *121* (4), 421-427.
113. Dhillon, A. S.; Hagan, S.; Rath, O.; Kolch, W., MAP kinase signalling pathways in cancer. *Oncogene* **2007**, *26* (22), 3279-3290.
114. Mendoza, M. C.; Er, E. E.; Blenis, J., The Ras-ERK and PI3K-mTOR pathways: cross-talk and compensation. *Trends in Biochemical Sciences* **2011**, *36* (6), 320-328.
115. Prior, I. A.; Lewis, P. D.; Mattos, C., A Comprehensive Survey of Ras Mutations in Cancer. *Cancer Research* **2012**, *72* (10), 2457-2467.
116. Won, S. J.; Martin, B. R., Temporal Profiling Establishes a Dynamic S-Palmitoylation Cycle. *ACS Chem Biol* **2018**, *13* (6), 1560-1568.
117. Cravatt, B., Late stage assay provider results from the probe development effort to identify inhibitors of Fam108b: gel-based activity based protein profiling (ABPP) assay to assess HTS hit compounds inhibition and selectivity against a recombinant soluble form of Fam108b. National Center for Biotechnology Information: PubChem BioAssay Database, 2011.
118. Cravatt, B., Late stage assay provider results from the probe development effort to identify inhibitors of Fam108b: gel-based activity-based protein profiling (ABPP) assay to assess HTS hit compound inhibition and selectivity against a recombinant soluble form of Fam108b in a complex proteome. National Center for Biotechnology Information: PubChem BioAssay Database, 2011.
119. Won, S. J.; Davda, D.; Labby, K. J.; Hwang, S. Y.; Pricer, R.; Majmudar, J. D.; Armacost, K. A.; Rodriguez, L. A.; Rodriguez, C. L.; Chong, F. S.; Torossian, K. A.; Palakurthi, J.; Hur, E. S.; Meagher, J. L.; Brooks, C. L., 3rd; Stuckey, J. A.; Martin, B. R.,

- Molecular Mechanism for Isoform-Selective Inhibition of Acyl Protein Thioesterases 1 and 2 (APT1 and APT2). *ACS Chem Biol* **2016**, *11* (12), 3374-3382.
120. Roth, A. F.; Wan, J. M.; Bailey, A. O.; Sun, B. M.; Kuchar, J. A.; Green, W. N.; Phinney, B. S.; Yates, J. R.; Davis, N. G., Global analysis of protein palmitoylation in yeast. *Cell* **2006**, *125* (5), 1003-1013.
121. Percher, A.; Ramakrishnan, S.; Thinon, E.; Yuan, X.; Yount, J. S.; Hang, H. C., Mass-tag labeling reveals site-specific and endogenous levels of protein S-fatty acylation. *Proc Natl Acad Sci U S A* **2016**, *113* (16), 4302-7.
122. Ohno, Y.; Kashio, A.; Ogata, R.; Ishitomi, A.; Yamazaki, Y.; Kihara, A., Analysis of substrate specificity of human DHHC protein acyltransferases using a yeast expression system. *Mol Biol Cell* **2012**, *23* (23), 4543-51.
123. Rossin, A.; Durivault, J.; Chakhtoura-Feghali, T.; Lounnas, N.; Gagnoux-Palacios, L.; Hueber, A. O., Fas palmitoylation by the palmitoyl acyltransferase DHHC7 regulates Fas stability. *Cell Death Differ* **2015**, *22* (4), 643-53.
124. Abrami, L.; Leppla, S. H.; van der Goot, F. G., Receptor palmitoylation and ubiquitination regulate anthrax toxin endocytosis. *J Cell Biol* **2006**, *172* (2), 309-20.
125. Donnelly, M. I.; Zhou, M.; Millard, C. S.; Clancy, S.; Stols, L.; Eschenfeldt, W. H.; Collart, F. R.; Joachimiak, A., An expression vector tailored for large-scale, high-throughput purification of recombinant proteins. *Protein Expr Purif* **2006**, *47* (2), 446-54.
126. Huth, J. R.; Bewley, C. A.; Jackson, B. M.; Hinnebusch, A. G.; Clore, G. M.; Gronenborn, A. M., Design of an expression system for detecting folded protein domains and mapping macromolecular interactions by NMR. *Protein Sci* **1997**, *6* (11), 2359-64.
127. DelProposto, J.; Majmudar, C. Y.; Smith, J. L.; Brown, W. C., Mocr: A novel fusion tag for enhancing solubility that is compatible with structural biology applications. *Protein Expr Purif* **2009**, *63* (1), 40-9.
128. TM, K.; KE, K., Studies of the esterase activity of cytosolic aldehyde dehydrogenase with resorufin acetate as substrate. *Biochemical Journal* **1997**, *322* (Pt. 3), 701-708.
129. Teshima, T.; Griffin, J. C.; Powers, J. C., A new class of heterocyclic serine protease inhibitors. Inhibition of human leukocyte elastase, porcine pancreatic elastase, cathepsin G, and bovine chymotrypsin A alpha with substituted benzoxazinones, quinazolines, and anthranilates. *J Biol Chem* **1982**, *257* (9), 5085-91.
130. Powers, J. C.; Asgian, J. L.; Ekici, O. D.; James, K. E., Irreversible inhibitors of serine, cysteine, and threonine proteases. *Chem Rev* **2002**, *102* (12), 4639-750.
131. Kit, M. C. S.; Martin, B. R., Enrichment of S-Palmitoylated Proteins for Mass Spectrometry Analysis. In *Protein Lipidation*, Springer: 2019; pp 71-79.
132. Khoury, G. A.; Baliban, R. C.; Floudas, C. A., Proteome-wide post-translational modification statistics: frequency analysis and curation of the swiss-prot database. *Sci Rep* **2011**, *1*.
133. Craven, S. E.; El-Husseini, A. E.; Brecht, D. S., Synaptic targeting of the postsynaptic density protein PSD-95 mediated by lipid and protein motifs. *Neuron* **1999**, *22* (3), 497-509.
134. Collins, M. O.; Woodley, K. T.; Choudhary, J. S., Global, site-specific analysis of neuronal protein S-acylation. *Scientific reports* **2017**, *7* (1), 4683.
135. Shen, L.-F.; Chen, Y.-J.; Liu, K.-M.; Haddad, A. N. S.; Song, I.-W.; Roan, H.-Y.; Chen, L.-Y.; Yen, J. J.; Chen, Y.-J.; Wu, J.-Y., Role of S-Palmitoylation by ZDHHC13 in Mitochondrial function and Metabolism in Liver. *Scientific reports* **2017**, *7* (1), 2182.

136. Thinon, E.; Fernandez, J. P.; Molina, H.; Hang, H. C., Selective enrichment and direct analysis of protein S-palmitoylation sites. *Journal of proteome research* **2018**, *17* (5), 1907-1922.
137. Drosten, M.; Dhawahir, A.; Sum, E. Y.; Urosevic, J.; Lechuga, C. G.; Esteban, L. M.; Castellano, E.; Guerra, C.; Santos, E.; Barbacid, M., Genetic analysis of Ras signalling pathways in cell proliferation, migration and survival. *EMBO J* **2010**, *29* (6), 1091-104.
138. Ren, J.; Wen, L.; Gao, X.; Jin, C.; Xue, Y.; Yao, X., CSS-Palm 2.0: an updated software for palmitoylation sites prediction. *Protein Eng Des Sel* **2008**, *21* (11), 639-44.
139. Cox, J.; Hein, M. Y.; Lubner, C. A.; Paron, I.; Nagaraj, N.; Mann, M., Accurate proteome-wide label-free quantification by delayed normalization and maximal peptide ratio extraction, termed MaxLFQ. *Mol Cell Proteomics* **2014**, *13* (9), 2513-26.
140. Gould, N. S.; Evans, P.; Martinez-Acedo, P.; Marino, S. M.; Gladyshev, V. N.; Carroll, K. S.; Ischiropoulos, H., Site-Specific Proteomic Mapping Identifies Selectively Modified Regulatory Cysteine Residues in Functionally Distinct Protein Networks. *Chem Biol* **2015**, *22* (7), 965-75.
141. Gilbert, L. A.; Horlbeck, M. A.; Adamson, B.; Villalta, J. E.; Chen, Y.; Whitehead, E. H.; Guimaraes, C.; Panning, B.; Ploegh, H. L.; Bassik, M. C.; Qi, L. S.; Kampmann, M.; Weissman, J. S., Genome-Scale CRISPR-Mediated Control of Gene Repression and Activation. *Cell* **2014**, *159* (3), 647-61.
142. Horlbeck, M. A.; Gilbert, L. A.; Villalta, J. E.; Adamson, B.; Pak, R. A.; Chen, Y.; Fields, A. P.; Park, C. Y.; Corn, J. E.; Kampmann, M.; Weissman, J. S., Compact and highly active next-generation libraries for CRISPR-mediated gene repression and activation. *Elife* **2016**, *5*.
143. Larson, M. H.; Gilbert, L. A.; Wang, X.; Lim, W. A.; Weissman, J. S.; Qi, L. S., CRISPR interference (CRISPRi) for sequence-specific control of gene expression. *Nat Protoc* **2013**, *8* (11), 2180-96.
144. Amara, N.; Foe, I. T.; Onguka, O.; Garland, M.; Bogoyo, M., Synthetic Fluorogenic Peptides Reveal Dynamic Substrate Specificity of Depalmitoylases. *Cell Chem Biol* **2019**, *26* (1), 35-47.e7.
145. Ahn, K.; McKinney, M. K.; Cravatt, B. F., Enzymatic pathways that regulate endocannabinoid signaling in the nervous system. *Chem Rev* **2008**, *108* (5), 1687-707.
146. Mileni, M.; Johnson, D. S.; Wang, Z.; Everdeen, D. S.; Liimatta, M.; Pabst, B.; Bhattacharya, K.; Nugent, R. A.; Kamtekar, S.; Cravatt, B. F.; Ahn, K.; Stevens, R. C., Structure-guided inhibitor design for human FAAH by interspecies active site conversion. *Proc Natl Acad Sci U S A* **2008**, *105* (35), 12820-4.
147. Palermo, G.; Bauer, I.; Campomanes, P.; Cavalli, A.; Armirotti, A.; Giroto, S.; Rothlisberger, U.; De Vivo, M., Keys to Lipid Selection in Fatty Acid Amide Hydrolase Catalysis: Structural Flexibility, Gating Residues and Multiple Binding Pockets. *PLoS Comput Biol* **2015**, *11* (6), e1004231.
148. Welsch, M. E.; Kaplan, A.; Chambers, J. M.; Stokes, M. E.; Bos, P. H.; Zask, A.; Zhang, Y.; Sanchez-Martin, M.; Badgley, M. A.; Huang, C. S.; Tran, T. H.; Akkiraju, H.; Brown, L. M.; Nandakumar, R.; Cremers, S.; Yang, W. S.; Tong, L.; Olive, K. P.; Ferrando, A.; Stockwell, B. R., Multivalent Small-Molecule Pan-RAS Inhibitors. *Cell* **2017**, *168* (5), 878-889.e29.
149. Ntai, I.; Fornelli, L.; DeHart, C. J.; Hutton, J. E.; Doubleday, P. F.; LeDuc, R. D.; van Nispen, A. J.; Fellers, R. T.; Whiteley, G.; Boja, E. S.; Rodriguez, H.; Kelleher, N. L., Precise

- characterization of KRAS4b proteoforms in human colorectal cells and tumors reveals mutation/modification cross-talk. *Proc Natl Acad Sci U S A* **2018**, *115* (16), 4140-4145.
150. Jiang, H.; Zhang, X.; Chen, X.; Aramsangtienchai, P.; Tong, Z.; Lin, H., Protein Lipidation: Occurrence, Mechanisms, Biological Functions, and Enabling Technologies. *Chem Rev* **2018**, *118* (3), 919-988.
151. Gao, X.; Hannoush, R. N., A Decade of Click Chemistry in Protein Palmitoylation: Impact on Discovery and New Biology. *Cell Chem Biol* **2018**, *25* (3), 236-246.
152. Zhang, M. M.; Wu, P. Y.; Kelly, F. D.; Nurse, P.; Hang, H. C., Quantitative control of protein S-palmitoylation regulates meiotic entry in fission yeast. *PLoS Biol* **2013**, *11* (7), e1001597.